

1968

Nuclear Quasi-Equilibrium During Silicon Burning

David Bodansky
University of Washington

Donald D. Clayton
Clemson University, claydonald@gmail.com

William A. Fowler
California Institute of Technology

Follow this and additional works at: https://tigerprints.clemson.edu/physastro_pubs

Recommended Citation

Please use publisher's recommended citation.

This Article is brought to you for free and open access by the Physics and Astronomy at TigerPrints. It has been accepted for inclusion in Publications by an authorized administrator of TigerPrints. For more information, please contact kokeefe@clemson.edu.

NUCLEAR QUASI-EQUILIBRIUM DURING SILICON BURNING*

DAVID BODANSKY†

University of Washington, Seattle, and California Institute of Technology, Pasadena

DONALD D. CLAYTON‡

Rice University, Houston, Texas, and Institute of Theoretical Astronomy, Cambridge, England

AND

WILLIAM A. FOWLER

California Institute of Technology, Pasadena, and Institute of Theoretical
Astronomy, Cambridge, England*Received February 23, 1968*ANAXAGORAS: By fiery vapors rose this rock you're seeing.—GOETHE, *Faust*,
Part 2, Act II

ABSTRACT

The evolution of nuclear abundances starting from pure ^{28}Si is traced under assumed conditions of constant temperature and density. Calculations are carried out for temperatures from $T_9 = 3.4$ to $T_9 = 5.0$ and for densities from $\rho = 10^6$ to $\rho = 10^9$ g cm $^{-3}$. It is shown that the abundance distributions may be approximated by a succession of quasi-equilibrium configurations in which the number densities of the nuclei between $A = 28$ and $A = 62$ correspond to quasi-equilibrium with the remaining ^{28}Si and the free alpha particles and nucleons. The time rate at which the system progresses through the successive quasi-equilibrium configurations is calculated from the photodisintegration rates in the alpha-particle nuclei below ^{28}Si , particularly the $^{24}\text{Mg}(\gamma, \alpha)^{20}\text{Ne}$ rate. The concentrations of ^{20}Ne , ^{16}O , and ^{12}C are generally not in alpha-particle equilibrium with ^{28}Si and are much less abundant relative to ^{28}Si than they are in natural solar-system composition.

For temperatures and densities in a band extending from $T_9 = 3.8$ and $\rho = 10^7$ g cm $^{-3}$ to $T_9 = 5.0$ and $\rho = 10^9$ g cm $^{-3}$, it is found that the quasi-equilibrium abundances, when about 65 per cent of the ^{28}Si has been consumed, correspond to the natural solar-system abundances in important aspects. The quasi-equilibrium distributions are peaked in the alpha-particle nuclei, accounting (sometimes after beta decays) for the observed abundances of the dominant $A = 4n$ nuclei from $A = 28$ to $A = 56$. The observed abundances in the iron group, $A = 49$ through $A = 57$, can also be understood largely in terms of nuclei formed in quasi-equilibrium. In the quasi-equilibrium solutions the peak abundance occurs at $A = 56$, almost entirely in the form of ^{56}Ni which subsequently decays to ^{56}Fe , the most abundant nucleus in the natural iron-group abundance distribution. For the remaining nuclei between $A = 28$ and $A = 62$, the quasi-equilibrium calculations predict abundances which are usually much lower than the natural abundances.

The number of beta-decay and electron-capture events is sufficiently small under the conditions examined that the mean value of \bar{Z}/\bar{N} remains close to unity. However, even small departures from unity can have appreciable effects on the ratio of free-nucleon densities, n_p/n_n , and on the abundances. The role of these weak decays in the burning of pure ^{28}Si is considered in detail. The main contribution to decay processes is found to come from electron capture in ^{56}Ni . As the temperature of silicon burning is lowered, the beta decays and subsequent strong interactions cause ^{54}Fe to replace ^{56}Ni as the most abundant iron-group nucleus.

In view of the agreement between calculated and observed abundances, and in view of the emergence of silicon burning as a natural stage in the history of a thermonuclear gas, it is plausible to attribute the natural solar-system abundances of the $A = 4n$ nuclei ($A = 28$ through $A = 56$) and the dominant

* Supported in part by the National Science Foundation (GP-7976, formerly GP-5391), the Office of Naval Research [Nonr-220(47)], the Air Force Office of Scientific Research (AFOSR-855-65), and the Atomic Energy Commission [AT(45-1)-1388].

† John Simon Guggenheim Fellow.

‡ Alfred P. Sloan Research Fellow.

nuclei in the lower part of the iron group ($A = 49$ through $A = 57$) to the results of a superposition of quasi-equilibrium ^{28}Si -burning sequences. Subsequent secondary processes such as neutron capture are apparently responsible for the abundances of the remaining, less abundant, nuclei.

The ^{28}Si burning is found to be endoergic at the beginning of the ^{28}Si conversion and at relatively high temperatures and low densities. For most of the region considered, however, the process is strongly exoergic, with typical energy releases of 10^{15} – 10^{18} ergs $\text{g}^{-1} \text{sec}^{-1}$. This power will provide for a short epoch of thermonuclear stability in presupernova cores.

The distinctive conclusions of the present analysis are the following: (1) the synthesis of the alpha-particle nuclei and the synthesis of the iron-group nuclei occur simultaneously in silicon burning (to be explicit, the α -process and the e -process of Burbidge *et al.* and Fowler and Hoyle occur simultaneously); (2) the chief equilibrium product in the iron group is ^{56}Ni , the decay to ^{56}Fe occurring after the termination of the quasi-equilibrium silicon burning; and (3) under the most likely conditions, the production of the iron-group nuclei in silicon burning is accompanied by a large release of nuclear energy.

I. INTRODUCTION

The idea that equilibrium between nuclear species may occur at some time and place in stellar evolution and that the associated abundance patterns may persist in the stellar matter when ultimately dispersed into space is an old and attractive one. In principle, the assumption of equilibrium circumvents the problem of determining detailed reaction rates; one needs only to know the binding energies and partition functions of the various nuclear species. To establish equilibrium there must be reactions connecting all components, and a time must be available which is large compared with the lifetimes of the interacting nuclei.

As early as 1922 Tolman (1922) studied thermodynamic equilibrium between hydrogen and helium as a possible explanation of their relative abundances. Urey and Bradley (1931) examined the isotope ratios in the light elements in order to determine whether or not the observed relative abundances of those isotopes might indicate a single thermodynamic equilibrium, and in the same year Pokrowski (1931) formulated an equilibrium theory for the relative abundances of the elements. Only partial success was achieved, and the difficulties were made even more apparent in a detailed investigation by Chandrasekhar and Henrich (1942). An equilibrium origin for *all* the elements was ruled out by these investigations.

In the work of Hoyle (1946) and Klein, Beskow, and Treffenberg (1946) it was suggested that the abundance peak in the iron group, where the binding energy per nucleon is a maximum, might nonetheless be due to a thermodynamic equilibrium, in which case other sources of the light and very heavy elements would be required. This point of view was adopted by Burbidge, Burbidge, Fowler, and Hoyle (1957; hereinafter referred to as "B²FH"), who determined the astrophysical environment which best reproduced the iron-group nuclei and simultaneously postulated non-equilibrium events to synthesize the remainder of the elements in stars. Clifford and Tayler (1965) made an extensive computation of the composition of matter in nuclear statistical equilibrium for the range of environments suggested by B²FH. Every detail of the iron-group elements cannot be reproduced in this way, and indeed some of the important abundance ratios, such as Fe/Ni, are also not well established observationally. Nevertheless, these results have been so suggestive that there is little doubt that these prominent nuclei owe their high abundances to some type of equilibrium process.

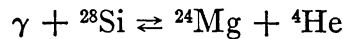
At the time of the writing of their paper it appeared to B²FH that the dominance of the intermediate alpha-particle nuclei (^{24}Mg , ^{28}Si , ^{32}S , ^{36}Ar , ^{40}Ca) was to be interpreted as being due to a chain of alpha-particle captures (called the α -process) involving these intermediate-mass nuclei and that the composition of the iron group was established by a complete nuclear equilibrium (called the e -process) at a subsequent time. In this paper we investigate the possibility that the situation is actually more unified than the one presumed for an α, e -sequence—that, in fact, *the abundances of the most abundant nuclei between ^{28}Si and the iron group, up to and including ^{57}Fe , have been established by a partial equilibrium in which the nuclei heavier than ^{28}Si are in equilibrium with ^{28}Si under the ex-*

change of photons, nucleons, and alpha particles. The ^{28}Si itself is not in equilibrium with those light particles, and the heavy nuclei are not in equilibrium among themselves, because the only effective reaction links are those involving light particles and photons.

We find that the correctness of this idea is strongly attested to by two results which we will discuss: (1) the corresponding abundance pattern bears a remarkable resemblance to the observed solar-system abundances; and (2) the burning of silicon, which now appears to be a fundamental late stage of nuclear burning in stars, leads naturally to such a partial equilibrium. We call this partial equilibrium "quasi-equilibrium" to distinguish it from true nuclear equilibrium, in which ^{28}Si is a negligible constituent. These results constitute a major refinement of the α, e -sequence described by Fowler and Hoyle (1964) and Fowler (1966*a, b*), which corresponds approximately to that special case of silicon burning in which the ^{28}Si is quickly depleted to a very small value, followed by a protracted phase of nuclear equilibrium during which beta decays gradually shift the dominant nucleus from ^{56}Ni ($N = Z$) through ^{54}Fe ($N = Z + 2$) to ^{56}Fe ($N = Z + 4$).

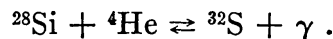
Because of the conceptual difficulty associated with this process and the reasons why it should occur, we first describe in broad terms the sequence of events that occurs when pure ^{28}Si is heated to temperatures in the vicinity of four billion degrees ($T_9 \approx 4$). It should be acknowledged at this point that our understanding of this process took root from a numerical investigation by Truran, Cameron, and Gilbert (1966; hereinafter referred to as "TCG") and from an unpublished analysis by Finzi and Wolf (1966). The possibility of a process of this type seems to have been mentioned first by Hayashi *et al.* (1959; see p. 122).

When ^{28}Si is heated to temperatures in excess of $T_9 = 3$, light particles begin to be ejected at a significant rate, both by $^{28}\text{Si}(\gamma, \alpha)^{24}\text{Mg}$ and by $^{28}\text{Si}(\gamma, p)(\gamma, n)(\gamma, n)^{24}\text{Mg}$. A pool of free alpha particles is established, so that the abundance of ^{24}Mg stabilizes at a value of the order of 10^{-3} of the ^{28}Si concentration when the inverse reactions

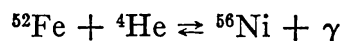
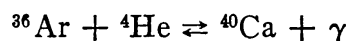
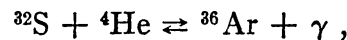


come into equilibrium with the free alpha particles and the thermal photons. Subsequent depletion of ^{28}Si occurs via (γ, α) reactions on ^{24}Mg , followed in turn by (γ, α) reactions on ^{20}Ne , ^{16}O , and ^{12}C . The equilibrium between ^{28}Si and ^{24}Mg greatly slows the disintegration of ^{28}Si into seven alpha particles. The rate for the over-all process is calculated in § III.

Most of the liberated alpha particles do not remain free, of course. Initially they are consumed rapidly by the reaction $^{28}\text{Si}(\alpha, \gamma)^{32}\text{S}$, resulting in a buildup of ^{32}S . However, since the ^{32}S undergoes photoejection *with shorter lifetime than* ^{28}Si , the capture of alpha particles and the buildup of ^{32}S are halted by the equilibration of the inverse reactions



In a similar manner the reactions



also achieve equilibrium. This situation is possible basically because the other (γ, α) lifetimes are all shorter than the effective (γ, α) lifetime of ^{28}Si . Thus we have a situation in

which the concentrations of the heavy nuclei build up to such a value that they liberate alpha particles at almost the same rate at which they consume alpha particles, i.e., *the alpha-particle density assumes a quasi-static value*. On a much longer time scale, the ^{28}Si slowly “melts,” thereby injecting more alpha particles into the bath. These new alpha particles are captured in the formation of more heavy nuclei, thereby establishing a new quasi-equilibrium with more iron-group nuclei and less ^{28}Si . The quasi-static equilibrium can be maintained because the intermediate nuclei capture and lose alpha particles at rates much greater than the actual rates of change of their abundances.

The equilibria are characterized by a series of Saha equations similar to the following one for $^{28}\text{Si} + ^4\text{He} \rightleftharpoons ^{32}\text{S} + \gamma$:

$$\frac{n(^{32}\text{S})}{n(^{28}\text{Si})} = n_\alpha \frac{\omega(^{32}\text{S})}{\omega(^{28}\text{Si})} \left[\frac{A(^{32}\text{S})}{A(^{28}\text{Si})A(^4\text{He})} \right]^{3/2} \left(\frac{2\pi\hbar^2}{M_u kT} \right)^{3/2} \exp \frac{B_\alpha(^{32}\text{S})}{kT}, \quad (1)$$

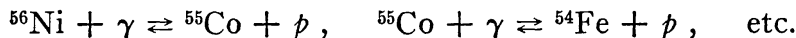
where the partition functions ω are approximately unity for alpha-particle nuclei; the A 's are the atomic masses in units of M_u , the atomic mass unit; and $B_\alpha(^{32}\text{S})$ is the separation energy of an alpha particle from the ground state of ^{32}S . Numerically,

$$(2\pi\hbar^2/M_u kT)^{3/2} = 1.6827 \times 10^{-34} T_9^{-3/2} \text{ cm}^{-3}.$$

It turns out that near $T_9 = 4$ the nuclear system is in the process of building up ^{56}Ni as the most abundant heavy nucleus because it has the greatest binding energy per nucleon of those nuclei having $Z = N$. From the product of seven equations like the one above, we see at once that the free-alpha-particle density grows slowly as ^{28}Si is converted into ^{56}Ni ; in fact, $n_\alpha \propto [n(^{56}\text{Ni})/n(^{28}\text{Si})]^{1/7}$. When this relationship is coupled with those like equation (1) it becomes clear that the concentration of each alpha-particle nucleus may be regarded as a function of temperature and of the concentrations of ^{28}Si and of ^{56}Ni . Note that these equations imply equilibrium only with respect to alpha particles and photons—we do not have the relationship $n(^{56}\text{Ni}) \propto [n(^{28}\text{Si})]^2$, for instance, which would be true if the equilibrium were complete.

As n_α grows, the equilibrium amount of ^{24}Mg decreases, as does, therefore, the effective photodisintegration rate of ^{28}Si , and the quasi-equilibrium becomes more nearly exact. For this and other reasons to be detailed later, it turns out that, as the conversion of ^{28}Si to ^{56}Ni progresses, the rate of that conversion falls rapidly. At long times the distribution asymptotically approaches that of complete nuclear statistical equilibrium, in which ^{28}Si is a quite negligible constituent (Clifford and Tayler 1965).

Not all the nuclei are alpha-particle nuclei, of course. Consider the neutron-rich nuclei, of which ^{54}Fe is one of the most interesting examples. Because of its very large neutron separation energy, $B_n(^{54}\text{Fe}) = 13.6$ MeV, it frequently happens that ^{54}Fe is the most abundant of the neutron-rich nuclei. On a very short time scale an equilibrium proton density is established by photoejection such that the following inverse reactions come into equilibrium:



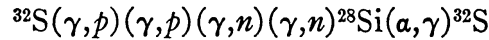
Thus the abundances of prominent neutron-rich species such as ^{54}Fe and the free-proton density n_p are determined by equations of the form

$$n(^{54}\text{Fe})n_p^2 = f(T)n(^{56}\text{Ni}), \quad (2)$$

together with the conservation of nuclear charge in nuclear reactions. To clarify this point, suppose, as an example which is often not far from the truth, that no beta decays have occurred and that ^{54}Fe is overwhelmingly the most abundant neutron-rich nucleus. Then we would have immediately from charge conservation that $n_p \approx 2n(^{54}\text{Fe})$, a relationship that yields both n_p and $n(^{54}\text{Fe})$ as being proportional to $n(^{56}\text{Ni})^{1/3}$. When beta

decay is significant, this relationship is replaced by the more complete, but similar, relationship $n_p \approx 2n(^{54}\text{Fe}) - 2D$, where D is the total number of beta-decay and electron-capture events which change protons to neutrons. The inclusion of the remainder of the neutron-rich nuclei only makes the arithmetic more complicated, while leaving the essence of the equilibration the same as when only ^{54}Fe is considered.

A relatively small density of free neutrons n_n is also maintained by the gas. The value of n_n is in equilibrium with the densities of free protons and alpha particles, viz., $n_p^2 n_n^2 \propto n_\alpha$. This equilibrium is maintained by rapid cycles of the type



plus their inverses. With the aid of this assembly of equations, the relative quasi-equilibrium abundance at a given temperature of every nucleus heavier than ^{28}Si can be computed from two densities, say, n_p and n_α or ^{54}Fe and ^{56}Ni .

The preceding discussion was for typical events near $T_9 = 4$, but we can now easily describe the contrasting features at other temperatures. The densities of free protons, neutrons, and alpha particles are sharply rising functions of temperature. For $T_9 > 5$ the equilibrium $^{54}\text{Fe} + 2p \rightleftharpoons ^{56}\text{Ni}$ switches toward $^{54}\text{Fe} + 2p$, with the result that ^{56}Ni is no longer the dominant iron-group nucleus, and for $T_9 > 6$ the buildup of an iron-group peak is suppressed in favor of merely tearing down ^{28}Si into a free-alpha-particle gas. At lower temperatures the conversion of ^{28}Si to the iron group becomes so slow that beta decay and electron capture occur at competitive rates, with the result that the iron peak grows from a gas that is increasingly neutron-rich. At $T_9 \approx 3$ the conversion is slow enough so that the neutron-rich nucleus ^{54}Fe exceeds ^{56}Ni , and for $T_9 < 3$ the conversion becomes so slow that ^{56}Fe is the dominant product. We may look ahead at this point to remark that the dominance of ^{56}Fe in solar abundances could be due either to the dominant production of ^{56}Fe in long-lasting equilibrium processes or to the subsequent decay of ^{56}Ni , which is formed as the dominant product in rapid equilibrium processes (for $T_9 \leq 5$).

This sequence of events is related to the nuclear evolution of the core of a presupernova star. It is now believed (Fowler 1968) that helium burning results in the production of approximately equal amounts of ^{12}C and ^{16}O in stars in the wide range of masses from 0.5 to $50 M_\odot$. The result of carbon burning followed by oxygen burning in the presence of the debris of carbon burning has not been worked out at the present time. However, general arguments indicate that the dominant nuclear species at the end of this stage of stellar evolution will be ^{28}Si and ^{32}S . In any case, the remarks now to be made are illustrative of the complexities which arise when nuclei other than ^{28}Si are included in the stellar material prior to silicon burning. As the residue of carbon-oxygen burning is heated, the ^{32}S undergoes photoejection more quickly than does the ^{28}Si , about half the ^{32}S reverting to ^{28}Si and about half transforming to heavier nuclei in equilibrium with ^{28}Si and the free light particles. This system is describable by an extension of the techniques of this paper. A similar extension can be made in those cases where a nucleus lighter than ^{28}Si , such as ^{24}Mg , is mixed in substantial proportions with the ^{28}Si . Thus the problem under consideration is an instructive step in the study of the nuclear evolution of a star.

This quasi-equilibrium technique is quite different from that of the related investigation of TCG, who followed the abundances numerically as the explicit network of reactions dictated their evolution. We have been motivated to the present investigation because the assumption of quasi-equilibrium is valid after relatively short relaxation times, it greatly simplifies the conceptual understanding of the process, and it provides abundance information that is readily calculated and interpreted. The method to be presented will be inaccurate at early times, when the abundances are in the process of relaxing toward their quasi-equilibrium values, but at later stages of the calculation it

has greater numerical accuracy than does a method based on the explicit inclusion of each pair of inverse reactions.

II. CHARACTERISTICS OF QUASI-EQUILIBRIUM SOLUTIONS

It has long been known that it is not possible to match the full range of natural solar-system abundances by a true equilibrium model. The failure is particularly pronounced for nuclei heavier than the iron group, but the failure at intermediate masses has also been severe except at the embarrassingly high temperatures required to keep the abundances from collapsing into the iron group. For this reason most modern comparisons of natural and equilibrium abundances have concentrated on the region of the iron peak. The novel feature of the present calculation within the history of equilibrium calculations is the starting point of ^{28}Si , whose slow rate of destruction allows its abundance to remain much larger than a true equilibrium value. The ^{28}Si starting point has already been recognized by others as being important. Fowler and Hoyle (1964) discussed this and decided that the alpha-particle nuclei would be abundant during silicon burning because of the prominent role of (α, γ) and (γ, α) reactions. TCG carried out numerical integrations of the differential equations during silicon burning which revealed these same abundance features. But neither group of authors emphasized the quasi-equilibrium nature of the burning process or indicated the crucial factors in the determination of its rate. We hope to clarify these points in this paper.

The quasi-equilibrium solutions of the present analysis are exact solutions to the following *Gedanken* problem: "What are the steady-state abundances at fixed temperature T , fixed mass density ρ , and fixed ^{28}Si mass fraction f , if it is assumed that the photodisintegration lifetime of ^{28}Si is infinite, if no beta decays occur to change \bar{Z}/\bar{N} , and if the heavy nuclei are able to interact only with photons, nucleons, and alpha particles?" (We adopt the notation of Fowler and Hoyle 1964 in letting \bar{Z}/\bar{N} designate the *total* proton-to-neutron ratio of the nuclear gas; Clifford and Tayler 1965 used the symbol R for that ratio.) The burning of ^{28}Si at constant T and ρ may be approximated by a succession of such solutions in which f and \bar{Z}/\bar{N} are decreased slowly as the ^{28}Si conversion progresses. In advancing from one solution to the next, quasi-equilibrium can be very nearly achieved in the actual system because of the fast rates for reactions induced by alpha particles and nucleons and for the photodisintegration of nuclei heavier than ^{28}Si . These processes dominate the consumption and liberation of the free nucleons and alpha particles. In particular, the net rate of liberation of alpha particles by the photodisintegration of ^{28}Si is negligible compared with the rates of liberation and capture of alpha particles in heavier nuclei. This feature is necessary for quasi-equilibrium solutions to be a good approximation to the real situation.

In this section we search for the existence of quasi-equilibrium solutions with abundances which match the observed natural abundances of elements. We defer until subsequent sections the crucial but separate question: Can these abundances be reached as silicon burning proceeds?

Because the quasi-equilibrium abundances relative to ^{28}Si are determined by the number densities of free alpha particles, protons, and neutrons, it is convenient to express the equilibrium number density $n(^A Z)$ in the form

$$n(^A Z) = C(^A Z) n(^{28}\text{Si}) n_\alpha^{\delta_\alpha} n_p^{\delta_p} n_n^{\delta_n}, \quad (3)$$

where δ_α , δ_p , and δ_n specify the numbers of alpha particles and nucleons in $(^A Z)$ in excess of the number in ^{28}Si . These numbers are computed with respect to the largest alpha-particle nucleus contained within $(^A Z)$. If this largest alpha-particle nucleus contains N' neutrons and Z' protons ($N' = Z'$), then it follows that the integers δ_α , δ_p , and δ_n are given by

$$\delta_\alpha = \frac{1}{4}(N' + Z' - 28), \quad \delta_p = Z - Z', \quad \delta_n = N - N'. \quad (4)$$

The nucleus ${}_{19}^{38}\text{K}$, for example, may be thought of as being composed of ${}_{18}^{36}\text{Ar}$, the nearest alpha-particle nucleus within ${}^{38}\text{K}$, plus one proton and one neutron. Thus $\delta_a = 2$, $\delta_p = 1$, and $\delta_n = 1$.

The quantities $C(^AZ)$ are functions of temperature but are independent of all densities. Again representing the partition function of the nucleus (^AZ) by $\omega(^AZ)$, taking $\omega_a = 1$ and $\omega_p = \omega_n = 2$, we have

$$C(^AZ) = \frac{\omega(^AZ)}{\omega(^{28}\text{Si})} 2^{-(\delta_p+\delta_n)} [\mathfrak{U}(^AZ)]^{3/2} \left(\frac{M_u kT}{2\pi\hbar^2} \right)^{-3(\delta_a+\delta_p+\delta_n)/2} \exp \left[\frac{Q(^AZ)}{kT} \right], \quad (5)$$

where, in terms of the atomic masses, we have

$$\mathfrak{U}(^AZ) = \frac{A(^AZ)}{A(^{28}\text{Si})} A(^4\text{He})^{-\delta_a} A_p^{-\delta_p} A_n^{-\delta_n}, \quad (6)$$

and where

$$Q(^AZ) = B(^AZ) - B(^{28}\text{Si}) - \delta_a B(^4\text{He}) \quad (7)$$

is the energy required to decompose (^AZ) into ${}^{28}\text{Si} + \delta_a(^4\text{He}) +$ nucleons, $B(^AZ)$ being the total binding energy of (^AZ) . The alpha particles, protons, and neutrons maintain an internal equilibrium via chains, such as the chain cited above for ${}^{32}\text{S} \rightleftharpoons {}^{28}\text{Si}$, so that

$$n_a = C_a n_n^2 n_p^2, \quad (8)$$

where

$$C_a = \frac{1}{16} \left[\frac{A(^4\text{He})}{A_p^2 A_n^2} \right]^{3/2} \left(\frac{M_u kT}{2\pi\hbar^2} \right)^{-9/2} \exp \left[\frac{B(^4\text{He})}{kT} \right]. \quad (9)$$

The equilibrium abundance of each heavy element relative to ${}^{28}\text{Si}$ can be characterized by any *two independent* number densities or by appropriate combinations of the densities. These may be taken to be n_a and n_p , n_p/n_n and $n_p n_n$, n_p/n_n and n_a , n_p and ${}^{54}\text{Fe}$, ${}^{54}\text{Fe}$ and ${}^{56}\text{Ni}$, etc. The particular pairs chosen in subsequent discussions are selected as a matter of convenience.

In Table 1 we list for each nucleus considered the quantities δ_p , δ_n , δ_a , $Q(^AZ)$, and the alpha-particle and nucleon separation energies, which are temperature-independent, and the values at several temperatures of $C(^AZ)$. In calculating $C(^AZ)$, the numerical values of the partition functions $\omega(^AZ)$ are taken in most cases from the (temperature-dependent) prescription of TCG. For those few nuclei which are included here but which are not considered by TCG, the approximate (temperature-independent) prescription employed by Clifford and Tayler (1965) was used. The partition functions, at most, vary only weakly with temperature, and therefore, for illustrative purposes, their values at $T_9 = 4.0$ are also presented in Table 1. The Q -values are obtained from the tabulations of Mattauch, Thiele, and Wapstra (1965).¹ Approximate values of $C(^AZ)$ at intermediate temperatures may be obtained from Table 1 by interpolation, using the functional form of equation (5) and neglecting the temperature dependence in $\omega(^AZ)$.

The character of the quasi-equilibrium abundance distributions depends upon the magnitudes of $n(^{28}\text{Si})$, n_a , n_p , and n_n . For a very wide region of number densities, and in particular for the values which will be seen to occur in the conversion of ${}^{28}\text{Si}$, the following

¹ *Note added in proof.*—For a number of proton-rich nuclei, where data were not given by Mattauch *et al.* (1965), $Q(^AZ)$ was calculated from a tabulation of binding energies by Clifford and Tayler (1965), as indicated in Table 1. The corresponding atomic masses are 1–4 MeV less than masses derived from Coulomb displacement energies, as analyzed by Harchol *et al.* (M. Harchol, A. A. Jaffe, J. Miron, I. Unna, and J. Zioni, 1967, *Nucl. Phys.*, **A90**, 459). If the latter estimates are correct, then the present calculation has greatly overestimated the equilibrium abundances of these nuclei. The consequences are significant only at $A = 45$ and $A = 47$, where the corrected total abundances are roughly one-half and one-fifth, respectively, of the abundances indicated in Figures 3, 14, and 21.

TABLE 1. PARAMETERS FOR NUCLEI ENTERING INTO THE QUASI-EQUILIBRIUM CALCULATION*

Nucleus	δ		Q _i (^A Z) (MeV)	Separation Energy (MeV)			ω(^A Z) T ₉ = 4.0	-log c(^A Z)		
	p	n		α	p	n		α	T ₉ = 3.8	T ₉ = 4.4
Mg 24	0	0	-1	11.694	16.532	9.317	1.10	-22.243	-24.161	-25.636
Si 28	0	0	0	11.583	17.175	9.981	1.01	0.000	0.000	0.000
Si 29	0	1	0	12.327	8.475	11.128	2.15	23.362	24.978	26.210
P 29	1	0	0	2.744	17.356	10.439	8.91	30.339	30.935	31.403
Si 30	0	2	0	13.510	10.617	10.650	1.01	44.533	48.177	50.968
P 30	1	1	0	5.592	11.323	10.411	15.80	50.001	52.741	54.848
S 30	2	0	0	4.434		9.383	1.35	60.205	61.699	62.859
P 31	1	2	0	7.287	12.312	9.666	2.11	69.479	74.527	78.392
S 31	2	1	0	6.084	12.973	9.031	8.91	77.109	81.044	84.071
S 32	0	0	1	8.864	15.092	6.948	1.02	26.239	27.589	28.625
S 33	0	1	1	9.569	8.641	7.114	4.22	49.094	52.098	54.401
Cl 33	1	0	1	2.290	16.275	6.494	8.91	57.189	59.055	60.499
S 34	0	2	1	10.888	11.422	7.919	0.99	69.502	74.675	78.640
Cl 34	1	1	1	5.157	11.508	6.679	15.80	76.608	80.651	83.760
Ar 34	2	0	1	4.669		6.729	1.35	86.746	89.552	91.721
Cl 35	1	2	1	6.370	12.635	7.002	2.11	95.661	102.070	106.979
Ar 35	2	1	1	5.889	12.728	6.484	8.91	103.977	109.180	113.182
Cl 36	1	3	1	7.961	8.577	7.642	5.95	118.772	126.814	132.973
Ar 36	0	0	2	8.506	15.252	6.644	1.01	52.904	55.553	57.588
Cl 37	1	4	1	8.399	10.317	7.855	4.09	140.177	150.203	157.887
Ar 37	0	1	2	8.720	8.791	6.793	4.10	75.569	79.900	83.221
K 37	1	0	2	1.867	16.151	6.221	8.91	84.410	87.497	89.879

(continued)

TABLE 1 (continued)

Nucleus	δ			$Q(^A_Z)$ (MeV)	Separation Energy (MeV)			$\omega(^A_Z)^{\dagger}$ $T_9 = 4.0$	ξ		
	p	n	α		p	n	α		$T_9 = 3.8$	$T_9 = 4.4$	$T_9 = 5.0$
Ar 38	0	2	2	34.221	10.242	11.839	7.209	0.99	101.987	107.026	
K 38	1	1	2	27.506	5.124	12.047	6.760	15.80	103.117	112.599	
Ca 38	2	0	2	19.628	4.169		5.721	1.10	114.721	121.696	
Ar 39	0	3	2	40.812	10.724	6.591	6.816	8.25	128.688	134.565	
K 39	1	2	2	40.595	6.374	13.089	7.214	3.99	121.288	135.114	
Ca 39	2	1	2	33.309	5.803	13.681	6.674	8.91	130.602	142.110	
Ar 40	0	4	2	50.684	12.527	9.872	6.808	1.09	143.415	160.564	
K 40	1	3	2	48.396	7.584	7.801	6.438	16.91	145.254	161.704	
Ca 40	0	0	3	20.632	8.333	15.619	7.041	0.99	79.051	86.171	
K 41	1	4	2	58.487	7.803	10.091	6.212	4.50	167.383	187.193	
Ca 41	0	1	3	28.996	8.896	8.364	6.614	8.03	101.983	111.931	
Sc 41	1	0	3	21.719	1.086	15.816	6.260	8.91	111.588	119.228	
Ca 42	0	2	3	40.467	10.276	11.471	6.246	1.11	122.573	136.289	
Sc 42	1	1	3	33.286	4.290	11.567	5.780	15.80	130.932	142.433	
Th 42	2	0	3	25.486	3.767		5.858	1.10	142.434	151.452	
Ca 43	0	3	3	48.395	10.667	7.928	7.583	11.37	145.985	162.399	
Sc 43	1	2	3	45.390	4.923	12.104	4.795	9.86	150.027	165.502	
Th 43	2	1	3	37.774	4.488	12.288	4.465	8.91	160.163	173.271	
Ca 44	0	4	3	59.530	12.170	11.135	8.846	1.19	167.133	187.255	
Sc 44	1	3	3	55.101	6.706	9.710	6.704	19.36	171.805	190.476	
Th 44	0	0	4	25.867	8.773	16.389	5.235	1.11	107.550	116.446	
Ca 45	0	5	3	66.950	12.737	7.420	10.166	12.09	191.216	213.918	
Sc 45	1	4	3	66.420	6.890	11.319	7.933	11.43	191.950	214.430	
Th 45	0	1	4	35.283	8.478	9.415	6.287	14.65	128.875	140.971	
[†] V 45	1	0	4	29.045				8.91	137.358	147.509	

(continued)

TABLE 1 (continued)

Nucleus	δ		$Q(^A_Z)$ (MeV)	Separation Energy (MeV)			$\omega(^A_Z)$ [†] $T_9 = 4.0$	$-\log C(^A_Z)$ [§]	
	p	n		p	n	α		$T_9 = 3.8$	$T_9 = 4.4$
Ca 46	0	6	77.351	13.797	10.401	11.143	1.09	213.401	239.581
Sc 46	1	5	75.186	8.236	8.767	9.162	28.50	214.862	240.325
Ti 46	0	2	48.475	10.351	13.192	8.008	1.39	147.348	163.758
V 46	1	1	40.630	5.347		7.344	15.80	156.680	170.697
[†] Cr 46	2	0	33.782				1.35	166.830	178.667
Sc 47	1	6	85.828	8.477	10.642	10.172	9.09	236.173	265.227
Ti 47	0	3	57.350	10.460	8.875	8.955	11.47	169.590	189.053
V 47	1	2	53.651	5.176	13.021	8.261	9.79	174.571	192.811
[†] Cr 47	2	1	47.712				8.91	182.471	198.922
Ti 48	0	4	68.978	11.446	11.628	9.448	1.31	190.052	213.346
V 48	1	3	64.182	6.832	10.531	9.082	14.53	195.369	217.135
Cr 48	0	0	33.447	8.092		7.580	1.31	132.922	144.370
Ti 49	0	5	77.124	11.342	8.146	10.174	8.20	213.376	239.523
V 49	1	4	75.734	6.756	11.552	9.314	16.41	214.925	240.592
[†] Cr 49	0	1	44.095	8.209	10.648	8.813	7.13	152.995	168.052
Mn 49	1	0	37.014				8.91	162.280	175.146
Ti 50	0	6	86.068	12.171	10.944	10.717	1.05	234.695	264.485
V 50	1	5	85.071	7.947	9.337	9.885	19.23	237.414	266.204
Cr 50	0	2	57.026	9.588	12.930	8.551	1.57	171.451	190.747
[†] Mn 50	1	1	48.642	4.547		8.013	15.80	181.545	198.292
Fe 50	2	0	43.633				1.35	189.256	204.408
V 51	1	6	96.126	8.057	11.055	10.297	12.85	257.864	290.365
Cr 51	0	3	66.295	9.520	9.269	8.945	9.08	193.319	215.810
[†] Mn 51	1	2	62.326	5.300	13.683	8.675	10.34	198.528	219.760
Fe 51	2	1	55.484				8.91	207.657	226.760
Cr 52	0	4	78.330	10.501	12.035	9.352	1.10	213.214	239.691
Mn 52	1	3	72.839	6.544	10.513	8.657	16.51	219.319	244.063
Fe 52	0	0	41.387	7.357		7.940	1.16	157.934	172.121

(continued)

TABLE 1 (continued)

Nucleus	δ			Q_α (MeV)	Separation Energy (MeV)			$\omega(^A Z)$ $T_9 = 4.0$	δ		
	p	n	α		p	n	α		$T_9 = 3.8$	$T_9 = 4.4$	$T_9 = 5.0$
Cr 53	0	5	5	86.272	11.134	7.941	9.148	5.07	236.959	253.481	266.133
Mn 53	1	4	5	84.891	6.560	12.051	9.157	10.07	238.485	254.778	267.268
Fe 53	0	1	6	51.828	7.285	10.441	7.733	8.25	178.164	188.202	195.904
Co 53	1	0	6	44.823				8.91	187.417	196.197	202.949
Cr 54	0	6	5	95.993	12.039	9.721	7.925	1.50	259.540	277.897	291.952
Mn 54	1	5	5	93.832	7.560	8.941	8.761	12.35	261.488	279.456	293.220
Fe 54	0	2	6	65.447	8.852	13.619	8.421	1.13	195.910	208.482	218.108
Mn 55	1	6	5	104.056	8.063	10.224	7.951	12.56	282.851	302.787	318.062
Fe 55	0	3	6	74.746	9.210	9.299	8.451	7.46	217.706	232.029	243.004
Co 55	1	2	6	70.504	5.057	14.091	8.179	8.19	223.272	236.881	247.319
Ni 55	2	1	6	62.562				8.91	233.766	245.945	255.301
Fe 56	0	4	6	85.950	10.190	11.203	7.619	1.45	238.495	254.945	267.542
Co 56	1	3	6	80.593	5.846	10.088	7.754	15.44	244.565	260.066	271.951
Ni 56	0	0	7	49.382	7.174		7.996	1.00	182.885	192.482	199.848
Fe 57	0	5	6	93.591	10.561	7.642	7.320	13.11	262.341	280.275	294.017
Co 57	1	4	6	91.972	6.022	11.379	7.082	8.17	264.678	282.362	295.919
Ni 57	0	1	7	59.659	7.362	10.276	7.851	4.21	203.572	215.117	223.972
Fe 58	0	6	6	103.634	11.955	10.042	7.641	1.62	284.877	304.899	319.874
Co 58	1	5	6	100.543	6.951	8.571	6.711	20.84	287.855	307.149	321.935
Ni 58	0	2	7	71.854	8.178	12.195	6.407	1.10	222.922	236.752	247.344
Co 59	1	6	6	111.009	7.375	10.466	6.953	8.90	309.278	330.572	346.862
Ni 59	0	3	7	80.856	8.610	9.002	6.110	7.71	245.089	260.613	272.509
Cu 59	1	2	7	75.274	3.420	12.771	4.770	8.91	252.408	266.982	278.169
Ni 60	0	4	7	92.240	9.527	11.383	6.290	1.16	265.747	283.442	296.989
Cu 60	1	3	7	85.352	4.476	10.058	4.740	15.80	273.759	290.247	302.900
Zn 60	0	0	8	52.094	5.116		2.712	1.35	214.657	224.847	232.681

(continued)

TABLE 1 (concluded)

Nucleus	δ		$Q_c(^AZ)$		Separation Energy (MeV)		$\omega(^AZ)$ †		$-\log C(^AZ)$ §		
	p	n	p	n	n	α	$T_9 = 4.0$	$T_9 = 3.8$	$T_9 = 4.4$	$T_9 = 5.0$	
Ni 61	0	5	7	7	9.858	7.821	6.469	8.91	289.414	308.661	323.421
Cu 61	1	4	7	7	4.802	11.709	5.070	8.91	293.417	312.118	326.464
Zn 61	0	1	8	8	5.523	10.465	2.901	8.91	234.898	247.076	256.432
Ni 62	0	6	7	7	11.107	10.599	7.026	1.10	311.205	332.464	348.765
Cu 62	1	5	7	7	5.882	8.900	5.400	15.80	316.304	336.710	352.362
Zn 62	0	2	8	8	6.428	12.614	3.320	1.35	253.926	268.481	279.654

* The values of $Q_c(^AZ)$ (eq. [7]) and the separation energies are based on tabulations of Mattauach, Thiele, and Wapstra (1965), unless otherwise indicated.

† The values of $\omega(^AZ)$ for these nuclei are obtained from a tabulation of binding energies by Clifford and Taylor (1965).

‡ Calculated from tabulation by Truran, Cameron, and Gilbert (1966). For those cases not covered by Truran et al., the following values were adopted for $\omega(^AZ)$ (after Clifford and Taylor 1965): even-even (magic) -- 1.10; even-even -- 1.35; odd -- 8.91; and odd-odd -- 15.80.

§ For convenience in tabulation, the negative of $\log [C(^AZ)]$ (eq. [5]) is listed. Values of $\log [C(^AZ)]$ at unlisted temperatures, T, can be calculated from the values at the nearest listed temperature, T_0 , from the approximate relation (which neglects the temperature dependence of the partition functions $\omega(^AZ)$):

$$\log [C(^AZ), T] \approx \log [C(^AZ), T_0] + \frac{3}{2} (\delta_p + \delta_n + \delta_\alpha) \log (T_0/T) + 5.040 Q_c(^AZ) [1/T - 1/T_0]$$

where $Q_c(^AZ)$ is expressed in MeV and T is expressed in 10^9 °K.

generalizations apply: (1) the alpha-particle nuclei ^{28}Si , ^{32}S , ^{36}Ar , and ^{40}Ca are much more abundant than any other nuclei between $A = 28$ and $A = 40$; (2) there is an abundance minimum in the range $40 < A < 50$; and (3) there is an abundance maximum at the iron group. These features are similar to the main features of the natural abundances of the nuclear species. A recent compilation (Cameron 1967) is shown in Figure 1, and the general features which we have listed as characterizing the quasi-equilibrium are quite evident in this figure.²

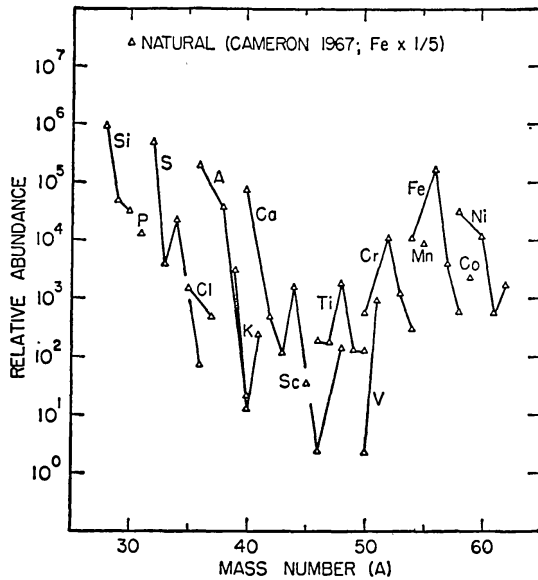


FIG. 1

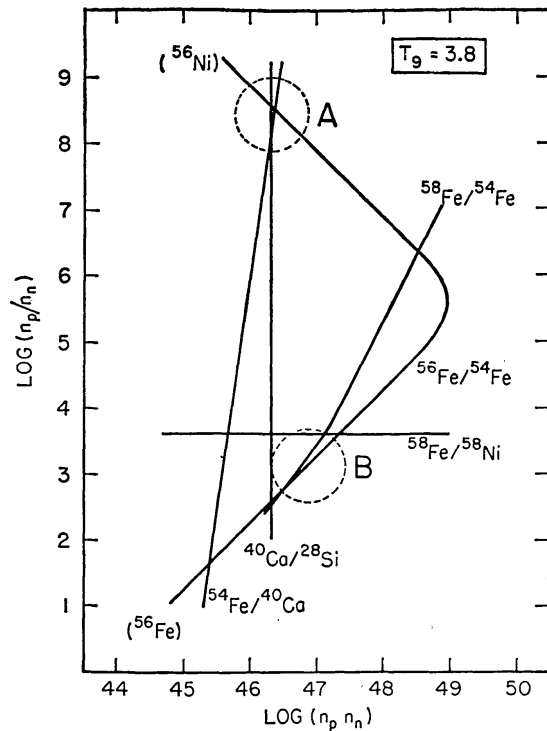


FIG. 2

FIG. 1.—Natural abundances of the elements in the solar system (Cameron 1967). Isotopes of the same element are connected by solid lines. Cameron's value for the iron abundance has been reduced by a factor of $\frac{1}{5}$, corresponding to a choice of the solar photospheric abundance for iron rather than the meteoritic abundance.

FIG. 2.—Determination of values of n_p/n_n and $n_p n_n$ which provide a match to the natural solar-system abundances of elements. Solid lines are loci of points for which the quasi-equilibrium abundances match the indicated natural abundance ratios. The regions labeled *A* and *B* represent two solutions corresponding to the best over-all matches.

In order to explore the possibility that the most abundant nuclei between $A = 28$ and $A = 60$ are formed in a quasi-equilibrium process, we have performed a search for free-nucleon concentrations that could account for the solar-system abundances shown in Figure 1. To this end, we have examined how key abundance ratios depend upon the parameters n_p/n_n and $n_p n_n$. The abundance ratios $^{40}\text{Ca}/^{28}\text{Si}$, $^{54}\text{Fe}/^{40}\text{Ca}$, $^{56}\text{Fe}/^{54}\text{Fe}$, and $^{58}\text{Fe}/^{58}\text{Ni}$ have been selected as providing important tests of a quasi-equilibrium solution. The locus of points in the $[\log(n_p/n_n), \log(n_p n_n)]$ -plane that satisfy the solar-system ratios of these abundances is shown in Figure 2 for the specific choice $T_9 = 3.8$.

The ratio $^{40}\text{Ca}/^{28}\text{Si}$, for example, involves nuclei with equal numbers of protons and neutrons and therefore defines a straight line at constant $n_p n_n$. A different natural ratio

² The Cameron (1967) abundance for iron has been reduced by $\frac{1}{5}$ to match the solar photospheric abundances. The iron-abundance problem is discussed in § IX.

of $^{40}\text{Ca}/^{28}\text{Si}$ would have resulted in a parallel line at a slightly different value of $n_p n_n$. In fact, we see from equations (3) and (8) that

$$\frac{n(^{40}\text{Ca})}{n(^{28}\text{Si})} = C(^{40}\text{Ca})n_a^3 = C(^{40}\text{Ca})C_a^3(n_p n_n)^6, \quad (10)$$

so that the product $n_p n_n$ is proportional to the one-sixth power of the chosen abundance ratio. Similarly, the ratio $^{58}\text{Fe}/^{58}\text{Ni}$ defines a straight line at constant n_p/n_n . The ratio $^{56}\text{Fe}/^{54}\text{Fe}$ leads to a more complicated curve because the observed ^{56}Fe may have come from several different mass-56 parents. The upper half of that curve, at high values of n_p/n_n , corresponds to an equilibrium condition for which the mass-56 nuclei are primarily in the form of ^{56}Ni (which ultimately decays to ^{56}Fe), whereas the half at low values of n_p/n_n corresponds to a condition for which ^{56}Fe is itself produced in the equilibrium.

The natural abundances are best accounted for in an equilibrium model by values of n_p and n_n corresponding to regions where the individual lines in Figure 2 intersect. There are two qualitatively distinct regions in Figure 2 where the agreements are most suggestive. One of these, designated as region *B*, offers simultaneous fits to the three ratios involving the isotopes of iron but provides a poor fit to the relative size of the iron group and the alpha-particle nuclei, as represented by the ratio $^{54}\text{Fe}/^{40}\text{Ca}$. For this region the iron-group nuclei are much more abundant than are the lighter nuclei, because this region corresponds to conditions of true nuclear statistical equilibrium where ^{28}Si is quite small. It was in this general region also that Fowler and Hoyle (1964), and B²FH before them, sought the nuclear equilibrium that best characterized the iron peak.

Another possibility, and it is this one that is really the subject of the present paper, is suggested by the agreements near region *A*. This solution fails to fit the $^{58}\text{Fe}/^{58}\text{Ni}$ and $^{58}\text{Fe}/^{54}\text{Fe}$ ratios, but it does preserve the $^{56}\text{Fe}/^{54}\text{Fe}$ ratio in the form of $^{56}\text{Ni}/^{54}\text{Fe}$, and it simultaneously provides a good representation of the abundances of the alpha-particle nuclei, relative to each other and relative to the iron group. We will find that abundances of this general character are naturally encountered in those stages of silicon burning in which a substantial amount of the original ^{28}Si remains. This suggests that a quasi-equilibrium with ^{28}Si , which appears in the sequence of thermonuclear burning stages in stars, may have played a very major role in nucleosynthesis.

At first one might hope that some other choice of temperature could result in the satisfaction of all abundance ratios. It appears, however, that such hopes are doomed to disappointment and that the situation in Figure 2 for $T_9 = 3.8$ is indeed characteristic of the situation throughout the temperature region in which equilibrium solutions of any sort are successful.

Examples of abundance distributions corresponding to these two regions are shown in Figures 3 and 4. Figure 3 illustrates the abundances for a solution corresponding to region *A* of Figure 2. The relatively large value $n_p/n_n = 10^{7.86}$ corresponds to a gas in which $\bar{Z}/\bar{N} \approx 1$ if we have (as illustrated in Fig. 3) a large unburned component of ^{28}Si . This last condition requires emphasis, because the work of Clifford and Tayler (1965) showed that complete nuclear equilibrium at that value of n_p/n_n is characterized by a negligible component of ^{28}Si and a value of \bar{Z}/\bar{N} near 0.9. This contrast illustrates the way in which this calculation differs from previous equilibrium calculations. This solution gives an excellent fit to the abundances of the alpha-particle nuclei and to the dominant iron-group nuclei up to $A = 57$, but it fails badly elsewhere, underestimating the abundances of the remaining nuclei.

In Figure 4, illustrating a solution of type *B*, there is no match to natural abundances for $A < 50$, but the fit is reasonably good between $A = 51$ and $A = 62$. This solution is essentially the same as that of Fowler and Hoyle (1964). It represents a very late stage of the burning when the ^{28}Si has almost vanished, and the gas has become neutron-rich

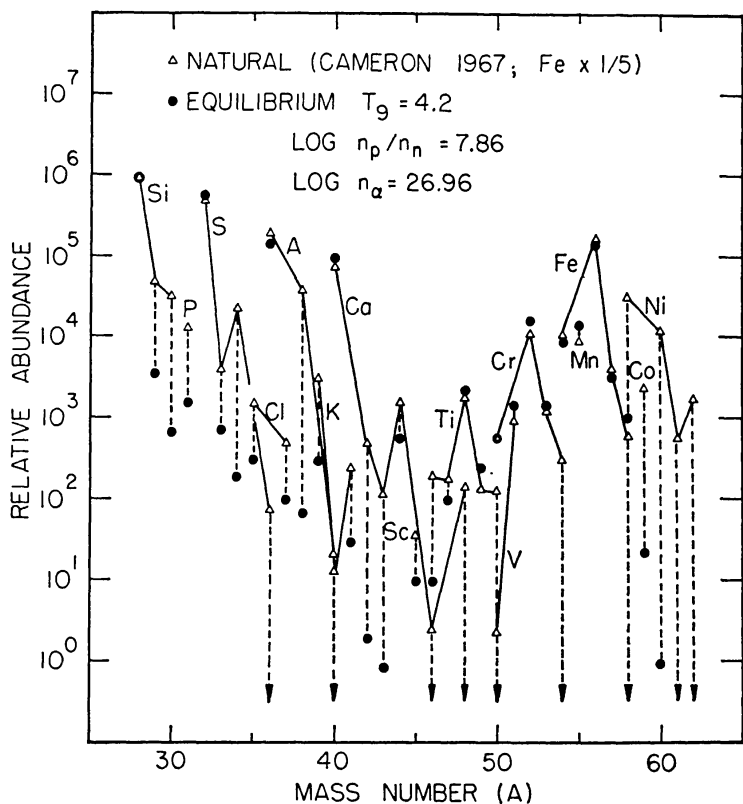


FIG. 3.—Comparison of natural solar-system abundances with quasi-equilibrium abundances for a Type *A* solution. The parameters are taken from Table 2. It will be found (§ *Vd*) that these values are closely achieved during ^{28}Si burning at $T_9 = 4.2$ and $\rho = 10^8 \text{ g cm}^{-3}$. Vertical lines with arrows represent cases in which the quasi-equilibrium abundances fall off-scale.

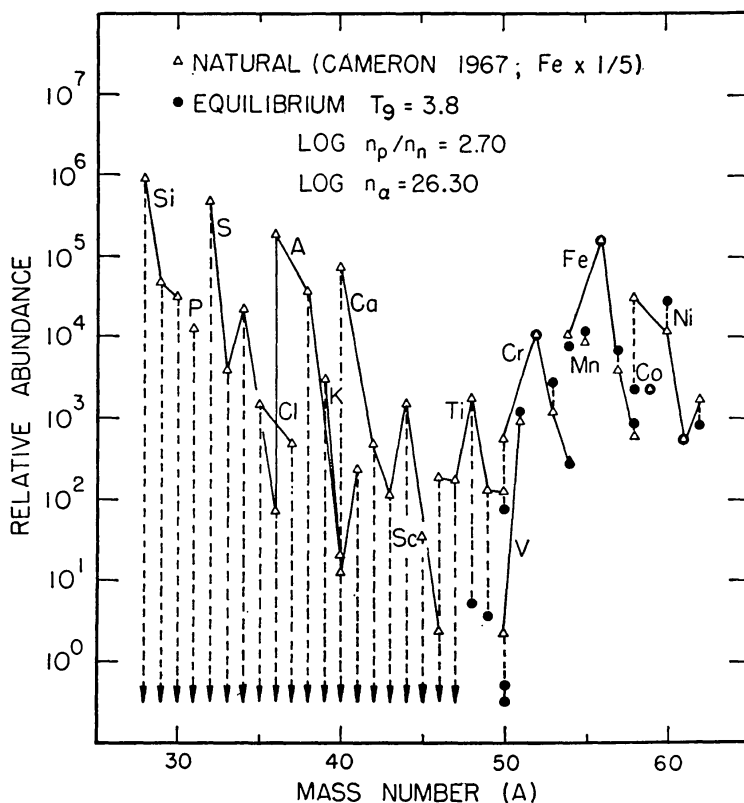


FIG. 4.—Comparison of natural solar-system abundances with quasi-equilibrium abundances for a Type *B* solution. The parameters correspond to the equilibrium solution found by Fowler and Hoyle (1964). Vertical lines with arrows represent cases in which the quasi-equilibrium abundances fall off-scale.

to the extent that $\bar{Z}/\bar{N} < 0.9$. The achievement of such values of \bar{Z}/\bar{N} in silicon burning, where $\bar{Z}/\bar{N} = 1.0$ initially, requires sufficient time for the necessary beta-decay and electron-capture processes to act. The ratio of *free*-proton to *free*-neutron density exceeds unity ($n_p/n_n = 10^{2.7}$) because neutron binding energies are greater than proton binding energies within the iron group.

A simple relationship between region *A* and region *B* exists within the context of silicon burning. As will be seen below, there exists a wide range of temperatures and densities for which n_p and n_n fall near region *A* at a time when about two-thirds of the ^{28}Si has been converted to heavier elements. At $T_9 = 4.0$, for example, this point is reached about 10 seconds after the start of the ^{28}Si conversion. If the system remains with temperature and density unchanged, the conversion of ^{28}Si into heavier elements, predominantly ^{56}Ni , will continue. Beta decay and electron capture gradually lower the value of \bar{Z}/\bar{N} below unity, with a corresponding (but much larger) decrease in n_p/n_n but on a time scale much longer (at $T_9 \geq 4.0$) than that required to reduce the ^{28}Si fraction to one-third. The decrease in n_p/n_n is accompanied by a transfer of the abundance peaks from the alpha-particle nuclei to the neutron-rich isotopes of iron. At that time the system has passed into region *B*.

The evidence for an equilibrium with ^{28}Si in region *A*, where the abundance of ^{56}Fe is identified with that of its ^{56}Ni progenitor, may be seen in another form of display of the observed abundance ratios of the alpha-particle nuclei. This display also provides, in principle, a systematic means for determining the values of the temperature, T , and alpha-particle density, n_a , that can account for the abundances. If equilibrium is assumed, it can be shown that the abundance ratios are given by

$$\begin{aligned} (N + Z - 28)^{-1} \log \left\{ \left[\frac{A(^{28}\text{Si})}{A(^A Z)} \right]^{3/2} \frac{\omega(^{28}\text{Si})n(^A Z)}{\omega(^A Z)n(^{28}\text{Si})} \right\} \\ = a(T, n_a) + b(T) \frac{B(^A Z) - B(^{28}\text{Si})}{N + Z - 28}, \end{aligned} \quad (11)$$

where

$$\begin{aligned} a(T, n_a) &= -\frac{3}{8} \log \left[A(^4\text{He}) \frac{M_u k T}{2\pi \hbar^2} \right] - \frac{1.260 B(^4\text{He})}{T_9} + \frac{1}{4} \log n_a, \\ b(T) &= 5.040/T_9. \end{aligned} \quad (12)$$

Thus a plot, as in Figure 5, of the left-hand side of equation (11) against the relative binding energy $[B(^A Z) - B(^{28}\text{Si})]/(N + Z - 28)$ should give a straight line whose slope determines T_9 and whose ordinate determines n_a . (For Fig. 5 we approximate $\omega(^A Z)/\omega(^{28}\text{Si})$ by its value at $T_9 = 4.0$.) The relation does indeed appear to be linear, although the sensitivity to temperature is not great enough to determine the temperature with any precision. Values ranging between $T_9 = 3.8$ and $T_9 = 5.0$ appear plausible, and temperatures outside this range cannot be definitely excluded.

The data points of Figure 5, together with equations (11) and (12), can be used to determine n_a at any given value of T_9 between 3.8 and 5.0. These values are presented in Table 2. At a given temperature, the proton number density, n_p , can be determined from the equilibrium $^{56}\text{Ni} \rightleftharpoons ^{54}\text{Fe} + 2p$, assuming that the equilibrium ratio $n(^{56}\text{Ni})/n(^{54}\text{Fe})$ is equal to the natural abundance ratio $n(^{56}\text{Fe})/n(^{54}\text{Fe})$. Finally, n_n can be determined with the aid of equation (8). The values of n_p and n_n which are found in this manner are also presented in Table 2. There is, of course, no assurance that these values are reached in ^{28}Si burning, but it will be found in § V that they can in fact be closely approached at certain densities, for temperatures between $T_9 = 4.0$ and $T_9 = 5.0$, when about 60 or 65 per cent of the ^{28}Si has been consumed. Approximate values of the densities at which this occurs are listed in the last column of Table 2.

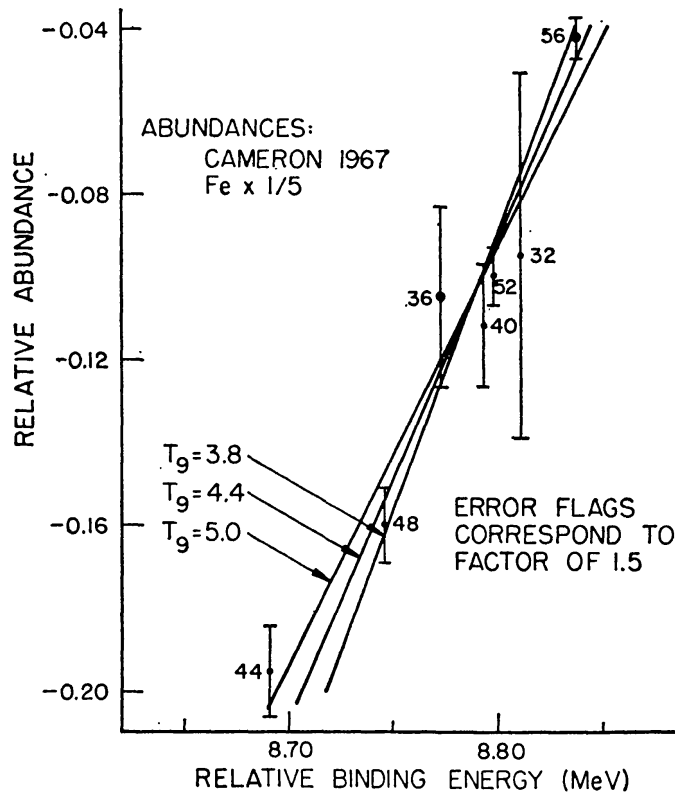


FIG. 5.—Systematics of the abundances of the alpha-particle nuclei. Coordinates for each nucleus are determined by the relative abundance (left-hand side of eq. [11]) and the relative binding energy (coefficient of $b(T)$ in eq. [11]). Solid lines are examples of fits to the points. The slope of the line determines the temperature T , and the position of the line determines n_α . For cases in which the alpha-particle nucleus is not stable ($A \geq 44$) the abundance is taken to equal the natural abundance of its stable beta-decay product.

TABLE 2
 NUCLEON AND ALPHA-PARTICLE NUMBER DENSITIES (cm^{-3}) FOR BEST MATCH
 TO THE NATURAL ABUNDANCES OF THE ALPHA-PARTICLE NUCLEI
 AND THE NATURAL RATIO $n(^{56}\text{Fe})/n(^{54}\text{Fe})$

Temperature (T_9)	$\log n_\alpha$	$\log n_p$	$\log n_n$	$\log (n_p/n_n)$	$\log \rho^*$
3.8.....	26.03	27.45	18.93	8.52
4.0.....	26.52	27.89	19.72	8.17	7.5
4.2.....	26.96	28.29	20.43	7.86	8.0
4.4.....	27.38	28.66	21.09	7.57	8.5
4.6.....	27.74	29.00	21.68	7.32	9.0
4.8.....	28.08	29.31	22.23	7.08	9.0
5.0.....	28.38	29.60	22.72	6.88	9.5

* Approximate values, from the analysis discussed in § V. The density ρ is in grams per cubic centimeter.

The linear relationship in Figure 5 is a striking one, despite the failure to determine T accurately, and it is difficult to see how it could be obtained except by alpha-particle equilibrium. If these abundances were due to an unimpeded flow of alpha-particle captures, they would be inversely correlated with the alpha-particle capture cross-sections rather than with the binding energies. We draw the conclusion that quasi-equilibrium events have been prominent contributors to nucleosynthesis in this mass range.

This suggestion has a practical consequence for observational astronomy, viz., *the abundances from ^{28}Si through the iron group should be strongly correlated in the interstellar medium.* A test is to be sought in the metal-deficient stars, where we expect these elements to be deficient by roughly the same factor. Elements synthesized in other burning stages, such as helium, carbon, nitrogen, oxygen, sodium, magnesium, and barium may, on the other hand, have uncorrelated deficiency factors, although they are by no means required to. Evidence along this line has been presented by Peat and Pemberton (1967), who have found that in the moderately metal-deficient old stars the elements calcium and iron appear underabundant by similar factors, whereas ^{16}O and ^{24}Mg do not seem to be as underabundant. It seems to us that observational studies of this type have important implications for the early evolution of the Galaxy.

It should be noted that this same argument cannot be applied to stars with large *overabundances* in the range from silicon to iron. Such stars have presumably mixed material to their surface that has been synthesized within the interior, or they have produced these elements on the surface. At the present time it appears impossible that any star can have an inner region pass through a nuclear burning phase as advanced as silicon burning and yet live sufficiently long to mix these products to the surface. A more promising approach to the cases of surface overabundances seems to lie with especially intense flash phenomena during helium or carbon burning, along the general lines suggested by Fowler *et al.* (1965), or with non-thermal surface reactions by preferentially accelerated alpha particles, along the general lines suggested by Brancazio and Cameron (1967).

Finally we must add that the element silicon, and perhaps also sulfur, may participate only partially in this correlation. In particular, it may be possible to synthesize ^{28}Si and ^{32}S at an earlier stage, namely, oxygen burning, without synthesizing the remainder of the heavier elements. This possibility depends upon regions of a star being expelled during oxygen burning, and we are not yet able to assess its likelihood under general circumstances. For the material which comprises the solar system, the agreement between the natural abundances and the predictions for quasi-equilibrium abundance distributions (especially those shown in Figs. 3 and 5) argues against such expulsion of pre-equilibrium ^{28}Si and ^{32}S having taken place in large quantity.

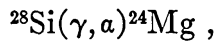
III. PHOTODISINTEGRATION FLOW DOWNWARD FROM ^{28}Si

We have assumed in the foregoing discussion that the densities n_a , n_p , and n_n take on quasi-static values determined from the quasi-equilibrium above ^{28}Si . That is to say, their densities are very slowly varying, inasmuch as they are determined by the near-equality of the rates of capture and photoejection within the nuclei near ^{28}Si . The relatively slow disintegration of ^{28}Si merely throws fresh nucleons into the pot, which are quickly captured in the establishment of the new quasi-equilibrium. We continue to make this assumption in the following discussion because the quantitative results will confirm its correctness. We now turn to a detailed consideration of the problem of converting the silicon in the face of established densities of protons, neutrons, and alpha particles that vary only slowly in time.

Because the great size of the Coulomb barrier virtually prohibits ^{28}Si from reacting with itself, the conversion from ^{28}Si into heavier elements proceeds by a process of photodisintegration rearrangement. Protons, neutrons, and alpha particles are liberated by two sequences leading to ^{24}Mg :



and



the first of which occurs at the more rapid rate (Fowler and Hoyle 1964; TCG; Fowler, Caughlan, and Zimmerman 1967 [hereinafter referred to as "FCZ"]). Although it might appear that the rates of these reactions would govern the consumption of ${}^{28}\text{Si}$, it was pointed out by Finzi and Wolf (1966) that the ${}^{24}\text{Mg}$ will quickly assume a concentration corresponding to equilibrium with ${}^{28}\text{Si}$. In this equilibrium each of the photodisintegration rates is balanced by the corresponding capture rate. For example, the rate of ${}^{24}\text{Mg}(\alpha, \gamma) {}^{28}\text{Si}$ will be as large as that of ${}^{28}\text{Si}(\gamma, \alpha) {}^{24}\text{Mg}$, and the rate of ${}^{28}\text{Si}(\gamma, p) {}^{27}\text{Al}$ is balanced by the rate of ${}^{27}\text{Al}(p, \gamma) {}^{28}\text{Si}$. Thus the ${}^{24}\text{Mg}$ concentration is determined by an equilibrium with ${}^{28}\text{Si}$ and the free-alpha-particle density:

$$n({}^{24}\text{Mg}) = C({}^{24}\text{Mg})n({}^{28}\text{Si})n_{\alpha}^{-1} . \tag{13}$$

The ratio $n({}^{24}\text{Mg})/n({}^{28}\text{Si})$ is always very small for alpha-particle concentrations large enough to correspond to an appreciable (say, > 5 per cent) conversion of ${}^{28}\text{Si}$ to other elements, because the binding energy of an alpha particle in ${}^{28}\text{Si}$ is large compared with the binding energy in the heavier alpha-particle nuclei (${}^{32}\text{S}, \dots, {}^{56}\text{Ni}$).

After the ${}^{24}\text{Mg}$ reaches its equilibrium concentration, further (net) disintegration of ${}^{28}\text{Si}$ can proceed only at a rate governed by the photodisintegration of ${}^{24}\text{Mg}$. The over-all effect is a reduction in the effective photodisintegration rate of ${}^{28}\text{Si}$, because the product of the ${}^{24}\text{Mg}$ concentration and its photodisintegration rate is much less than the corresponding product for ${}^{28}\text{Si}$, as indeed it must have been for the ${}^{24}\text{Mg}$ - ${}^{28}\text{Si}$ equilibrium to have been established. As the ${}^{28}\text{Si}$ conversion to the iron group proceeds, the flow downward is slowed even further because (a) the free-alpha-particle density is proportional to $[n({}^{56}\text{Ni})/n({}^{28}\text{Si})]^{1/7}$, with the result that over most of the conversion n_{α} rises and $n({}^{24}\text{Mg})/n({}^{28}\text{Si})$ falls, and (b) in some cases the alpha-particle capture in ${}^{20}\text{Ne}$ creates an appreciable flow upward (this point will be considered below in more detail). Thus ${}^{28}\text{Si}$ burning is characterized by the property that, as ${}^{28}\text{Si}$ is converted to iron-group nuclei, the rate of the conversion decreases.

We must next inquire into the fate of the ${}^{24}\text{Mg}$. FCZ have analyzed the nuclear data for the reactions ${}^{23}\text{Na}(p, \gamma) {}^{24}\text{Mg}$ and ${}^{20}\text{Ne}(\alpha, \gamma) {}^{24}\text{Mg}$. The photodisintegration rates determined from detailed balance are found to be

$$\begin{aligned} \lambda_{\gamma p}({}^{24}\text{Mg}) &= 5.08 \times 10^{15} T_9^{3/2} \exp\left(-\frac{140.75}{T_9}\right) \text{sec}^{-1} , \\ \lambda_{\gamma \alpha}({}^{24}\text{Mg}) &= 5.22 \times 10^{14} T_9^{3/2} \exp\left(-\frac{123.55}{T_9}\right) \text{sec}^{-1} . \end{aligned} \tag{14}$$

The (γ, p) rate is only 3 per cent of the (γ, α) rate at $T_9 = 3$, and it rises to 30 per cent at $T_9 = 5$. In what follows we will quantitatively include only the (γ, α) branch, with the following justification. In the lower temperature range we make an error of only a few per cent in the disintegration rate, whereas near $T_9 = 5$ the ${}^{20}\text{Ne}$ approaches alpha-particle equilibrium with ${}^{24}\text{Mg}$, with the result that the ${}^{24}\text{Mg}$ photodisintegration rate no longer controls the photodisintegration flow. (This situation is analogous to that of ${}^{24}\text{Mg}$ vis-à-vis ${}^{28}\text{Si}$.) Thus we use $\lambda_{\gamma \alpha}$ as the total photodisintegration rate of ${}^{24}\text{Mg}$ with very little error and with considerable simplification in the analysis below. The reaction ${}^{24}\text{Mg}(\gamma, \alpha) {}^{20}\text{Ne}$ is followed by ${}^{20}\text{Ne}(\gamma, \alpha) {}^{16}\text{O}$, ${}^{16}\text{O}(\gamma, \alpha) {}^{12}\text{C}$, and ${}^{12}\text{C}(\gamma, \alpha) {}^8\text{Be}(\alpha) {}^4\text{He}$. The net result is ${}^{28}\text{Si} \rightarrow 7 {}^4\text{He}$. We now calculate the rate of this over-all process.

Any simple quantitative estimate shows that the concentrations of the light alpha-

particle nuclei must be much less than that of ^{28}Si at all times during this process. In fact, each of these nuclei exists with a concentration just sufficient to produce a net downward photodisintegration flow equal to that received from above. After a rapid initial adjustment, the rate of change of the concentrations of ^{20}Ne , ^{16}O , and ^{12}C becomes much smaller than the alpha-particle flow in and out of each nucleus. If we define the net downward alpha-particle current from A to $A - 4$ as

$$J(A) = \lambda_{\gamma\alpha}(^AZ)n(^AZ) - \lambda_{\alpha\gamma}[^{A-4}(Z-2)]n[^{A-4}(Z-2)], \quad (15)$$

where $\lambda_{\alpha\gamma} = n_{\alpha}\langle\sigma(\alpha,\gamma)v\rangle$, the previously described assumption of conserved flow implies

$$J(24) = J(20) = J(16) = J(12). \quad (16)$$

This assumption will be valid if $dn(^AZ)/dt \ll J(A)$. These four equations can be solved simultaneously for the photodisintegration current, which we hereafter designate by J :

$$J = \frac{\lambda_{\gamma\alpha}(^{24}\text{Mg})n(^{24}\text{Mg}) - \eta(^{20}\text{Ne})\eta(^{16}\text{O})\eta(^{12}\text{C})r_{3\alpha}}{1 + \eta(^{20}\text{Ne})\{1 + \eta(^{16}\text{O})[1 + \eta(^{12}\text{C})]\}}, \quad (17)$$

where $\eta(^AZ)$ is the ratio of the alpha-capture rate to the photoalpha rate of (AZ),

$$\eta(^AZ) = \frac{\lambda_{\alpha\gamma}(^AZ)}{\lambda_{\gamma\alpha}(^AZ)}, \quad (18)$$

and where $r_{3\alpha}$ is the rate of the reaction $3\ ^4\text{He} \rightarrow ^{12}\text{C}$. The same equations may be solved for the concentrations of the light alpha-particle nuclei:

$$\begin{aligned} n(^{12}\text{C}) &= \frac{J + r_{3\alpha}}{\lambda_{\gamma\alpha}(^{12}\text{C})}, & n(^{16}\text{O}) &= \frac{J + \lambda_{\alpha\gamma}(^{12}\text{C})n(^{12}\text{C})}{\lambda_{\gamma\alpha}(^{16}\text{O})}, \\ n(^{20}\text{Ne}) &= \frac{J + \lambda_{\alpha\gamma}(^{16}\text{O})n(^{16}\text{O})}{\lambda_{\gamma\alpha}(^{20}\text{Ne})} \end{aligned} \quad (19)$$

These four equations give J , $n(^{12}\text{C})$, $n(^{16}\text{O})$, and $n(^{20}\text{Ne})$ in terms of the alpha-particle density n_{α} , the temperature, and the density of ^{24}Mg , which is in turn given by the density of ^{28}Si (eq. [13]). All reaction rates λ are taken from FCZ. This completes the prescription used for the calculation of the effective disintegration rate of ^{28}Si , which is equal to J , and of the concentrations of the light alpha-particle nuclei. It is this rate which controls the time scale for the conversion of ^{28}Si into heavier elements.

The constant-current hypothesis upon which the calculation is based is equivalent to assuming that the abundances of the light alpha-particle nuclei are constant. This assumption is of course not strictly correct, but it will be an excellent approximation to the extent that $J \gg dn/dt$. We now draw upon results of the final calculation to examine the validity of this assumption. Inspection of typical results of these calculations shows that ^{16}O is the most abundant of the nuclei ^{20}Ne , ^{16}O , and ^{12}C , and the condition for validity of our calculation becomes $J \gg dn(^{16}\text{O})/dt$. These two rates are compared in Figure 6 for a typical temperature and density. The condition is not fulfilled early in the burning when almost all the ^{28}Si remains, but it becomes increasingly better fulfilled as the burning proceeds. This and other results indicate that our calculations will be valid except for a brief initial period of time, which will be shown to have little effect on the total time required to burn a significant amount of ^{28}Si and will have virtually no effect on the nuclear abundances.

Further results of the final calculation can be used to obtain perspective on other qualitative features of this photodisintegration chain. In the region of interest for the present analysis ($T_9 = 3-5$, $\rho = 10^5-10^9\text{ g cm}^{-3}$, and the ^{28}Si reduced to not less than 5

per cent of its initial abundance) the rate $r_{3\alpha}$ is negligibly small. This fact is a consequence of reactions in nuclei above ^{28}Si , such as (α, γ) and (α, p) reactions, which remove free alpha particles before the alpha-particle density can approach equilibrium with ^{12}C . One can view the heavier nuclei as acting as alpha-particle absorbers. The low alpha-particle density forces the ^{12}C density to be small, and this condition of less-than-equilibrium concentration propagates upward to ^{20}Ne .

The ^{24}Mg achieves alpha-particle equilibrium with ^{28}Si throughout the region of interest primarily because the alpha-particle separation energies in both ^{28}Si and ^{24}Mg are unusually high. The high separation energy in ^{28}Si is responsible for the fact that the equilibrium ratio $n(^{24}\text{Mg})/n(^{28}\text{Si})$ is typically less than 10^{-3} , and the high separation energy in ^{24}Mg renders its photodisintegration rate sufficiently small that the ^{24}Mg can

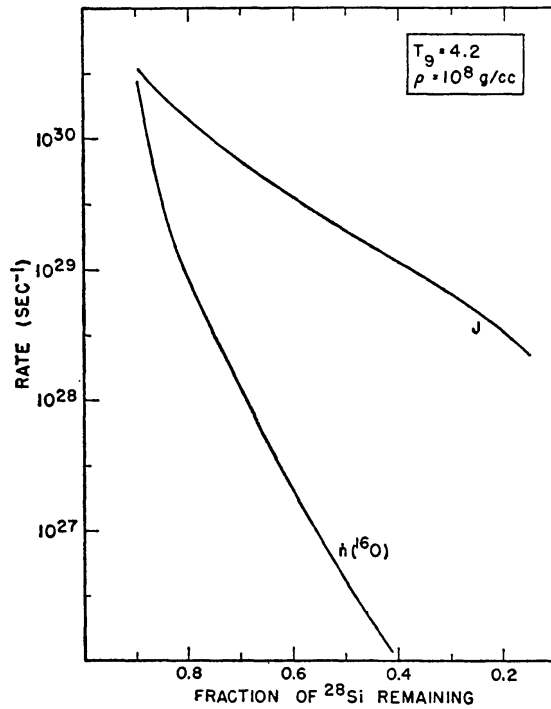


FIG. 6.—Examination of the extent to which the alpha-particle current J exceeds the rate of change of the abundance of ^{16}O , under typical conditions of ^{28}Si burning.

easily maintain its abundance at the equilibrium value. Thus, as mentioned above, the number of photodisintegrations per second, $n\lambda$, is much higher for ^{28}Si than for ^{24}Mg , even though $\lambda_{\gamma\alpha}(^{24}\text{Mg}) > \lambda_{\gamma\alpha}(^{28}\text{Si})$. The condition $\lambda_{\gamma\alpha}(^{28}\text{Si})n(^{28}\text{Si}) \gg J$ is easily satisfied, implying that equilibrium between ^{28}Si and ^{24}Mg is well achieved, whereas equilibrium between ^{24}Mg and ^{20}Ne may not be achieved.

Although the calculations of the present paper used the full expression for J (eq. [17]), it is interesting to note situations in which simpler relations give instructive approximations. At relatively low temperatures the product of n_α and $n(^{20}\text{Ne})$ is so small that there are no appreciable alpha-particle captures by ^{20}Ne , in which case $\eta(^{20}\text{Ne}) \approx 0$ and equation (17) reduces to

$$J \approx \lambda_{\gamma\alpha}(^{24}\text{Mg})n(^{24}\text{Mg}) . \tag{20}$$

Figure 7 displays the results of the final calculations (see § V) at $T_9 = 3.6$. It is seen here that J remains fairly close to the rate $\lambda_{\gamma\alpha}(^{24}\text{Mg})n(^{24}\text{Mg})$, confirming that alpha-particle capture in ^{20}Ne is relatively small. In other words, the ^{20}Ne concentration is well

below the value it would have in alpha-particle equilibrium with ^{24}Mg . The much larger rate for $^{20}\text{Ne}(\gamma, \alpha)^{16}\text{O}$ indicates that the equilibrium $^{20}\text{Ne} + \gamma \rightleftharpoons ^{16}\text{O} + ^4\text{He}$ has almost been established.

At higher temperatures the back current from $^{20}\text{Ne}(\alpha, \gamma)^{24}\text{Mg}$ becomes quite appreciable. Specific results at $T_9 = 4.4$ are displayed in Figure 8, which reveals an appreciable difference between J and $\lambda_{\gamma\alpha}(^{24}\text{Mg})n(^{24}\text{Mg})$ in the later stages of the burning. They differ by a factor of 6 when the ^{28}Si has been depleted to 5 per cent of its initial concentration. At that point the ^{20}Ne is nearly in alpha-particle equilibrium with ^{24}Mg , and a

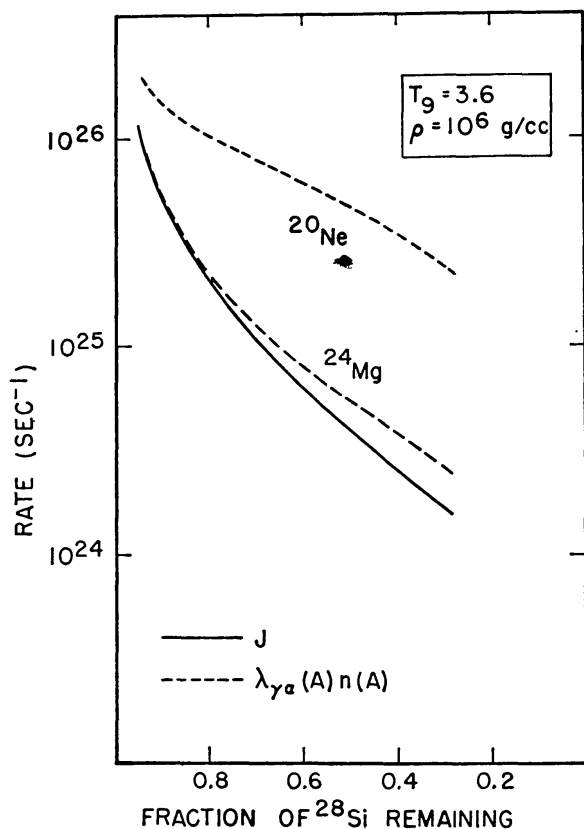


FIG. 7

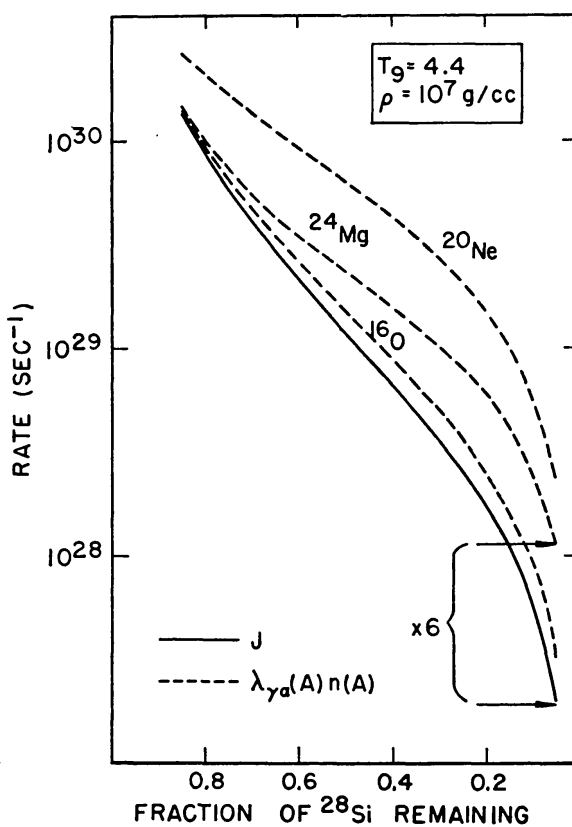


FIG. 8

FIG. 7.—Comparison of alpha-particle current J and photodisintegration rates λn under conditions of ^{28}Si burning where $J \simeq \lambda(^{24}\text{Mg})n(^{24}\text{Mg})$.

FIG. 8.—Comparison of alpha-particle current J and photodisintegration rates λn under conditions in which the back current from ^{20}Ne is important.

large departure from equilibrium does not occur until $^{16}\text{O} + \gamma \rightleftharpoons ^{12}\text{C} + ^4\text{He}$. We see that equation (20) is a poor approximation at temperatures as high as $T_9 = 4.4$. The value of $\lambda_{\gamma\alpha}(^{16}\text{O})$ replaces the value of $\lambda_{\gamma\alpha}(^{24}\text{Mg})$ as the most important rate in the determination of the photodisintegration flow at higher temperatures.

IV. METHOD OF CALCULATING QUASI-EQUILIBRIUM CONVERSION OF ^{28}Si

In this section we will outline the method used for calculating the quasi-equilibrium abundances and the method of determining the time scale for this conversion. The silicon-burning process could be calculated in the usual manner for studying a complex network of nuclear interactions, namely, by starting with the basic equations for the time rate of change of the abundance of each of the species:

$$dn(^AZ)/dt = R_+(^AZ) - R_-(^AZ), \quad (21)$$

where R_{\pm} are the production and destruction rates for nucleus (AZ) due to all relevant nuclear interactions. Integration of such a system of equations yields a self-consistent set of abundances as a function of time. TCG have integrated these equations numerically for two sets of conditions: $T_9 = 3$, $\rho = 10^6 \text{ g cm}^{-3}$, and $T_9 = 5$, $\rho = 10^7 \text{ g cm}^{-3}$. This is the most obvious way to handle the problem and the only one valid in some circumstances.

For a wide range of circumstances, however, the abundances are quasi-static in the sense that the time derivative in equation (21) is a small difference between two large and nearly equal numbers. In this case, the system of equations reduces to a simultaneous set of homogeneous linear algebraic equations, which implies that the abundance ratios are determined algebraically. It is then possible to determine the value of each by normalizing their sum to a desired density. In this section we present the numerical technique for evolving the abundances with the quasi-equilibrium assumption. We limit ourselves to the problem of silicon burning at constant density and temperature, as a first step toward the understanding of the probable situation in real stars.

The number densities $n({}^AZ)$ of nuclei in equilibrium with ${}^{28}\text{Si}$ are given by equations (3) and (8). Conservation of baryons and of charge impose two constraints upon the system:

1. The total number of nucleons, N_B , is constant; it is conveniently written as³

$$N_B = n_p + n_n + 4n_a + L + \sum_{A \geq 24} A n({}^AZ) \quad (22)$$

where

$$L = 12n({}^{12}\text{C}) + 16n({}^{16}\text{O}) + 20n({}^{20}\text{Ne}) \quad (23)$$

is the density of nucleons in those light nuclei which have appreciable abundances. These nuclei are generally not in equilibrium with ${}^{28}\text{Si}$, and their number densities are found from equation (18). The sum in the final term is over nuclei that do participate in the equilibrium, and their number densities are found from equation (3).

2. The number of free protons is related to the number of free neutrons by the expression

$$n_p = n_n + \Sigma(N - Z)n({}^AZ) - 2D, \quad (24)$$

where $2D$ is the total neutron excess of the gas. (When no limits are listed in a summation, the summation is to be taken over all nuclei of the calculation, namely, ${}^4\text{He}$, ${}^{12}\text{C}$, ${}^{16}\text{O}$, ${}^{20}\text{Ne}$, and the nuclei listed in Table 1. These represent the nuclei with appreciable abundances.) In a case like the present, where $Z/\bar{N} = 1$ initially, D is the net number of beta-decay and electron-capture events in which protons change to neutrons:

$$\frac{dD}{dt} = \Sigma n({}^AZ)[\lambda^{\beta^+}({}^AZ) + \lambda^{\text{ec}}({}^AZ) - \lambda^{\beta^-}({}^AZ)]. \quad (25)$$

In our numerical work we have used the extensive tables prepared by Hansen (1966) for the rates $\lambda({}^AZ)$.

The ${}^{28}\text{Si}$ is photodisintegrated at the rate J given in equation (17). The product $28J$ is therefore equal to the rate at which nucleons appear in the form of increased abundances of all nuclei other than ${}^{28}\text{Si}$. Thus

$$28J = \frac{dn_n}{dt} + \frac{dn_p}{dt} + 4 \frac{dn_a}{dt} + \sum_{A=12}^{27} A \frac{dn({}^AZ)}{dt} + \sum_{A \geq 29} (A - 28) \frac{dn({}^AZ)}{dt}. \quad (26)$$

³ In this equation and elsewhere A has its common meaning of atomic mass number. This is to be distinguished from our use of $A({}^AZ)$ for the atomic mass in amu.

With the aid of equation (22), this statement can be reduced to

$$J = - \sum_{A \geq 28} dn(^AZ)/dt \equiv -dS/dt, \quad (27)$$

where S is defined to be the sum of the concentrations of all nuclei having atomic weights greater than or equal to 28:

$$S = \sum_{A \geq 28} n(^AZ). \quad (28)$$

The evolution of the abundance distribution as a function of time is followed by obtaining a series of quasi-equilibrium distributions at discrete time steps, which are labeled by the subscript k . For instance, $n(^AZ)_k$ represents the concentration $n(^AZ)$ at the time $t = t_k$. Equation (27) is used to calculate the time elapsed between the k th distribution, where $S = S_k$, and the previous one, where $S = S_{k-1}$. The difference $(\Delta S)_k = S_k - S_{k-1}$ is related to the time by

$$t_k = t_{k-1} - \frac{(\Delta S)_k}{\langle J \rangle_k}, \quad (29)$$

where $\langle J \rangle_k$ is an appropriate average value of $J(t)$ between t_{k-1} and t_k . The proper average depends upon the functional form of $J(t)$; because we found that $J(t)$ generally decreased in a roughly exponential manner, we have taken $\langle J \rangle_k$ to be

$$\langle J \rangle_k = \frac{J_{k-1} - J_k}{\ln (J_{k-1}/J_k)}, \quad (30)$$

which is exact for an exponential dependence.

This prescription does not define $\langle J \rangle$ during the first time interval, during which the distribution changes from pure ^{28}Si to the first quasi-equilibrium distribution. However, a crude approximation to $\langle J \rangle_1$ suffices because the distribution initially changes with such rapidity that the time required to burn a small fraction of the ^{28}Si , say 10 per cent, is very much less than the time required to burn a substantial fraction, say 50 per cent. Thus an error in the initial time step eventually becomes a negligible error in the total elapsed time. We have found the approximation $\langle J \rangle_1 = 2J_1$ to be adequate for the first time interval, in which case we have

$$t_1 = - \frac{S_1 - N_B/28}{2J_1} \quad (31)$$

and equation (29) thereafter.

The increment in the number of proton-to-neutron transitions during the time interval $(\Delta t)_k$ has been calculated using a simple average of the abundances:

$$(\Delta D)_k = (\Delta t)_k \Sigma \frac{n(^AZ)_k + n(^AZ)_{k-1}}{2} [\lambda^{\beta^+}(^AZ) + \lambda^{\text{ec}}(^AZ) - \lambda^{\beta^-}(^AZ)], \quad (32)$$

and the accumulated number of transitions is

$$D_k = \sum_{\nu=1}^k (\Delta D)_\nu.$$

Before specifying in detail the manner in which the preceding equations are employed to calculate the abundance distributions, we will summarize the spirit of the procedure. For a selected temperature (T) and density (ρ or, equivalently, N_B) the silicon conversion is followed through a discrete succession of quasi-equilibrium solutions, each charac-

terized by a certain remaining mass fraction of ^{28}Si ($f = 28n(^{28}\text{Si})/N_B$) and a certain neutron excess ($2D$). As the ^{28}Si is consumed, f decreases and D increases. At each step in the succession, the quasi-equilibrium distribution is calculated through an iterative procedure in which T and N_B are specified constants, f assumes a value chosen for convenience, and D assumes a value dictated by the time scale and decay rates. Trial values of the alpha-particle and proton densities (and hence neutron density) are chosen and then readjusted in an iterative cycle until (a) the quasi-equilibrium abundances are consistent with the specified value of N_B and (b) the neutron excess equals $2D$. The inclusion of beta decays in the time evolution entails an appreciable complication because the value of $(\Delta D)_k$ is not known until the values of $n(^A Z)$ have been determined, but those values in turn depend upon D_k . Therefore, the iterative procedure must readjust $(\Delta t)_k$ and $(\Delta D)_k$ until a self-consistent solution is found.

The detailed procedure, for given values of T , N_B , and f , is as follows:

- a) Pick trial values of n_a , n_p , n_n , L , and D , where n_n is related to n_a and n_p by equation (8).
- b) Calculate $n(^{28}\text{Si})$ from equation (22) by expressing $n(^A Z)$ in terms of $n(^{28}\text{Si})$, n_a , n_p , and n_n , with the aid of equation (3) and factoring $n(^{28}\text{Si})$ out of the summation. This value of $n(^{28}\text{Si})$ will not generally equal the desired silicon mass fraction f .
- c) Readjust n_a to make $n(^{28}\text{Si})$ conform more closely to the desired value of f .
- d) Solve equation (24) for n_p with the aid of the equilibrium relations (3) and (8).
- e) Calculate n_n from equation (8).
- f) Recalculate $n(^{28}\text{Si})$ as in (b).
- g) Calculate $n(^A Z)$ from the latest values of $n(^{28}\text{Si})$, n_a , n_p , and n_n .
- h) Calculate S from equation (28).
- i) Calculate J and $\langle J \rangle$ from equations (17) and (30).
- j) Calculate L from equations (19) and (23).
- k) Calculate Δt from equation (29) or equation (31).
- l) Calculate D from equation (32).
- m) Return to step a, using the latest values of n_a , n_p , n_n , L , and D as the new trial values.
- n) Repeat the cycle until satisfactory convergence is reached. We have adopted the criterion that the mean of the absolute value of the change in $\log n(^A Z)$ (i.e., $\langle |\Delta \log n(^A Z)| \rangle$) must be less than 0.001. At this point a self-consistent set of quasi-equilibrium abundances has been obtained.
- o) Advance to the next value of the silicon mass fraction f and repeat the procedure.

This particular iterative procedure did not always bring rapid convergence, and in some cases diverging or oscillating solutions were encountered. Such difficulties frequently could be eliminated by bypassing some of the iterative steps. If convergence had not been achieved after eight cycles, the readjustment of n_a , step c above, was dropped. This introduces no error, but f no longer is held at the preset value. If after two more cycles convergence still had not been attained, steps h through l were omitted and the quantities S , J , L , Δt , and D were left frozen at their previous values. If this process brought convergence in $n(^A Z)$ within five more cycles, the abundances were recorded and new values of S , J , L , Δt , and D were calculated from them. The differences between the new and "frozen" values were examined to test the internal consistency of the calculation; small shifts (< 5 per cent) were accepted. Finally, if no convergence had been reached at this point, the calculation at this temperature and density was terminated, and the results for this last case were discarded.

We have found that this particular iteration procedure converges well if the temperature is not too low, if f is not too low, and if ρ is not too high. When these conditions are not met, the above algorithm cannot be cured by minor modifications. It has been constructed on the supposition that n_a rises monotonically as f decreases—a supposition that is incorrect for burning times long enough for significant beta decays (and electron

captures) to have occurred. For substantial beta decay, the chief abundances transfer to the neutron-rich nuclei such as ^{54}Fe , and even later to ^{56}Fe , at which time n_α and n_p/n_n begin to decrease as f decreases. In other words, the iteration is inappropriate whenever the conversion has substantially switched from region A toward region B of Figure 2. At each temperature and density, this iteration scheme is successful down to a minimum silicon mass fraction f_{\min} (no attempt was made to carry f below 0.05, although in many cases this would have been possible). Values of f_{\min} , for various temperatures and densities, are presented in Table 3. To pursue the burning to smaller values of f would require a different iteration scheme. In the present work, however, we limit ourselves to solutions near region A , where the computational program is adequate.

TABLE 3
MINIMUM VALUES OF THE FRACTION OF ^{28}Si REMAINING
FOR SATISFACTORY CONVERGENCE*

TEMPERATURE (T_9)	DENSITY (g cm^{-3})				
	10^5	10^6	10^7	10^8	10^9
3.4.....	0.47	0.52	0.62
3.6.....	.17	.28	.44	0.61
3.8.....	.05	.05	.19	.45	0.65
4.0.....	.05	.05	.05	.29	.54
4.2.....05	.05	.15	.45
4.4.....	.05	.05	.05	.05	.27
4.6.....	0.05	.05	.05	.05	.15
4.8.....05	.05	.05	.05
5.0.....	0.05	0.05	0.05	0.05

* No attempt was made to carry the calculation below $f=0.05$, even in the many cases where convergence might have been achieved for $f<0.05$.

V. EVOLUTION OF ABUNDANCES DURING ^{28}Si BURNING

The raw results of the calculations we have carried out on ^{28}Si burning consist of computer outputs in which the following quantities, among others, are listed at successively decreasing values of the ^{28}Si concentration (typically at $f = 0.95, 0.85, \dots, 0.05$): elapsed time; $n_\alpha, n_p, n_n, n(^A Z)$ for all nuclei listed in Table 1 and for the light alpha-particle nuclei (^{12}C , ^{16}O , and ^{20}Ne); \bar{Z}/\bar{N} ; D ; J ; $\lambda_{\alpha\gamma}(^A Z)n(^A Z)$ and $\lambda_{\gamma\alpha}(^A Z)n(^A Z)$ for the light alpha-particle nuclei; the energy release due to the change in total rest mass of the nuclei; the fractional contributions of individual nuclei to the beta-decay rates; and quantities bearing on the convergence of the iteration procedure. Some of these numerical results are presented in Table 4.

In the present section we summarize the main features of the results. We are especially interested in considering the following aspects: (a) the time scale of the conversion; (b) the role of electron capture and beta decay; (c) the abundances during the conversion; and (d) a comparison with the natural abundances.

a) Time Scale for the Conversion of ^{28}Si

The ^{28}Si conversion times are strongly temperature-dependent. Typical results are displayed in Figure 9, where the time required to burn 65 per cent of the ^{28}Si is plotted as a function of temperature. The required time falls from $t = 1000$ sec at $T_9 = 3.6$ to $t = 0.003$ sec at $T_9 = 5.0$, both at $\rho = 10^7$ g cm^{-3} , reflecting the strong temperature dependence of the photodisintegration rates (see § III).

TABLE 4
RESULTS OF THE SILICON-BURNING CALCULATION: TIME SCALE, KEY
ABUNDANCES, BETA DECAYS, NUCLEAR ENERGY GENERATION

TABLE 4.01 $\rho = 1.0 \times 10^6 \text{ gm cm}^{-3}$

	$T_9 = 3.0$									
	1	2	3	4	5	6	7	8	9	10
k	0.910	0.880	0.850	0.821	0.799					
f^*	4.296	4.618	4.904	5.152	5.321					
$\log t^\dagger$	6.288	6.355	6.420	6.360	6.230					
$\log n_p/n_n$	22.844	22.907	22.959	22.940	22.878					
$\log n_p$	16.556	16.552	16.539	16.580	16.648					
$\log n_n$	22.547	22.664	22.743	22.786	22.798					
$\log n_\alpha$	28.292	28.277	28.262	28.247	28.235					
$\log n(^{28}\text{Si})$	25.128	25.811	26.245	26.566	26.764					
$\log n(^{54}\text{Fe})$	21.777	22.586	23.124	23.406	23.481					
$\log n(^{56}\text{Ni})$	4.389	3.856	3.462	3.150	2.957					
$-(\log d)^\ddagger$	11.339	11.061	10.990	10.948	10.927					
$\log \epsilon_\S$	4.5	7.1	11.0	16.6	22.5					
q^\parallel										

TABLE 4.02 $\rho = 1.0 \times 10^5 \text{ gm cm}^{-3}$

	$T_9 = 3.4$									
	1	2	3	4	5	6	7	8	9	10
k	0.950	0.900	0.850	0.800	0.750					
f^*	0.984	1.539	1.960	2.282	2.552					
$\log t^\dagger$	5.715	5.950	6.400	6.858	7.234					
$\log n_p/n_n$	24.313	24.510	24.782	25.045	25.259					
$\log n_p$	18.597	18.560	18.382	18.187	18.025					
$\log n_n$	23.729	24.049	24.237	24.372	24.476					
$\log n_\alpha$	27.310	27.287	27.262	27.236	27.208					
$\log n(^{28}\text{Si})$	21.747	23.565	24.314	24.705	24.983					
$\log n(^{54}\text{Fe})$	18.742	20.955	22.247	23.164	23.870					
$\log n(^{56}\text{Ni})$	6.950	6.062	5.426	4.900	4.438					
$-(\log d)^\ddagger$	14.237	13.962	13.620	13.388	13.217					
$\log \epsilon_\S$	1.7	4.1	6.5	9.1	11.9					
q^\parallel										

TABLE 4—Continued

$T_g = 3.4$ $\rho = 1.0 \times 10^6 \text{ gm cm}^{-3}$

	1	2	3	4	5	6	7	8	9	10
k	0.950	0.900	0.850	0.800	0.750	0.700	0.650	0.600	0.551	0.523
f^*	0.988	1.537	1.945	2.259	2.527	2.776	3.021	3.262	3.482	3.601
$\log t^{\dagger}$	6.598	6.697	6.992	7.363	7.656	7.840	7.906	7.862	7.733	7.607
$\log n_p/n_n$	24.755	24.885	25.079	25.299	25.472	25.586	25.635	25.624	25.567	25.506
$\log n_p$	18.158	18.187	18.087	17.936	17.816	17.745	17.729	17.763	17.835	17.900
$\log n_n$	23.735	24.053	24.243	24.379	24.486	24.570	24.636	24.683	24.713	24.721
$\log n_{\alpha}$	28.310	28.287	28.262	28.236	28.208	28.178	28.146	28.111	28.074	28.051
$\log n(^{28}\text{Si})$	21.903	23.848	24.759	25.250	25.622	25.958	26.287	26.603	26.887	27.044
$\log n(^{54}\text{Fe})$	19.783	21.987	23.287	24.218	24.935	25.498	25.926	26.221	26.392	26.426
$\log n(^{56}\text{Ni})$	6.575	5.725	5.149	4.666	4.233	3.835	3.464	3.122	2.831	2.686
$-(\log d)^{\ddagger}$	14.295	13.986	13.662	13.456	13.305	13.195	13.115	13.054	13.007	12.987
$\log \epsilon^{\S}$	2.0	4.5	7.0	9.8	13.0	17.2	23.4	32.5	45.2	54.8
q^{\parallel}										

$T_g = 3.4$ $\rho = 1.0 \times 10^7 \text{ gm cm}^{-3}$

	1	2	3	4	5	6	7	8	9	10
k	0.950	0.900	0.850	0.800	0.750	0.700	0.650	0.616	0.587	0.560
f^*	0.989	1.537	1.943	2.257	2.528	2.786	3.054	3.244	3.444	3.560
$\log t^{\dagger}$	7.315	7.040	7.143	7.440	7.661	7.743	7.642	7.438	7.236	7.080
$\log n_p/n_n$	25.114	25.056	25.155	25.338	25.475	25.536	25.500	25.402	25.300	25.220
$\log n_p$	17.799	18.016	18.012	17.898	17.814	17.793	17.858	17.965	18.060	18.140
$\log n_n$	23.736	24.054	24.243	24.380	24.486	24.568	24.625	24.644	24.620	24.580
$\log n_{\alpha}$	29.310	29.287	29.262	29.236	29.208	29.178	29.146	29.122	29.090	29.060
$\log n(^{28}\text{Si})$	22.195	24.510	25.613	26.178	26.617	27.040	27.480	27.782	27.950	28.000
$\log n(^{54}\text{Fe})$	20.793	22.992	24.292	25.222	25.936	26.482	26.850	26.957	26.948	26.880
$\log n(^{56}\text{Ni})$	6.179	5.410	4.938	4.513	4.098	3.676	3.236	2.948	2.700	2.580
$-(\log d)^{\ddagger}$	14.308	13.991	13.669	13.470	13.325	13.224	13.168	13.149	13.130	13.110
$\log \epsilon^{\S}$	2.1	4.6	7.1	10.0	13.4	18.1	26.1	35.2	45.2	54.8
q^{\parallel}										

TABLE 4—Continued

TABLE 4.05

$T_9 = 3.6$

$\rho = 1.0 \times 10^5 \text{ gm cm}^{-3}$

k	1	2	3	4	5	6	7	8	9	10
f^*	0.950	0.850	0.750	0.650	0.550	0.450	0.350	0.248	0.172	
$\log t^\dagger$	-0.157	0.714	1.376	1.852	2.259	2.623	2.949	3.256	3.486	
$\log n_p/n_n$	5.017	5.598	6.399	6.977	7.369	7.606	7.701	7.648	7.477	
$\log n_p$	24.721	25.141	25.600	25.927	26.150	26.287	26.349	26.334	26.255	
$\log n_n$	19.704	19.543	19.201	18.950	18.781	18.682	18.648	18.686	18.778	
$\log n_\alpha$	24.317	24.834	25.069	25.221	25.329	25.405	25.462	25.507	25.533	
$\log n(^{28}\text{Si})$	27.310	27.262	27.208	27.146	27.073	26.986	26.877	26.727	26.569	
$\log n(^{54}\text{Fe})$	21.805	24.536	25.209	25.560	25.793	25.967	26.132	26.329	26.512	
$\log n(^{56}\text{Ni})$	18.529	22.098	23.690	24.696	25.374	25.823	26.112	26.278	26.303	
$-(\log d)^\ddagger$	7.900	6.529	5.492	4.712	4.046	3.469	2.978	2.554	2.273	
$\log \epsilon^\S$	15.064	14.982	14.353	13.989	13.817	13.736	13.667	13.576	13.468	
q^\parallel	0.8	5.3	9.6	14.4	21.9	35.3	57.9	93.6	131.7	

TABLE 4.06

$T_9 = 3.6$

$\rho = 1.0 \times 10^6 \text{ gm cm}^{-3}$

k	1	2	3	4	5	6	7	8	9	10
f^*	0.950	0.850	0.750	0.650	0.550	0.450	0.345	0.281	0.205	
$\log t^\dagger$	-0.150	0.691	1.320	1.803	2.252	2.653	3.006	3.200	3.343	
$\log n_p/n_n$	5.903	6.361	7.151	7.734	8.034	8.039	7.838	7.643	7.477	
$\log n_p$	25.168	25.526	25.982	26.313	26.490	26.509	26.420	26.328	26.255	
$\log n_n$	19.265	19.164	18.831	18.579	18.456	18.470	18.583	18.685	18.778	
$\log n_\alpha$	24.333	24.847	25.092	25.252	25.358	25.427	25.473	25.492	25.533	
$\log n(^{28}\text{Si})$	28.310	28.262	28.208	28.146	28.073	27.986	27.871	27.782	27.685	
$\log n(^{54}\text{Fe})$	22.021	24.861	25.605	26.000	26.321	26.675	27.061	27.288	27.468	
$\log n(^{56}\text{Ni})$	19.638	23.194	24.849	25.907	26.582	26.975	27.183	27.224	27.255	
$-(\log d)^\ddagger$	7.544	6.229	5.217	4.399	3.681	3.099	2.637	2.405	2.273	
$\log \epsilon^\S$	15.329	15.066	14.510	14.202	14.016	13.982	13.753	13.648	13.576	
q^\parallel	1.6	6.6	12.0	19.0	31.4	52.8	85.9	112.1	131.7	

TABLE 4—Continued

TABLE 4.07

$T_9 = 3.6$ $\rho = 1.0 \times 10^7 \text{ gm cm}^{-3}$

	1	2	3	4	5	6	7	8	9	10
k	0.950	0.850	0.750	0.650	0.550	0.442				
f^*	-0.146	0.688	1.305	1.793	2.266	2.707				
$\log t^\dagger$	6.783	7.062	7.683	8.076	7.993	7.592				
$\log n_p/n_n$	25.609	25.877	26.249	26.485	26.469	26.282				
$\log n_p$	18.826	18.815	18.566	18.410	18.476	18.690				
$\log n_\alpha$	24.337	24.850	25.097	25.257	25.358	25.410				
$\log n(^{28}\text{Si})$	29.310	29.262	29.208	29.146	29.073	28.978				
$\log n(^{54}\text{Fe})$	22.169	25.181	26.106	26.695	27.357	28.004				
$\log n(^{56}\text{Ni})$	20.668	24.216	25.884	26.946	27.576	27.848				
$-(\log d)^\ddagger$	7.082	5.826	4.885	4.081	3.321	2.673				
$\log \epsilon_\S$	15.372	15.079	14.549	14.262	14.081	13.963				
q^\parallel	1.7	6.9	12.5	20.5	37.7	66.6				

TABLE 4.08

$T_9 = 3.6$ $\rho = 1.0 \times 10^8 \text{ gm cm}^{-3}$

	1	2	3	4	5	6	7	8	9	10
k	0.950	0.900	0.850	0.800	0.750	0.700	0.650	0.613		
f^*	-0.146	0.358	0.765	1.081	1.349	1.602	1.868	2.082		
$\log t^\dagger$	7.303	7.141	7.065	7.262	7.466	7.536	7.397	7.135		
$\log n_p/n_n$	25.869	25.869	25.878	26.011	26.140	26.196	26.142	26.017		
$\log n_p$	18.566	18.728	18.814	18.749	18.674	18.661	18.746	18.882		
$\log n_\alpha$	24.338	24.660	24.851	24.988	25.095	25.181	25.243	25.267		
$\log n(^{28}\text{Si})$	30.310	30.287	30.262	30.236	30.208	30.178	30.146	30.120		
$\log n(^{54}\text{Fe})$	22.654	24.891	26.179	26.847	27.314	27.769	28.280	28.670		
$\log n(^{56}\text{Ni})$	21.673	23.909	25.216	26.151	26.875	27.443	27.845	27.986		
$-(\log d)^\ddagger$	6.357	5.619	5.151	4.762	4.361	3.916	3.412	3.037		
$\log \epsilon_\S$	15.382	15.212	14.847	14.632	14.472	14.354	14.288	14.270		
q^\parallel	1.8	4.4	7.0	9.8	12.9	17.1	23.9	32.9		

TABLE 4—Continued

$T_g = 3.8$ $\rho = 1.0 \times 10^5 \text{ gm cm}^{-3}$

	1	2	3	4	5	6	7	8	9	10
k	0.950	0.850	0.750	0.650	0.550	0.450	0.350	0.250	0.150	0.050
f^*	-1.164	-0.346	0.368	0.842	1.227	1.568	1.885	2.195	2.528	2.982
$\log t^\dagger$	4.390	4.866	5.561	6.095	6.485	6.771	6.980	7.132	7.226	7.206
$\log n_p/n_n$	25.080	25.453	25.858	26.161	26.383	26.546	26.668	26.758	26.821	26.833
$\log n_p$	20.690	20.587	20.297	20.067	19.898	19.776	19.688	19.627	19.595	19.627
$\log n_n$	24.817	25.358	25.586	25.733	25.839	25.920	25.987	26.047	26.108	26.196
$\log n_\alpha$ (^{28}Si)	27.310	27.262	27.208	27.146	27.073	26.986	26.877	26.731	26.508	26.031
$\log n$ (^{54}Fe)	21.683	24.672	25.410	25.764	25.991	26.150	26.266	26.355	26.437	26.548
$\log n$ (^{56}Ni)	18.145	21.881	23.427	24.388	25.059	25.545	25.904	26.174	26.381	26.516
$-(\log d)^\ddagger$	8.736	7.448	6.403	5.683	5.088	4.584	4.085	3.631	3.166	2.594
$\log \epsilon^\S$	16.216	15.920	15.183	14.698	14.462	14.390	14.324	14.204	14.034	13.759
q^\parallel	-1.2	2.1	5.1	7.5	10.5	15.6	24.3	37.5	57.7	94.7

$T_g = 3.8$ $\rho = 1.0 \times 10^6 \text{ gm cm}^{-3}$

	1	2	3	4	5	6	7	8	9	10
k	0.950	0.850	0.750	0.650	0.550	0.450	0.350	0.250	0.150	0.052
f^*	-1.151	-0.379	0.286	0.776	1.213	1.610	1.963	2.289	2.622	3.047
$\log t^\dagger$	5.264	5.664	6.398	6.997	7.417	7.684	7.831	7.866	7.752	7.331
$\log n_p/n_n$	25.527	25.859	26.287	26.626	26.864	27.017	27.105	27.136	27.092	26.897
$\log n_p$	20.263	20.196	19.889	19.629	19.447	19.333	19.275	19.270	19.340	19.566
$\log n_n$	24.857	25.386	25.629	25.788	25.898	25.977	26.037	26.088	26.139	26.203
$\log n_\alpha$ (^{28}Si)	28.310	28.262	28.208	28.146	28.073	27.986	27.877	27.731	27.509	27.049
$\log n$ (^{54}Fe)	22.067	25.062	25.850	26.220	26.448	26.603	26.736	26.888	27.113	27.490
$\log n$ (^{56}Ni)	19.424	23.082	24.726	25.775	26.478	26.940	27.249	27.462	27.598	27.586
$-(\log d)^\ddagger$	8.399	7.175	6.146	5.344	4.636	4.023	3.509	3.062	2.639	2.176
$\log \epsilon^\S$	15.982	16.161	15.515	15.155	14.926	14.758	14.598	14.424	14.217	13.911
q^\parallel	0.7	5.9	11.0	17.0	26.1	40.5	61.5	89.7	128.0	186.6

TABLE 4—Continued

TABLE 4.11

$T_9 = 3.8$ $\rho = 3.1 \times 10^6 \text{ gm cm}^{-3}$

k	1	2	3	4	5	6	7	8	9	10
f^*	0.950	0.850	0.750	0.650	0.550	0.450	0.350	0.250	0.149	
$\log t^\dagger$	-1.147	-0.383	0.267	0.756	1.207	1.619	1.978	2.306	2.636	
$\log n_p/n_n$	5.709	6.055	6.761	7.369	7.783	8.002	8.038	7.900	7.592	
$\log n_p$	25.751	26.056	26.470	26.815	27.049	27.178	27.210	27.153	27.010	
$\log n_n$	20.042	20.001	19.709	19.446	19.267	19.176	19.173	19.253	19.418	
$\log n_\alpha$	24.864	25.391	25.636	25.798	25.909	25.986	26.042	26.089	26.133	
$\log n(^{28}\text{Si})$	28.802	28.754	28.699	28.637	28.564	28.477	28.368	28.222	27.996	
$\log n(^{54}\text{Fe})$	22.159	25.192	26.025	26.403	26.640	26.833	27.058	27.355	27.721	
$\log n(^{56}\text{Ni})$	19.963	23.606	25.267	26.335	27.041	27.492	27.781	27.963	28.044	
$-(\log d)^\ddagger$	8.194	6.993	5.986	5.168	4.424	3.784	3.261	2.818	2.412	
$\log \epsilon^\S$	16.126	16.183	15.561	15.220	14.986	14.806	14.641	14.467	14.261	
q^\parallel	1.0	6.4	11.8	18.4	28.9	45.7	70.0	102.5	146.0	

TABLE 4.12

$T_9 = 3.8$ $\rho = 1.0 \times 10^7 \text{ gm cm}^{-3}$

k	1	2	3	4	5	6	7	8	9	10
f^*	0.950	0.850	0.750	0.650	0.550	0.450	0.350	0.245	0.193	
$\log t^\dagger$	-1.144	-0.384	0.256	0.745	1.205	1.626	1.990	2.325	2.484	
$\log n_p/n_n$	6.162	6.455	7.111	7.709	8.069	8.120	7.907	7.553	7.297	
$\log n_p$	25.979	26.257	26.646	26.986	27.194	27.238	27.144	26.977	26.852	
$\log n_n$	19.817	19.802	19.535	19.277	19.125	19.118	19.237	19.424	19.555	
$\log n_\alpha$	24.867	25.393	25.640	25.802	25.913	25.988	26.039	26.078	26.090	
$\log n(^{28}\text{Si})$	29.310	29.262	29.208	29.146	29.073	28.986	28.876	28.721	28.619	
$\log n(^{54}\text{Fe})$	22.238	25.315	26.206	26.604	26.894	27.239	27.678	28.130	28.359	
$\log n(^{56}\text{Ni})$	20.497	24.130	25.801	26.878	27.583	28.017	28.268	28.386	28.364	
$-(\log d)^\ddagger$	7.940	6.759	5.776	4.948	4.166	3.495	2.956	2.503	2.310	
$\log \epsilon^\S$	16.184	16.191	15.584	15.255	15.022	14.842	14.683	14.525	14.423	
q^\parallel	1.1	6.6	12.1	19.1	30.5	49.4	77.1	116.5	142.2	

TABLE 4—Continued

TABLE 4.13		$T_9 = 3.8$										$\rho = 1.0 \times 10^8 \text{ gm cm}^{-3}$									
		1	2	3	4	5	6	7	8	9	10	1	2	3	4	5	6	7	8	9	10
k		0.950	0.850	0.750	0.650	0.550	0.454														
f^*		-1.143	-0.384	0.250	0.743	1.228	1.650														
$\log t^\dagger$		6.864	7.047	7.504	7.854	7.652	7.162														
$\log n_p/n_n$		26.330	26.553	26.843	27.059	26.983	26.750														
$\log n_p$		19.466	19.506	19.339	19.205	19.332	19.587														
$\log n_\alpha$		24.870	25.395	25.642	25.804	25.906	25.951														
$\log n(^{28}\text{Si})$		30.310	30.262	30.208	30.146	30.073	29.990														
$\log n(^{54}\text{Fe})$		22.551	25.732	26.825	27.468	28.264	28.959														
$\log n(^{56}\text{Ni})$		21.513	25.140	26.814	27.887	28.533	28.760														
$-(\log d)^\ddagger$		7.133	5.991	5.077	4.244	3.376	2.697														
$\log \epsilon_\S$		16.222	16.196	15.601	15.293	15.096	14.989														
q^\parallel		1.2	6.8	12.4	20.1	34.8	62.9														
TABLE 4.14		$T_9 = 3.8$										$\rho = 1.0 \times 10^9 \text{ gm cm}^{-3}$									
		1	2	3	4	5	6	7	8	9	10	1	2	3	4	5	6	7	8	9	10
k		0.950	0.850	0.750	0.648	0.550	0.448														
f^*		-1.143	-0.383	0.271	0.855	1.337	1.768														
$\log t^\dagger$		6.937	6.535	6.705	6.511	6.111	5.511														
$\log n_p/n_n$		26.367	26.297	26.442	26.378	26.378	26.378														
$\log n_p$		19.430	19.762	19.737	19.868	19.868	19.868														
$\log n_\alpha$		24.870	25.394	25.636	25.768	25.768	25.768														
$\log n(^{28}\text{Si})$		31.310	31.262	31.208	31.144	31.144	31.144														
$\log n(^{54}\text{Fe})$		23.479	27.238	28.586	29.579	29.579	29.579														
$\log n(^{56}\text{Ni})$		22.514	26.133	27.773	28.637	28.637	28.637														
$-(\log d)^\ddagger$		5.927	4.888	4.047	3.103	2.257	1.514														
$\log \epsilon_\S$		16.231	16.200	15.631	15.429	15.231	15.144														
q^\parallel		1.3	6.9	13.3	28.0	48.0	82.0														

TABLE 4—Continued

TABLE 4.15

$T_g = 4.0$ $\rho = 1.0 \times 10^5 \text{ gm cm}^{-3}$

	1	2	3	4	5	6	7	8	9	10
k	0.950	0.850	0.750	0.650	0.550	0.450	0.350	0.250	0.150	0.050
f^*	-2.064	-1.360	-0.553	-0.077	0.289	0.606	0.904	1.202	1.534	2.008
$\log t^\dagger$	3.812	4.206	4.773	5.238	5.593	5.870	6.088	6.264	6.405	6.506
$\log n_p/n_n$	25.381	25.730	26.070	26.338	26.541	26.699	26.826	26.930	27.018	27.093
$\log n_p$	21.570	21.525	21.297	21.100	20.948	20.830	20.738	20.666	20.613	20.587
$\log n_\alpha$	25.201	25.810	26.036	26.175	26.277	26.358	26.428	26.493	26.561	26.661
$\log n(^{28}\text{Si})$	27.310	27.262	27.208	27.146	27.073	26.986	26.877	26.731	26.509	26.028
$\log n(^{54}\text{Fe})$	21.147	24.661	25.507	25.884	26.120	26.287	26.414	26.513	26.592	26.658
$\log n(^{56}\text{Ni})$	17.325	21.538	23.064	23.976	24.617	25.102	25.483	25.790	26.044	26.261
$-(\log d)^\ddagger$	9.504	8.348	7.231	6.568	6.048	5.597	5.180	4.769	4.328	3.736
$\log \epsilon_\S$	17.776	15.499	14.331	15.225	15.102	14.776	13.791	14.107	14.146	13.608
q^\parallel	-5.3	-5.2	-5.3	-6.3	-7.7	-9.0	-9.2	-8.2	-5.5	-2.7

TABLE 4.16

$T_g = 4.0$ $\rho = 1.0 \times 10^6 \text{ gm cm}^{-3}$

	1	2	3	4	5	6	7	8	9	10
k	0.950	0.850	0.750	0.650	0.550	0.450	0.350	0.250	0.150	0.050
f^*	-2.033	-1.379	-0.644	-0.140	0.288	0.675	1.028	1.364	1.717	2.120
$\log t^\dagger$	4.686	5.038	5.690	6.255	6.671	6.967	7.175	7.322	7.418	7.418
$\log n_p/n_n$	25.844	26.161	26.547	26.868	27.104	27.272	27.393	27.480	27.543	27.566
$\log n_p$	21.158	21.123	20.857	20.613	20.433	20.306	20.218	20.158	20.125	20.148
$\log n_n$	25.305	25.867	26.108	26.263	26.374	26.456	26.521	26.578	26.637	26.727
$\log n_\alpha$	28.310	28.262	28.208	28.146	28.073	27.986	27.877	27.731	27.509	27.031
$\log n(^{28}\text{Si})$	21.948	25.201	26.060	26.443	26.675	26.826	26.928	27.004	27.074	27.181
$\log n(^{54}\text{Fe})$	19.053	22.939	24.570	25.596	26.300	26.787	27.129	27.382	27.577	27.729
$\log n(^{56}\text{Ni})$	9.152	8.070	6.980	6.202	5.536	4.951	4.438	3.971	3.507	2.925
$-(\log d)^\ddagger$	17.040	17.204	16.394	15.980	15.727	15.559	15.393	15.194	14.934	14.526
$\log \epsilon_\S$	-1.1	4.3	9.1	14.0	20.7	31.2	46.4	66.6	92.3	129.0

TABLE 4—Continued

TABLE 4.17

$T_9 = 4.0$ $\rho = 1.0 \times 10^7 \text{ gm cm}^{-3}$

	1	2	3	4	5	6	7	8	9	10
k	0.950	0.850	0.750	0.650	0.550	0.450	0.350	0.250	0.150	0.051
f^*	-2.021	-1.382	-0.693	-0.188	0.272	0.696	1.071	1.414	1.765	2.218
$\log t^{\dagger}$	5.586	5.856	6.453	7.048	7.488	7.772	7.919	7.926	7.731	7.200
$\log n_p/n_n$	26.301	26.573	26.933	27.272	27.520	27.682	27.770	27.787	27.703	27.454
$\log n_p$	20.715	20.717	20.480	20.224	20.032	19.910	19.851	19.861	19.972	20.254
$\log n_{\alpha}$	25.331	25.881	26.128	26.290	26.403	26.483	26.543	26.596	26.648	26.717
$\log n(^{28}\text{Si})$	29.310	29.262	29.208	29.146	29.073	28.986	28.877	28.731	28.508	28.037
$\log n(^{54}\text{Fe})$	22.214	25.474	26.426	26.824	27.048	27.195	27.331	27.517	27.829	28.337
$\log n(^{56}\text{Ni})$	20.231	24.037	25.709	26.783	27.504	27.975	28.288	28.507	28.651	28.662
$-(\log d)^{\ddagger}$	8.701	7.660	6.627	5.807	5.038	4.350	3.770	3.267	2.791	2.261
$\log e^{\S}$	15.623	17.267	16.522	16.158	15.896	15.687	15.491	15.287	15.048	14.699
q^{\parallel}	-0.0	6.1	11.6	18.3	28.3	43.8	65.6	94.1	131.4	186.6

TABLE 4.18

$T_9 = 4.0$ $\rho = 1.0 \times 10^8 \text{ gm cm}^{-3}$

	1	2	3	4	5	6	7	8	9	10
k	0.950	0.850	0.750	0.650	0.550	0.450	0.346	0.291	0.246	0.200
f^*	-2.018	-1.380	-0.706	-0.204	0.268	0.709	1.101	1.290	1.481	1.721
$\log t^{\dagger}$	6.368	6.579	7.066	7.627	7.935	7.801	7.381	7.109	6.719	6.200
$\log n_p/n_n$	26.693	26.936	27.241	27.562	27.745	27.696	27.499	27.367	27.206	26.946
$\log n_p$	20.325	20.357	20.175	19.935	19.810	19.895	20.118	20.258	20.408	20.648
$\log n_{\alpha}$	25.337	25.884	26.132	26.296	26.409	26.484	26.532	26.548	26.548	26.548
$\log n(^{28}\text{Si})$	30.310	30.262	30.208	30.146	30.073	29.986	29.872	29.796	29.706	29.606
$\log n(^{54}\text{Fe})$	22.472	25.771	26.840	27.284	27.638	28.171	28.792	29.090	29.240	29.490
$\log n(^{56}\text{Ni})$	21.274	25.058	26.739	27.825	28.543	28.980	29.206	29.240	29.240	29.240
$-(\log d)^{\ddagger}$	7.862	6.846	5.865	5.026	4.176	3.417	2.801	2.531	2.261	1.911
$\log e^{\S}$	16.322	17.275	16.549	16.202	15.950	15.755	15.597	15.499	15.349	15.199
q^{\parallel}	0.2	6.5	12.1	19.2	30.6	49.8	80.6	103.0	131.4	186.6

TABLE 4—Continued

$T_9 = 4.2$ $\rho = 1.0 \times 10^6 \text{ gm cm}^{-3}$

	1	2	3	4	5	6	7	8	9	10
k	0.950	0.850	0.750	0.650	0.550	0.450	0.350	0.250	0.150	0.050
f^*	-2.816	-2.419	-1.502	-0.970	-0.549	-0.176	0.171	0.509	0.871	1.372
$\log t^\dagger$	4.149	4.476	5.035	5.552	5.948	6.243	6.464	6.632	6.760	6.848
$\log n_p/n_n$	26.108	26.434	26.774	27.070	27.296	27.464	27.592	27.691	27.771	27.839
$\log n_p$	21.959	21.959	21.739	21.519	21.348	21.221	21.128	21.059	21.011	20.991
$\log n_n$	25.641	26.293	26.533	26.685	26.794	26.878	26.947	27.008	27.071	27.167
$\log n_\alpha$ (^{28}Si)	28.310	28.262	28.208	28.146	28.073	27.986	27.877	27.731	27.509	27.030
$\log n$ (^{54}Fe)	21.396	25.255	26.206	26.612	26.856	27.018	27.132	27.214	27.278	27.331
$\log n$ (^{56}Ni)	18.222	22.734	24.364	25.363	26.057	26.557	26.926	27.206	27.429	27.619
$-(\log d)^\ddagger$	9.843	9.072	7.740	6.981	6.632	5.819	5.330	4.871	4.403	3.799
$\log \epsilon^\S$	18.492	18.405	17.128	16.641	16.346	16.193	16.056	15.874	15.606	15.125
q^\parallel	-4.9	1.1	4.9	8.4	12.4	18.6	28.2	41.8	59.4	81.7

$T_9 = 4.2$ $\rho = 1.0 \times 10^7 \text{ gm cm}^{-3}$

	1	2	3	4	5	6	7	8	9	10
k	0.950	0.850	0.750	0.650	0.550	0.450	0.350	0.250	0.150	0.050
f^*	-2.792	-2.380	-1.568	-1.032	-0.566	-0.139	0.244	0.600	0.968	1.465
$\log t^\dagger$	5.053	5.312	5.844	6.410	6.846	7.154	7.366	7.511	7.589	7.503
$\log n_p/n_n$	26.578	26.859	27.187	27.511	27.757	27.932	28.054	28.140	28.194	28.173
$\log n_p$	21.525	21.547	21.343	21.101	20.911	20.778	20.687	20.629	20.604	20.670
$\log n_n$	25.712	26.320	26.568	26.729	26.843	26.926	26.989	27.045	27.103	27.192
$\log n_\alpha$ (^{28}Si)	29.310	29.262	29.208	29.146	29.073	28.986	28.877	28.731	28.509	28.031
$\log n$ (^{54}Fe)	21.951	25.596	26.621	27.042	27.275	27.414	27.506	27.577	27.658	27.845
$\log n$ (^{56}Ni)	19.717	23.925	25.605	26.673	27.399	27.888	28.223	28.467	28.656	28.801
$-(\log d)^\ddagger$	9.383	8.616	7.408	6.588	5.844	5.171	4.585	4.062	3.550	2.918
$\log \epsilon^\S$	18.178	18.457	17.374	16.964	16.680	16.460	16.250	16.020	15.736	15.304
q^\parallel	-2.5	5.1	10.7	17.0	25.8	39.4	58.3	82.4	112.3	153.8

TABLE 4—Continued

TABLE 4.21 $\tau_g = 4.2$ $\rho = 3.0 \times 10^7 \text{ gm cm}^{-3}$

	1	2	3	4	5	6	7	8	9	10
k	0.950	0.850	0.750	0.650	0.550	0.450	0.350	0.250	0.150	0.050
f^*	-2.788	-2.371	-1.582	-1.048	-0.573	-0.134	0.256	0.615	0.982	1.468
$\log t^\dagger$	5.475	5.706	6.193	6.762	7.209	7.517	7.708	7.784	7.685	7.195
$\log n_p/n_n$	26.792	27.057	27.363	27.688	27.941	28.115	28.226	28.277	28.242	28.017
$\log n_p$	21.317	21.352	21.170	20.927	20.732	20.598	20.518	20.494	20.557	20.822
$\log n_n$	25.723	26.324	26.573	26.737	26.851	26.933	26.995	27.050	27.105	27.184
$\log n_\alpha$	29.788	29.739	29.685	29.623	29.550	29.463	29.354	29.208	28.986	28.508
$\log n(^{28}\text{Si})$	22.078	25.707	26.784	27.215	27.442	27.577	27.682	27.813	28.052	28.573
$\log n(^{54}\text{Fe})$	20.271	24.432	26.120	27.201	27.933	28.418	28.745	28.978	29.146	29.217
$\log n(^{56}\text{Ni})$	9.055	8.294	7.126	6.293	5.496	4.762	4.132	3.583	3.057	2.449
$-(\log d)^\ddagger$	18.102	18.454	17.405	17.011	16.724	16.493	16.276	16.051	15.786	15.397
$\log e_\S$	-2.1	5.6	11.4	18.1	27.9	42.9	63.8	90.8	125.5	176.7
q^\parallel										

TABLE 4.22 $\tau_g = 4.2$ $\rho = 1.0 \times 10^8 \text{ gm cm}^{-3}$

	1	2	3	4	5	6	7	8	9	10
k	0.950	0.850	0.750	0.650	0.550	0.450	0.350	0.250	0.148	0.050
f^*	-2.785	-2.366	-1.589	-1.058	-0.578	-0.131	0.264	0.624	0.987	1.468
$\log t^\dagger$	5.886	6.094	6.530	7.092	7.538	7.793	7.808	7.556	7.103	7.195
$\log n_p/n_n$	26.998	27.252	27.532	27.854	28.106	28.254	28.276	28.163	27.947	28.017
$\log n_p$	21.113	21.158	21.002	20.762	20.568	20.461	20.469	20.607	20.845	20.822
$\log n_n$	25.729	26.326	26.576	26.740	26.855	26.936	26.997	27.046	27.091	27.184
$\log n_\alpha$	30.310	30.262	30.208	30.146	30.073	29.986	29.877	29.730	29.502	28.508
$\log n(^{28}\text{Si})$	22.227	25.856	26.987	27.431	27.662	27.846	28.114	28.540	29.059	29.217
$\log n(^{54}\text{Fe})$	20.833	24.969	26.661	27.750	28.484	28.964	29.277	29.476	29.564	29.217
$\log n(^{56}\text{Ni})$	8.523	7.770	6.636	5.797	4.959	4.184	3.535	2.987	2.491	2.449
$-(\log d)^\ddagger$	18.055	18.452	17.420	17.036	16.750	16.518	16.311	16.106	15.878	15.397
$\log e_\S$	-1.9	5.9	11.7	18.7	29.0	45.2	68.5	99.8	142.9	176.7
q^\parallel										

TABLE 4—Continued

TABLE 4.23 $\rho = 3.0 \times 10^8 \text{ gm cm}^{-3}$

$T_9 = 4.2$

	1	2	3	4	5	6	7	8	9	10
k	0.950	0.850	0.750	0.650	0.550	0.450	0.349	0.253		
f^*	-2.785	-2.365	-1.592	-1.063	-0.578	-0.124	0.277	0.608		
$\log t^{\dagger}$	6.158	6.353	6.749	7.287	7.654	7.637	7.267	6.833		
$\log n_p/n_n$	27.135	27.382	27.642	27.952	28.164	28.175	28.004	27.795		
$\log n_p$	20.977	21.029	20.893	20.665	20.510	20.539	20.737	20.962		
$\log n_{\alpha}$	25.730	26.327	26.577	26.741	26.856	26.935	26.988	27.020		
$\log n(^{28}\text{Si})$	30.788	30.739	30.685	30.623	30.550	30.463	30.353	30.213		
$\log n(^{54}\text{Fe})$	22.443	26.078	27.251	27.721	28.029	28.469	29.071	29.575		
$\log n(^{56}\text{Ni})$	21.323	25.451	27.144	28.235	28.968	29.430	29.688	29.775		
$-(\log d)^{\ddagger}$	7.094	7.154	6.041	5.208	4.362	3.587	2.952	2.483		
$\log \epsilon^{\S}$	18.055	18.453	17.427	17.048	16.770	16.552	16.372	16.222		
q^{\parallel}	-1.8	6.0	11.9	18.9	29.8	47.8	75.6	113.0		

TABLE 4.24 $\rho = 1.0 \times 10^9 \text{ gm cm}^{-3}$

$T_9 = 4.2$

	1	2	3	4	5	6	7	8	9	10
k	0.950	0.850	0.750	0.650	0.550	0.446				
f^*	-2.785	-2.365	-1.593	-1.061	-0.565	-0.061				
$\log t^{\dagger}$	6.317	6.498	6.822	7.241	7.273	6.819				
$\log n_p/n_n$	27.214	27.454	27.679	27.929	27.973	27.762				
$\log n_p$	20.898	20.956	20.856	20.688	20.700	20.943				
$\log n_{\alpha}$	25.731	26.327	26.577	26.741	26.853	26.917				
$\log n(^{28}\text{Si})$	31.310	31.262	31.208	31.146	31.073	30.982				
$\log n(^{54}\text{Fe})$	22.810	26.457	27.701	28.289	28.909	29.693				
$\log n(^{56}\text{Ni})$	21.849	25.975	27.669	28.757	29.465	29.827				
$-(\log d)^{\ddagger}$	7.171	6.422	5.329	4.517	3.682	2.902				
$\log \epsilon^{\S}$	18.026	18.453	17.431	17.062	16.807	16.639				
q^{\parallel}	-1.8	6.1	12.0	19.3	31.6	56.8				

TABLE 4—Continued

TABLE 4.25 $T_9 = 4.4$ $\rho = 1.0 \times 10^5 \text{ gm cm}^{-3}$

	1	2	3	4	5	6	7	8	9	10
k	0.850	0.750	0.650	0.550	0.450	0.350	0.250	0.149	0.048	
f^*	-2.752	-2.193	-1.736	-1.398	-1.115	-0.853	-0.588	-0.286	0.171	
$\log t^\dagger$	3.027	3.343	3.666	3.929	4.143	4.324	4.478	4.608	4.702	
$\log n_p/n_n$	26.156	26.384	26.582	26.739	26.866	26.973	27.067	27.150	27.222	
$\log n_p$	23.130	23.041	22.916	22.810	22.723	22.650	22.589	22.542	22.520	
$\log n_\alpha$	26.444	26.724	26.870	26.971	27.050	27.119	27.185	27.255	27.357	
$\log n(^{28}\text{Si})$	27.262	27.208	27.146	27.073	26.986	26.877	26.730	26.506	26.015	
$\log n(^{54}\text{Fe})$	23.705	25.150	25.717	26.035	26.249	26.408	26.535	26.637	26.717	
$\log n(^{56}\text{Ni})$	19.891	21.791	22.754	23.385	23.853	24.228	24.541	24.809	25.034	
$-(\log d)^\ddagger$	9.659	8.784	8.175	7.748	7.403	7.098	6.806	6.500	6.083	
$\log \epsilon_\delta$	<u>19.350</u>	<u>18.661</u>	<u>18.181</u>	<u>17.904</u>	<u>17.675</u>	<u>17.471</u>	<u>17.251</u>	<u>17.008</u>	<u>16.677</u>	
q^{\parallel}	-41.1	-63.1	-81.9	-99.9	-118.0	-137.4	-159.2	-186.6	-234.1	

TABLE 4.26 $T_9 = 4.4$ $\rho = 1.0 \times 10^6 \text{ gm cm}^{-3}$

	1	2	3	4	5	6	7	8	9	10
k	0.850	0.750	0.650	0.550	0.450	0.350	0.250	0.150	0.050	
f^*	-2.715	-2.174	-1.696	-1.302	-0.952	-0.621	-0.290	0.073	0.586	
$\log t^\dagger$	3.962	4.426	4.884	5.248	5.532	5.757	5.934	6.076	6.184	
$\log n_p/n_n$	26.678	26.972	27.238	27.447	27.610	27.740	27.845	27.933	28.012	
$\log n_p$	22.717	22.546	22.354	22.199	22.078	21.983	21.911	21.857	21.827	
$\log n_\alpha$	26.663	26.909	27.057	27.164	27.249	27.319	27.384	27.451	27.551	
$\log n(^{28}\text{Si})$	28.262	28.208	28.146	28.073	27.986	27.877	27.731	27.509	27.030	
$\log n(^{54}\text{Fe})$	25.190	26.271	26.715	26.974	27.151	27.278	27.374	27.449	27.508	
$\log n(^{56}\text{Ni})$	22.420	24.088	25.064	25.741	26.244	26.631	26.937	27.187	27.404	
$-(\log d)^\ddagger$	9.279	8.390	7.688	7.123	6.632	6.182	5.749	5.296	4.698	
$\log \epsilon_\delta$	<u>18.404</u>	<u>17.565</u>	<u>16.901</u>	<u>16.406</u>	<u>16.371</u>	<u>16.371</u>	<u>16.292</u>	<u>16.060</u>	<u>15.486</u>	
q^{\parallel}	-5.1	-3.2	-2.1	-1.4	0.2	3.3	8.8	16.8	25.3	

TABLE 4—Continued

		$\rho = 1.0 \times 10^7 \text{ gm cm}^{-3}$									
		$T_9 = 4.4$									
k	l	2	3	4	5	6	7	8	9	10	
f^*	0.850	0.750	0.650	0.550	0.450	0.350	0.250	0.150	0.050		
$\log t^\dagger$	-2.719	-2.241	-1.757	-1.310	-0.893	-0.509	-0.145	0.235	0.752		
$\log n_p/n_n$	4.818	5.285	5.816	6.238	6.547	6.770	6.935	7.058	7.133		
$\log n_p$	27.119	27.416	27.721	27.961	28.136	28.264	28.361	28.438	28.499		
$\log n_n$	22.302	22.130	21.905	21.723	21.590	21.494	21.427	21.380	21.366		
$\log n_\alpha$ (^{28}Si)	26.714	26.965	27.125	27.239	27.324	27.390	27.448	27.509	27.602		
$\log n$ (^{54}Fe)	29.262	29.208	29.146	29.073	28.986	28.877	28.731	28.509	28.032		
$\log n$ (^{56}Ni)	25.668	26.776	27.226	27.473	27.625	27.723	27.790	27.842	27.897		
$\log n$ (^{56}Ni)	23.779	25.481	26.541	27.267	27.770	28.124	28.386	28.591	28.767		
$-(\log d)^\ddagger$	8.896	8.066	7.285	6.576	5.930	5.352	4.825	4.300	3.639		
$\log \epsilon_\S$	18.213	18.151	17.680	17.367	17.143	16.932	16.697	16.395	15.904		
q^\parallel	3.2	8.8	14.7	22.3	33.6	49.7	70.7	96.5	129.1		

		$\rho = 1.0 \times 10^8 \text{ gm cm}^{-3}$									
		$T_9 = 4.4$									
k	l	2	3	4	5	6	7	8	9	10	
f^*	0.850	0.750	0.650	0.550	0.450	0.350	0.250	0.150	0.050		
$\log t^\dagger$	-2.716	-2.267	-1.794	-1.327	-0.880	-0.476	-0.104	0.277	0.781		
$\log n_p/n_n$	5.636	6.020	6.552	7.002	7.322	7.527	7.613	7.516	6.987		
$\log n_p$	27.532	27.787	28.094	28.348	28.529	28.647	28.704	28.670	28.425		
$\log n_n$	21.895	21.767	21.542	21.346	21.207	21.120	21.091	21.153	21.438		
$\log n_\alpha$ (^{28}Si)	26.726	26.979	27.144	27.260	27.343	27.407	27.462	27.519	27.599		
$\log n$ (^{54}Fe)	30.262	30.208	30.146	30.073	29.986	29.877	29.731	29.509	29.031		
$\log n$ (^{54}Fe)	25.929	27.133	27.609	27.844	27.978	28.078	28.205	28.450	29.018		
$\log n$ (^{56}Ni)	24.865	26.579	27.670	28.412	28.908	29.245	29.486	29.662	29.741		
$-(\log d)^\ddagger$	8.075	7.294	6.498	5.687	4.919	4.253	3.672	3.118	2.480		
$\log \epsilon_\S$	18.392	18.232	17.795	17.481	17.228	16.995	16.756	16.478	16.074		
q^\parallel	4.9	11.1	18.0	27.7	42.6	63.3	90.1	124.5	175.4		

TABLE 4—Continued

TABLE 4.29 $T_9 = 4.4$ $\rho = 1.0 \times 10^9 \text{ gm cm}^{-3}$

	1	2	3	4	5	6	7	8	9	10
k	0.850	0.750	0.650	0.550	0.450	0.349	0.271			
f^*	-2.715	-2.274	-1.804	-1.331	-0.870	-0.453	-0.173			
$\log t^\dagger$	6.138	6.458	6.953	7.318	7.307	6.921	6.545			
$\log n_p/n_n$	27.783	28.006	28.295	28.507	28.521	28.342	28.160			
$\log n_p$	21.645	21.548	21.342	21.189	21.214	21.420	21.615			
$\log n_n$	26.728	26.981	27.147	27.263	27.343	27.397	27.422			
$\log n_\alpha$	31.262	31.208	31.146	31.073	30.986	30.875	30.766			
$\log n(^{28}\text{Si})$	26.441	27.710	28.229	28.548	28.993	29.613	30.043			
$\log n(^{54}\text{Fe})$	25.879	27.595	28.692	29.434	29.908	30.169	30.235			
$\log n(^{56}\text{Ni})$	6.699	5.942	5.162	4.337	3.559	2.912	2.518			
$-(\log d)^\ddagger$	18.422	18.248	17.824	17.520	17.287	17.100	16.963			
$\log \epsilon^\S$	5.3	11.5	18.7	29.3	47.0	75.3	105.7			
q^\parallel										

TABLE 4.30 $T_9 = 4.6$ $\rho = 1.0 \times 10^5 \text{ gm cm}^{-3}$

	1	2	3	4	5	6	7	8	9	10
k	0.849	0.750	0.650	0.550	0.451	0.350	0.250	0.149	0.048	
f^*	-3.623	-3.147	-2.597	-2.219	-1.925	-1.663	-1.404	-1.113	-0.670	
$\log t^\dagger$	2.500	2.685	2.933	3.164	3.355	3.514	3.649	3.759	3.827	
$\log n_p/n_n$	26.289	26.480	26.649	26.793	26.910	27.008	27.092	27.165	27.223	
$\log n_p$	23.789	23.794	23.716	23.630	23.556	23.494	23.443	23.406	23.396	
$\log n_n$	26.534	26.924	27.107	27.222	27.308	27.380	27.448	27.517	27.616	
$\log n_\alpha$	27.262	27.208	27.146	27.073	26.986	26.877	26.730	26.506	26.015	
$\log n(^{28}\text{Si})$	22.084	24.381	25.258	25.703	25.984	26.185	26.340	26.460	26.540	
$\log n(^{54}\text{Fe})$	17.859	20.536	21.752	22.485	23.000	23.397	23.720	23.985	24.182	
$\log n(^{56}\text{Ni})$	10.534	9.752	9.022	8.565	8.226	7.939	7.676	7.408	7.059	
$-(\log d)^\ddagger$	20.400	19.972	19.339	19.012	18.774	18.558	18.343	18.097	17.760	
$\log \epsilon^\S$	-61.9	-107.9	-149.1	-186.5	-222.5	-259.3	-299.8	-348.7	-430.0	
q^\parallel										

TABLE 4--Continued

$T_9 = 4.6$ $\rho = 1.0 \times 10^6 \text{ gm cm}^{-3}$

k	1	2	3	4	5	6	7	8	9	10
f^*	0.850	0.750	0.650	0.550	0.450	0.350	0.250	0.150	0.049	
$\log t^\dagger$	-3.413	-2.899	-2.405	-2.018	-1.681	-1.365	-1.046	-0.688	-0.171	
$\log n_p/n_n$	3.483	3.856	4.251	4.576	4.840	5.055	5.234	5.382	5.498	
$\log n_p$	26.890	27.143	27.377	27.566	27.719	27.844	27.950	28.042	28.126	
$\log n_n$	23.407	23.286	23.126	22.990	22.879	22.789	22.717	22.660	22.628	
$\log n_\alpha$	26.969	27.234	27.383	27.488	27.572	27.644	27.711	27.781	27.884	
$\log n(^{28}\text{Si})$	28.262	28.208	28.146	28.073	27.986	27.877	27.731	27.509	27.027	
$\log n(^{54}\text{Fe})$	24.931	26.224	26.733	27.020	27.213	27.356	27.466	27.554	27.626	
$\log n(^{56}\text{Ni})$	21.906	23.705	24.683	25.347	25.846	26.240	26.563	26.835	27.073	
$-(\log d)^\ddagger$	9.892	9.055	8.361	7.837	7.393	6.988	6.596	6.179	5.618	
$\log \epsilon_\delta$	<u>19.590</u>	<u>18.436</u>	<u>18.006</u>	<u>17.774</u>	<u>17.523</u>	<u>17.198</u>	<u>16.859</u>	<u>16.494</u>	<u>16.244</u>	
q^{\parallel}	-15.6	-18.0	-20.8	-24.3	-28.2	-31.9	-35.4	-39.1	-47.6	

$T_9 = 4.6$ $\rho = 1.0 \times 10^7 \text{ gm cm}^{-3}$

k	1	2	3	4	5	6	7	8	9	10
f^*	0.850	0.750	0.650	0.550	0.450	0.350	0.250	0.150	0.050	
$\log t^\dagger$	-3.403	-2.951	-2.447	-1.999	-1.587	-1.205	-0.836	-0.445	0.088	
$\log n_p/n_n$	4.364	4.772	5.260	5.662	5.967	6.195	6.368	6.502	6.602	
$\log n_p$	27.354	27.622	27.906	28.136	28.310	28.441	28.543	28.625	28.699	
$\log n_n$	22.990	22.851	22.647	22.474	22.343	22.246	22.175	22.124	22.098	
$\log n_\alpha$	27.065	27.323	27.482	27.596	27.682	27.751	27.811	27.875	27.971	
$\log n(^{28}\text{Si})$	29.262	29.208	29.146	29.073	28.986	28.877	28.731	28.509	28.031	
$\log n(^{54}\text{Fe})$	25.671	26.885	27.370	27.635	27.801	27.910	27.987	28.043	28.088	
$\log n(^{56}\text{Ni})$	23.576	25.325	26.378	27.102	27.616	27.988	28.268	28.490	28.683	
$-(\log d)^\ddagger$	9.490	8.709	7.928	7.248	6.633	6.074	5.551	5.021	4.346	
$\log \epsilon_\delta$	<u>17.100</u>	<u>18.866</u>	<u>18.309</u>	<u>17.956</u>	<u>17.725</u>	<u>17.522</u>	<u>17.292</u>	<u>16.988</u>	<u>16.472</u>	
q^{\parallel}	0.1	5.6	10.7	16.8	25.5	38.1	55.1	76.5	103.1	

TABLE 4—Continued

TABLE 4.33 $T_9 = 4.6$ $\rho = 1.0 \times 10^8 \text{ gm cm}^{-3}$

k	1	2	3	4	5	6	7	8	9	10
f^*	0.850	0.750	0.650	0.550	0.450	0.350	0.250	0.150	0.050	
$\log t^\dagger$	-3.396	-2.985	-2.495	-2.017	-1.564	-1.151	-0.767	-0.371	0.159	
$\log n_p/n_n$	5.209	5.548	6.045	6.482	6.808	7.041	7.204	7.301	7.221	
$\log n_p$	27.782	28.016	28.306	28.554	28.738	28.871	28.967	29.030	29.013	
$\log n_n$	22.573	22.468	22.261	22.072	21.930	21.830	21.763	21.730	21.793	
$\log n_{\alpha}$	27.088	27.346	27.511	27.629	27.714	27.779	27.837	27.897	27.988	
$\log n(^{28}\text{Si})$	30.262	30.208	30.146	30.073	29.986	29.877	29.731	29.509	29.032	
$\log n(^{54}\text{Fe})$	25.975	27.259	27.774	28.027	28.167	28.252	28.316	28.389	28.583	
$\log n(^{56}\text{Ni})$	24.735	26.488	27.582	28.330	28.839	29.190	29.446	29.646	29.806	
$-(\log d)^\ddagger$	8.664	7.943	7.145	6.352	5.598	4.929	4.334	3.757	3.054	
$\log \epsilon^\S$	18.900	19.004	18.490	18.143	17.874	17.629	17.371	17.062	16.595	
$q^ $	3.3	9.9	16.9	26.1	39.8	58.9	83.4	113.8	155.2	

TABLE 4.34 $T_9 = 4.6$ $\rho = 1.0 \times 10^9 \text{ gm cm}^{-3}$

k	1	2	3	4	5	6	7	8	9	10
f^*	0.850	0.750	0.650	0.550	0.450	0.350	0.250	0.149		
$\log t^\dagger$	-3.394	-2.993	-2.512	-2.029	-1.561	-1.137	-0.748	-0.366		
$\log n_p/n_n$	5.793	6.075	6.550	6.988	7.257	7.268	6.968	6.465		
$\log n_p$	28.076	28.281	28.560	28.809	28.964	28.985	28.848	28.607		
$\log n_n$	22.282	22.206	22.010	21.821	21.707	21.718	21.880	22.142		
$\log n_{\alpha}$	27.092	27.350	27.517	27.635	27.720	27.783	27.833	27.875		
$\log n(^{28}\text{Si})$	31.262	31.208	31.146	31.073	30.986	30.877	30.730	30.505		
$\log n(^{54}\text{Fe})$	26.417	27.760	28.307	28.563	28.756	29.047	29.527	30.079		
$\log n(^{56}\text{Ni})$	25.764	27.518	28.623	29.376	29.881	30.214	30.419	30.489		
$-(\log d)^\ddagger$	7.257	6.563	5.783	4.968	4.183	3.505	2.930	2.426		
$\log \epsilon^\S$	18.981	19.030	18.531	18.188	17.918	17.685	17.465	17.234		
$q^ $	4.0	10.8	18.1	28.1	43.6	66.5	98.3	143.0		

TABLE 4—Continued

TABLE 4.35

$T_9 = 4.8$ $\rho = 1.0 \times 10^6 \text{ gm cm}^{-3}$

k	1	2	3	4	5	6	7	8	9	10
f^*	0.850	0.750	0.650	0.550	0.450	0.350	0.250	0.150	0.049	
$\log t^\dagger$	-4.079	-3.638	-3.101	-2.704	-2.373	-2.069	-1.761	-1.414	-0.902	
$\log n_p/n$	3.030	3.315	3.651	3.938	4.174	4.373	4.542	4.685	4.796	
$\log n_p$	27.062	27.283	27.491	27.661	27.800	27.917	28.019	28.108	28.190	
$\log n_n$	24.032	23.968	23.840	23.723	23.626	23.544	23.477	23.423	23.394	
$\log n_{\alpha}$	27.190	27.504	27.662	27.769	27.853	27.925	27.993	28.065	28.169	
$\log n(^{28}\text{Si})$	28.262	28.208	28.146	28.073	27.986	27.877	27.731	27.508	27.022	
$\log n(^{54}\text{Fe})$	24.304	26.011	26.638	26.974	27.194	27.355	27.481	27.583	27.665	
$\log n(^{56}\text{Ni})$	20.999	23.149	24.192	24.867	25.366	25.761	26.090	26.371	26.616	
$-(\log d)^\ddagger$	10.507	9.768	9.027	8.519	8.109	7.744	7.393	7.023	6.526	
$\log \epsilon_\S$	<u>20.557</u>	<u>19.838</u>	<u>19.226</u>	<u>18.915</u>	<u>18.658</u>	<u>18.414</u>	<u>18.156</u>	<u>17.868</u>	<u>17.512</u>	
$q^ $	-31.2	-41.6	-51.4	-61.5	-72.2	-83.7	-96.8	-113.0	-142.3	

TABLE 4.36

$T_9 = 4.8$ $\rho = 1.0 \times 10^7 \text{ gm cm}^{-3}$

k	1	2	3	4	5	6	7	8	9	10
f^*	0.850	0.750	0.650	0.550	0.450	0.350	0.250	0.150	0.050	
$\log t^\dagger$	-4.024	-3.621	-3.098	-2.635	-2.229	-1.851	-1.481	-1.085	-0.539	
$\log n_p/n$	3.944	4.294	4.736	5.113	5.409	5.638	5.817	5.959	6.067	
$\log n_p$	27.564	27.808	28.068	28.285	28.455	28.587	28.693	28.780	28.859	
$\log n_n$	23.620	23.513	23.332	23.172	23.046	22.949	22.875	22.821	22.791	
$\log n_{\alpha}$	27.371	27.643	27.803	27.916	28.003	28.074	28.138	28.204	28.302	
$\log n(^{28}\text{Si})$	29.262	29.208	29.146	29.073	28.986	28.877	28.731	28.509	28.030	
$\log n(^{54}\text{Fe})$	25.571	26.935	27.468	27.754	27.936	28.060	28.148	28.215	28.267	
$\log n(^{56}\text{Ni})$	23.271	25.122	26.177	26.896	27.417	27.806	28.105	28.347	28.556	
$-(\log d)^\ddagger$	10.033	9.327	8.526	7.872	7.292	6.760	6.250	5.724	5.044	
$\log \epsilon_\S$	<u>19.731</u>	<u>19.540</u>	<u>18.843</u>	<u>18.424</u>	<u>18.181</u>	<u>17.997</u>	<u>17.784</u>	<u>17.486</u>	<u>16.949</u>	
$q^ $	-5.3	-0.1	4.1	8.2	13.8	22.3	34.2	49.8	68.9	

TABLE 4—Continued

TABLE 4.37

$T_9 = 4.8$ $\rho = 1.0 \times 10^8 \text{ gm cm}^{-3}$

k	1	2	3	4	5	6	7	8	9	10
f^*	0.850	0.750	0.650	0.550	0.450	0.350	0.250	0.150	0.050	
$\log t^\dagger$	-4.009	-3.656	-3.142	-2.649	-2.189	-1.769	-1.375	-0.969	-0.422	
$\log n_p/n_n$	4.809	5.111	5.573	5.993	6.316	6.554	6.731	6.864	6.940	
$\log n_p$	28.007	28.225	28.498	28.737	28.920	29.056	29.160	29.242	29.303	
$\log n_n$	23.198	23.114	22.925	22.744	22.605	22.503	22.429	22.378	22.363	
$\log n_{\alpha}^{28}$	27.413	27.681	27.847	27.965	28.051	28.119	28.178	28.240	28.334	
$\log n(^{28}\text{Si})$	30.262	30.208	30.146	30.073	29.986	29.877	29.731	29.509	29.032	
$\log n(^{54}\text{Fe})$	25.974	27.360	27.917	28.190	28.344	28.437	28.498	28.546	28.605	
$\log n(^{56}\text{Ni})$	24.560	26.382	27.484	28.237	28.756	29.121	29.389	29.601	29.783	
$-(\log d)^\ddagger$	9.198	8.563	7.742	6.961	6.223	5.558	4.956	4.366	3.637	
$\log \epsilon_\S$	18.842	19.766	19.131	18.741	18.455	18.203	17.938	17.615	17.104	
q^\parallel	0.7	8.1	15.2	23.8	36.3	53.8	76.3	104.2	139.9	

TABLE 4.38

$T_9 = 4.8$ $\rho = 1.0 \times 10^9 \text{ gm cm}^{-3}$

k	1	2	3	4	5	6	7	8	9	10
f^*	0.850	0.750	0.650	0.550	0.450	0.350	0.250	0.150	0.051	
$\log t^\dagger$	-4.006	-3.667	-3.167	-2.666	-2.187	-1.752	-1.350	-0.942	-0.430	
$\log n_p/n_n$	5.463	5.710	6.148	6.585	6.915	7.114	7.150	6.907	6.220	
$\log n_p$	28.336	28.527	28.788	29.036	29.223	29.339	29.371	29.263	28.937	
$\log n_n$	22.873	22.816	22.640	22.451	22.308	22.224	22.221	22.357	22.717	
$\log n_{\alpha}^{28}$	27.421	27.688	27.856	27.976	28.062	28.128	28.185	28.241	28.311	
$\log n(^{28}\text{Si})$	31.262	31.208	31.146	31.073	30.986	30.877	30.731	30.509	30.040	
$\log n(^{54}\text{Fe})$	26.374	27.809	28.403	28.669	28.814	28.936	29.124	29.511	30.178	
$\log n(^{56}\text{Ni})$	25.618	27.435	28.551	29.313	29.831	30.185	30.437	30.609	30.624	
$-(\log d)^\ddagger$	7.766	7.163	6.365	5.555	4.774	4.083	3.477	2.905	2.291	
$\log \epsilon_\S$	19.287	19.807	19.192	18.806	18.509	18.249	18.994	17.710	17.323	
q^\parallel	2.0	9.7	17.2	27.0	41.5	62.1	89.7	126.7	182.7	

TABLE 4—Continued

$T_9 = 5.0$ $\rho = 1.0 \times 10^6 \text{ gm cm}^{-3}$

	1	2	3	4	5	6	7	8	9	10
k										
f^*	0.843	0.750	0.650	0.550	0.450	0.350	0.250	0.149	0.048	
$\log t^\dagger$	-4.750	-4.600	-3.851	-3.394	-3.049	-2.745	-2.444	-2.106	-1.603	
$\log n_p/n_n$	2.578	2.800	3.074	3.329	3.542	3.721	3.875	4.005	4.100	
$\log n_p$	27.164	27.392	27.576	27.733	27.861	27.969	28.063	28.146	28.220	
$\log n_n$	24.586	24.593	24.502	24.403	24.319	24.248	24.188	24.141	24.119	
$\log n_\alpha$ (^{28}Si)	27.234	27.703	27.889	28.005	28.092	28.166	28.235	28.307	28.411	
$\log n$ (^{54}Fe)	28.259	28.208	28.146	28.073	27.986	27.877	27.731	27.507	27.018	
$\log n$ (^{56}Ni)	22.728	25.502	26.378	26.804	27.071	27.261	27.407	27.524	27.612	
$\log n$ (^{56}Ni)	19.050	22.280	23.524	24.263	24.786	25.192	25.527	25.810	26.045	
$-(\log d)^\ddagger$	11.211	10.882	9.758	9.204	8.800	8.458	8.139	7.810	7.378	
$\log \epsilon_\S$	<u>21.455</u>	<u>21.427</u>	<u>20.268</u>	<u>19.885</u>	<u>19.614</u>	<u>19.372</u>	<u>19.126</u>	<u>18.849</u>	<u>18.481</u>	
q^\parallel	-52.5	-72.8	-95.1	-116.0	-136.8	-159.0	-183.8	-214.8	-268.4	

$T_9 = 5.0$ $\rho = 1.0 \times 10^7 \text{ gm cm}^{-3}$

	1	2	3	4	5	6	7	8	9	10
k										
f^*	0.850	0.750	0.650	0.550	0.450	0.350	0.250	0.150	0.050	
$\log t^\dagger$	-4.594	-4.286	-3.701	-3.233	-2.831	-2.459	-2.093	-1.694	-1.139	
$\log n_p/n_n$	3.547	3.847	4.241	4.588	4.870	5.096	5.278	5.426	5.543	
$\log n_p$	27.746	27.972	28.209	28.411	28.574	28.706	28.813	28.904	28.988	
$\log n_n$	24.199	24.125	23.969	23.823	23.704	23.609	23.535	23.478	23.445	
$\log n_\alpha$ (^{28}Si)	27.623	27.927	28.090	28.202	28.290	28.363	28.429	28.498	28.599	
$\log n$ (^{54}Fe)	29.262	29.208	29.146	29.073	28.986	28.877	28.731	28.509	28.030	
$\log n$ (^{56}Ni)	25.287	26.909	27.512	27.827	28.027	28.166	28.268	28.347	28.407	
$-(\log d)^\ddagger$	22.773	24.846	25.925	26.643	27.168	27.571	27.888	28.149	28.377	
$\log \epsilon_\S$	10.543	9.975	9.102	8.460	7.914	7.414	6.929	6.418	5.745	
q^\parallel	<u>20.724</u>	<u>20.242</u>	<u>19.215</u>	<u>18.636</u>	<u>18.363</u>	<u>18.232</u>	<u>18.083</u>	<u>17.809</u>	<u>17.185</u>	
	-14.0	-9.2	-6.7	-5.0	-2.9	0.6	6.4	14.5	22.8	

TABLE 4—Continued

TABLE 4.41

$T_9 = 5.0$

$\rho = 1.0 \times 10^9 \text{ gm cm}^{-3}$

	1	2	3	4	5	6	7	8	9	10
k	0.850	0.750	0.650	0.550	0.450	0.350	0.250	0.150	0.050	
f^*	-4.564	-4.303	-3.748	-3.233	-2.766	-2.340	-1.939	-1.522	-0.962	
$\log t^\dagger$	4.433	4.704	5.131	5.533	5.849	6.088	6.270	6.412	6.520	
$\log n_p/n_n$	28.208	28.415	28.670	28.901	29.081	29.218	29.324	29.411	29.489	
$\log n_p$	23.775	23.711	23.540	23.368	23.232	23.130	23.054	22.999	22.969	
$\log n_\alpha$	27.699	27.985	28.153	28.272	28.360	28.429	28.490	28.554	28.650	
$\log n(^{28}\text{Si})$	30.262	30.208	30.146	30.073	29.986	29.877	29.731	29.509	29.032	
$\log n(^{54}\text{Fe})$	25.899	27.430	28.036	28.331	28.500	28.604	28.673	28.722	28.762	
$\log n(^{56}\text{Ni})$	24.308	26.253	27.370	28.127	28.656	29.034	29.315	29.538	29.733	
$-(\log d)^\ddagger$	9.686	9.190	8.302	7.522	6.803	6.147	5.542	4.943	4.199	
$\log \epsilon_\S$	20.095	20.581	19.728	19.283	18.977	18.720	18.452	18.122	17.590	
q^\parallel	-3.5	5.3	12.5	20.5	31.6	47.1	67.5	92.9	124.8	

TABLE 4.42

$T_9 = 5.0$

$\rho = 1.0 \times 10^9 \text{ gm cm}^{-3}$

	1	2	3	4	5	6	7	8	9	10
k	0.850	0.750	0.650	0.550	0.450	0.350	0.250	0.150	0.050	
f^*	-4.556	-4.314	-3.781	-3.254	-2.760	-2.313	-1.901	-1.480	-0.924	
$\log t^\dagger$	5.145	5.366	5.768	6.189	6.527	6.770	6.926	6.964	6.615	
$\log n_p/n_n$	28.568	28.749	28.992	29.233	29.424	29.563	29.655	29.690	29.538	
$\log n_p$	23.423	23.383	23.225	23.044	22.897	22.793	22.730	22.726	22.922	
$\log n_\alpha$	27.715	27.997	28.168	28.289	28.377	28.445	28.504	28.565	28.653	
$\log n(^{28}\text{Si})$	31.262	31.208	31.146	31.073	30.986	30.877	30.731	30.509	30.031	
$\log n(^{54}\text{Fe})$	26.289	27.849	28.496	28.785	28.932	29.022	29.104	29.240	29.684	
$\log n(^{56}\text{Ni})$	25.418	27.341	28.475	29.246	29.774	30.141	30.408	30.614	30.753	
$-(\log d)^\ddagger$	8.231	7.772	6.916	6.098	5.322	4.628	4.009	3.411	2.699	
$\log \epsilon_\S$	19.634	20.641	19.817	19.376	19.054	18.777	18.501	18.185	17.731	
q^\parallel	-1.2	8.2	16.1	25.8	39.6	59.0	84.3	116.8	164.9	

NOTES TO TABLE 4

* f = fraction of ^{28}Si remaining after iteration step k .

† t = cumulative time in seconds through iteration step k .

‡ $d_k = D_k/N_B$, where D_k is the net number of transitions of protons to neutrons through beta decay and electron capture, cumulative through iteration step k (see eq. [32]).

§ $\epsilon_k = [(\Delta M)_k - (\Delta M)_{k-1}]/\rho(t_k - t_{k-1})$, in units of $\text{ergs g}^{-1} \text{sec}^{-1}$; ϵ_k is the average rate of nuclear energy generation during the interval t_{k-1} to t_k . See eq. (33) for definition of ΔM . When ϵ is negative, $\log(-\epsilon)$ is tabulated and is underlined.

|| $q_k = (\Delta M)_k/N_B$, in units of keV per nucleon; q_k is the total nuclear energy released per nucleon from the start of the silicon burning through the time t_k . To compare with Figs. 15 and 16, q_k must be divided by $(1 - f)$, since these figures display the nuclear energy released per *converted* nucleon.

On the other hand, the times are almost independent of density, as illustrated in the lower part of Figure 9. This insensitivity can be understood by noting that the term $[n(^{56}\text{Ni})/n(^{28}\text{Si})]^{1/7}$, which is nearly fixed by the choice $f = 0.35$, determines n_a and hence fixes ratios such as $n(^{24}\text{Mg})/n(^{28}\text{Si})$. Increasing the density at constant f leads to little change in $n(^{24}\text{Mg})/\rho$ and J/ρ and therefore leads to little change in the time.

The rate of silicon burning has a further very significant property: the rate is a rapidly decreasing function of time. That is, the magnitude of df/dt falls markedly as f decreases. Figure 10 shows the time required at several temperatures to deplete the silicon to the indicated mass fraction. It is seen that at each temperature the early burning is much more rapid than the later burning. For example, the time required to reduce f from 0.8 to 0.7 is in each case a small fraction of the time required to reduce f from 0.4 to 0.3. Because of this fact we expect partially burned silicon, say $0.8 < f < 0.2$, to be common under astrophysical circumstances. The initial burning rate is relatively rapid, so that whenever ^{28}Si begins to burn we may expect to burn at least 20 per cent. On the other hand, the final 20–30 per cent takes so much longer to be consumed that we may expect the burning to have been truncated if, for example, it takes place in non-central zones that may be ejected by the more rapid evolution of the presupernova stellar core. It does not seem surprising, therefore, that the abundance distribution of the elements in this mass range resembles the distribution for partially burned silicon.

The decrease in the burning rate with decreasing f may be understood as the result of several factors: (1) It is a general property of a system relaxing toward equilibrium that it does so in an exponential fashion if the individual reaction rates are constant (thus one might expect $df/dt \propto f$). The initial change is relatively rapid, but the equilibrium is approached asymptotically. (2) The value of n_a increases during the burning because of its dependence on $[n(^{56}\text{Ni})/n(^{28}\text{Si})]^{1/7}$. Thus the abundance of ^{24}Mg , which limits the disintegration current J , falls more rapidly with decreasing f than is implied by the decrease in $n(^{28}\text{Si})$ alone. (3) As the burning progresses, the reverse flow from alpha-particle capture in ^{20}Ne becomes more significant, and J becomes increasingly smaller than $\lambda_{\gamma\alpha}(^{24}\text{Mg})n(^{24}\text{Mg})$, as has been seen in Figures 7 and 8.

In Figure 10 we have also plotted results obtained by TCG at $T_9 = 3.0$ and $T_9 = 5.0$ as dashed lines. Exact agreement cannot be expected, inasmuch as we have adopted somewhat different nuclear parameters. For example, our value for $\lambda_{\gamma\alpha}(^{24}\text{Mg})$, which was taken from FCZ, is about a factor of 3 smaller than the value used by TCG. This difference turns out to be unimportant at $T_9 = 5.0$, where the burning is not controlled by $\lambda_{\gamma\alpha}(^{24}\text{Mg})$ alone, but at $T_9 = 3.0$ it becomes significant, as do secondary effects involving beta-decay rates. Test calculations with the parameters used by TCG confirmed our expectation that the difference in the results can be attributed largely to differences in parameters. Therefore we conclude that either computational technique is valid for the determination of the time required to burn a substantial amount of silicon.

b) *The Roles of Electron Capture and Beta Decay*

A system of nuclei evolving from ^{28}Si initially has an equal number of neutrons and protons. As the system moves toward higher mass numbers, the most stable nuclei include nuclei with $Z < A/2$ (such as ^{54}Fe). In the absence of electron or positron emission and electron capture (called, generically, beta decay), the free-neutron density, n_n , will perforce be much less than the free-proton density, n_p , and this in turn will inhibit the rise in the abundance of neutron-rich nuclei. This explains the high density of ^{56}Ni for much of the region studied here, in the face of the tighter binding of both ^{54}Fe and ^{56}Fe .

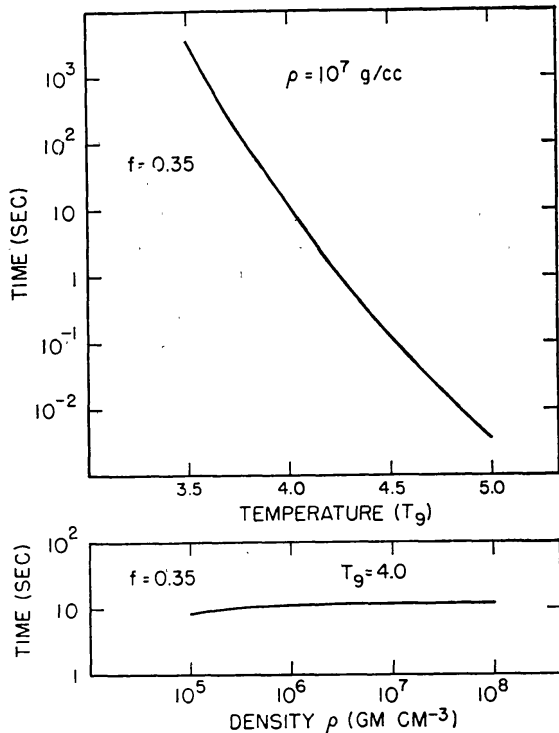


FIG. 9

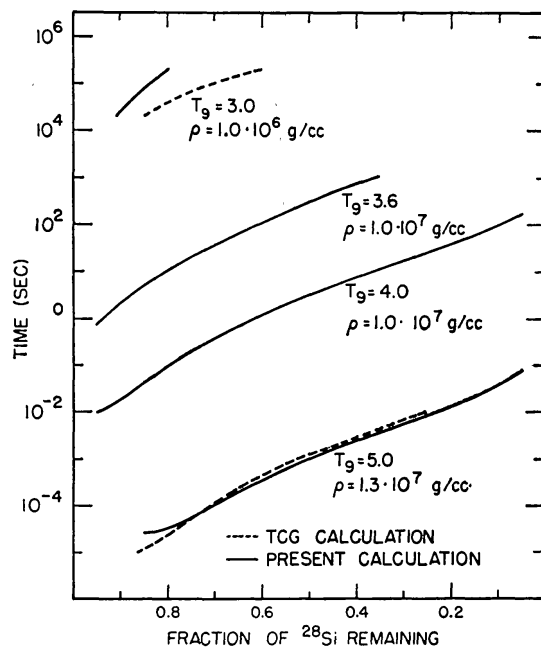


FIG. 10

FIG. 9.—Time required in ^{28}Si burning to deplete ^{28}Si to 35 per cent of its initial density. *Top*: as a function of temperature at fixed density. *Bottom*: as a function of density at fixed temperature.

FIG. 10.—Time required in ^{28}Si burning to deplete ^{28}Si to a given fraction f . Dotted curves give analogous results from the calculations of Truran, Cameron, and Gilbert (1966).

Even a relatively small number of conversions of neutrons to protons by beta decay can alter the abundance ratios considerably. One expects that the values of n_p/n_n will be significantly reduced when the number of past decays, D_2 has become comparable in magnitude to n_p . Commonly, this point is reached when \bar{Z}/\bar{N} is still very close to unity, e.g., $\bar{Z}/\bar{N} \approx 1 - 4d \gtrsim 0.99$, where $d = D/N_B$ (see Table 4).

The computer program kept track of the number of beta-decay events attributable to each nuclear species as the ^{28}Si conversion progressed, using rates calculated from the tables of Hansen (1966). These rates are dependent upon density and temperature, the density dependence of the electron-capture rate being particularly strong. At $T_9 = 4.0$ the capture lifetime for ^{56}Ni is 2600 sec at $\rho = 10^6 \text{ g cm}^{-3}$ and 16 sec at $\rho = 10^8 \text{ g cm}^{-3}$. The importance of electron capture and its dependence upon density stem from the high concentrations of free electrons at high densities. (In contrast, there are relatively few free positrons; hence positron capture has been neglected.) For much of the region con-

sidered in the present study the most important single contributor to all beta-decay and electron-capture processes is ^{56}Ni , by virtue of its large abundance and large capture rate. For example, at $T_9 = 4.2$, $\rho = 10^8 \text{ g cm}^{-3}$, and $f = 0.35$, about 70 per cent of the total magnitude of D is attributable to electron capture in ^{56}Ni alone.

Although for most aspects of the present study nuclei with $Z > A/2$ could be neglected as having negligibly small abundances, their high rate of positron emission can make them important at low densities (where electron capture is slow) and low temperatures (where the ^{28}Si conversion is slow). Thus, at $T_9 = 3.4$ and $\rho = 10^6 \text{ g cm}^{-3}$, positron emission in ^{29}P and ^{31}S accounts for over half the magnitude of D during the early stages of ^{28}Si depletion ($f \geq 0.6$). At this point the free-proton density, n_p , has already begun to fall because of the relatively long time (1800 sec) required to reach $f = 0.6$, and thus the positron emission has had a decisive effect on the character of the abundance distribution. It is for this reason that these nuclei are included in the present calculation.

The over-all consequence of beta decay is to reduce the relative abundances of proton-rich nuclei, such as ^{56}Ni , and to raise the relative abundances of neutron-rich nuclei, such as ^{54}Fe or ^{56}Fe . As discussed above, and displayed in §§ Vc and Vd below, these effects will be strongest at low temperatures, at high densities, and late in the conversion (low f). A corollary to the sensitivity of the abundance to beta decay and electron capture is the unimportance of these processes for the over-all energy balance. If we continue to be interested in solutions corresponding to the production of a large amount of ^{56}Ni , we are limited to small values of D/N_B . Hence, even if several MeV are lost in each event through neutrino emission, the total energy loss is small compared with the total nuclear energy release. More detailed consideration of the energy balance is presented in § VI.

c) Nuclear Abundances during the Conversion

The evolution of some of the more interesting nuclear abundances is shown in Figure 11, at several values of temperature and density. Among the notable general features

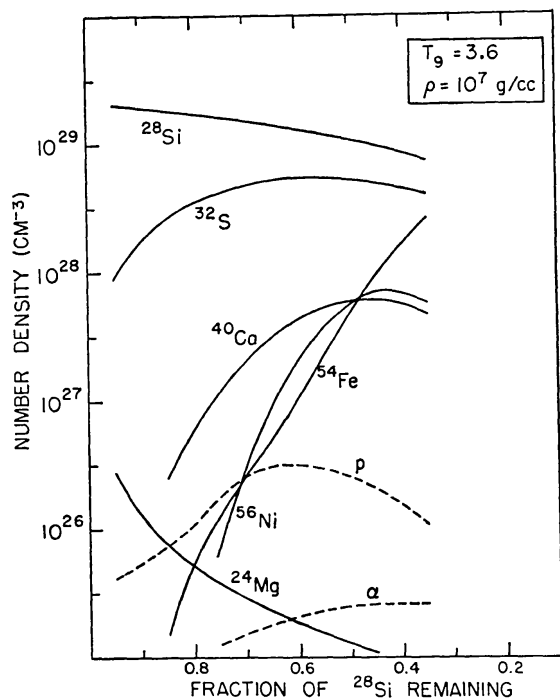


FIG. 11a

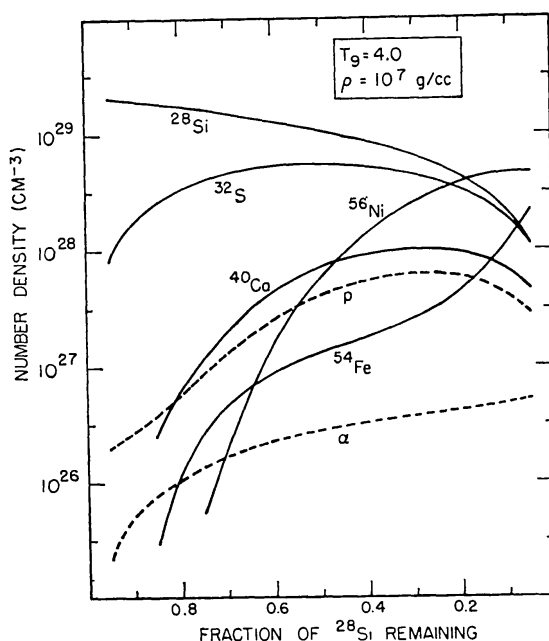


FIG. 11b

FIG. 11a.—Evolution of nuclear abundances during ^{28}Si burning at $T_9 = 3.6$ and $\rho = 10^7 \text{ g cm}^{-3}$.

FIG. 11b.—Evolution of nuclear abundances during ^{28}Si burning at $T_9 = 4.0$ and $\rho = 10^7 \text{ g cm}^{-3}$.

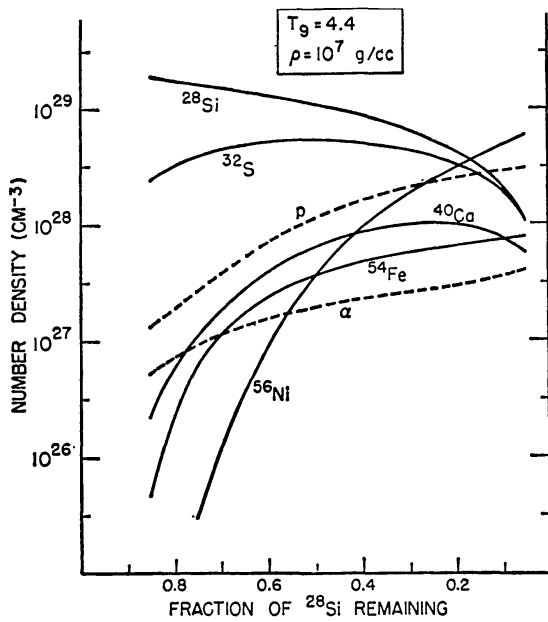


FIG. 11c

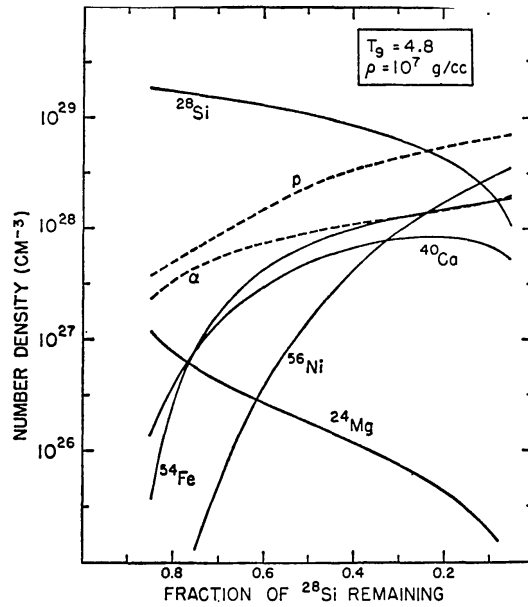


FIG. 11d

FIG. 11c.—Evolution of nuclear abundances during ^{28}Si burning at $T_9 = 4.4$ and $\rho = 10^7 \text{ g cm}^{-3}$.
 FIG. 11d.—Evolution of nuclear abundances during ^{28}Si burning at $T_9 = 4.8$ and $\rho = 10^7 \text{ g cm}^{-3}$.

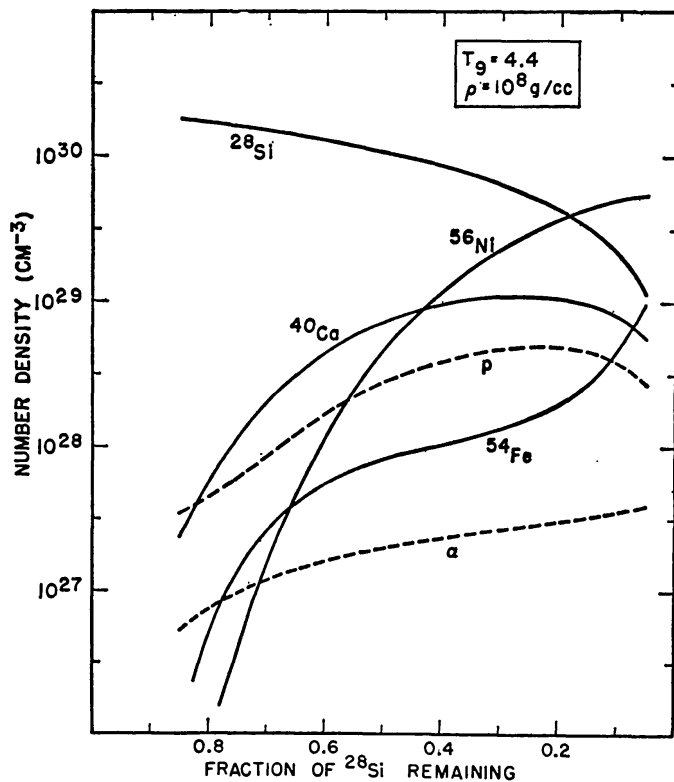


FIG. 11e.—Evolution of nuclear abundances during ^{28}Si burning at $T_9 = 4.4$ and $\rho = 10^8 \text{ g cm}^{-3}$

are (a) the monotonic rise in n_a over the region displayed; (b) the rise in n_p and its subsequent turnover when electron capture begins to take hold; (c) the interchanges in the relative magnitudes of $n(^{54}\text{Fe})$ and $n(^{56}\text{Ni})$, correlated with the magnitude of n_p ; (d) the early turnover of ^{32}S and the later turnover of ^{40}Ca , as the fall in $n(^{28}\text{Si})$ becomes more important than the rise in n_a ; and (e) the decrease in $n(^{24}\text{Mg})$, which is closely related to the decrease in the burning rate discussed above.

At smaller values of f than those illustrated in Figure 11a, the values of n_a pass through a maximum and begin to decrease. It is at this point that the iterative procedure becomes inappropriate. The phenomenon occurs when the accumulated beta decays cause dominance in the iron group to switch sufficiently from ^{56}Ni to ^{54}Fe , and thereafter to ^{56}Fe . Because n_a is proportional to $[n(^{56}\text{Ni})/n(^{28}\text{Si})]^{1/7}$, its value begins to decrease when this shift to neutron-rich nuclei causes $n(^{56}\text{Ni})$ to decrease faster than $n(^{28}\text{Si})$. The onset of this region is clearly apparent in Figure 11a, where the calculation was performed terminated near $f = 0.35$.

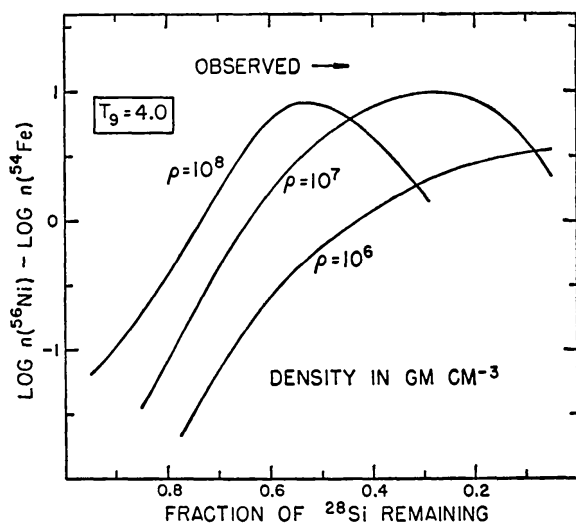


FIG. 12a

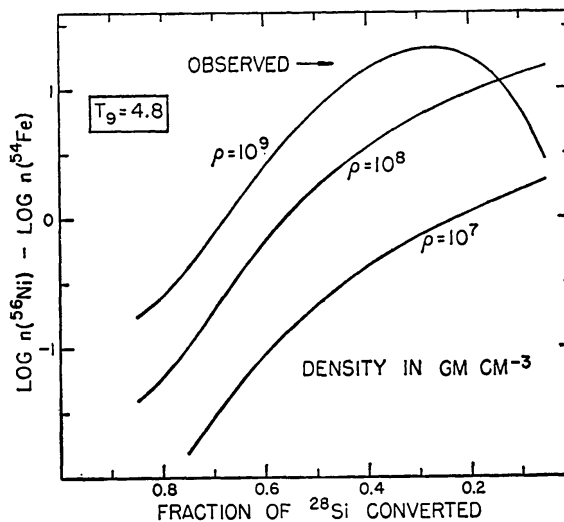


FIG. 12b

FIG. 12a.—Evolution of the ratio $n(^{56}\text{Ni})/n(^{54}\text{Fe})$ during ^{28}Si burning at $T_9 = 4.0$ for several densities. Arrow indicates observed natural magnitude (solar system) of the ratio $n(^{56}\text{Fe})/n(^{54}\text{Fe})$.

FIG. 12b.—Evolution of ratio $n(^{56}\text{Ni})/n(^{54}\text{Fe})$ during ^{28}Si burning at $T_9 = 4.8$ for several densities. Arrow indicates observed natural magnitude (solar system) of the ratio $n(^{56}\text{Fe})/n(^{54}\text{Fe})$.

The proton turnover which marks the advent of the beta-decay processes occurs near $f = 0.6$ at $T_9 = 3.6$ and $\rho = 10^7 \text{ g cm}^{-3}$ (see Fig. 11a), but at $T_9 = 4.4$ and $\rho = 10^7 \text{ g cm}^{-3}$ it does not occur until the silicon is almost entirely gone (see Fig. 11c). This reflects the fact that as the temperature increases the time rate of silicon burning rises and the decay processes do not compete so successfully. Examination of Figure 11 also shows that both n_p and n_a increase with temperature for the same values of f and density.

At the beginning of the conversion, when n_p is small, $n(^{54}\text{Fe})$ will always exceed $n(^{56}\text{Ni})$. As n_p rises, $n(^{56}\text{Ni})$ rises more rapidly than $n(^{54}\text{Fe})$ and, in the absence of beta decay, eventually becomes dominant. This dominance lasts until such time as n_p has substantially fallen because of beta decay. These characteristics can be seen in Figure 11 and are displayed more explicitly in Figures 12a and 12b, where the ratio $n(^{56}\text{Ni})/n(^{54}\text{Fe})$ is displayed as a function of the fraction of ^{28}Si remaining. Without beta decay this ratio would be highest at high densities, because then n_p is highest, and at low temperatures, because then the tendency to the dissociation $^{56}\text{Ni} \rightarrow ^{54}\text{Fe} + 2p$ is least. However, in just these conditions the decay processes are most important. The consequences of these

conflicting effects are seen in Figure 12, where at low temperatures and high densities (e.g., $T_9 = 4.0$ and $\rho = 10^8 \text{ g cm}^{-3}$) the ratio starts relatively high but soon reaches a peak and then falls. On the other hand, at high temperatures and low densities (e.g., $T_9 = 4.8$ and $\rho = 10^7 \text{ g cm}^{-3}$) the ratio starts so low that, although it rises throughout the region displayed, it is still comparatively small even when f has been reduced to values as low as $f = 0.05$. The highest values of the ratio are attained at high temperatures and high densities.

These considerations enable us to understand the results of TCG, who found ^{54}Fe to be the most abundant iron-group nucleus produced in two different special cases: one at $T_9 = 3.0$ and $\rho = 10^6 \text{ g cm}^{-3}$ and the other at $T_9 = 5.0$ and $\rho = 1.3 \times 10^7 \text{ g cm}^{-3}$. At $T_9 = 3.0$ the temperature is sufficiently low that the beta-decay and electron-capture processes have had ample time to establish ^{54}Fe as the dominant iron-group nucleus. At $T_9 = 5.0$ and $\rho = 1.3 \times 10^7 \text{ g cm}^{-3}$ the dominance of ^{56}Ni does not occur until a late stage in the burning, at values of f lower than those considered by TCG. However, in a large and important range including much of the region depicted in Figure 12, ^{56}Ni is characteristically the dominant iron-group nucleus produced in incomplete ^{28}Si burning.

d) Comparison with Natural Abundances

As discussed in § II, the natural abundances of elements in the solar system can be partially accounted for in terms of quasi-equilibrium with ^{28}Si . A comparison was presented in Figure 3 between the observed abundances and the quasi-equilibrium abundances calculated for a set of values of T , n_α , and n_p/n_n chosen to match the observed relative abundances of the alpha-particle nuclei and the observed natural ratio $n(^{56}\text{Fe})/n(^{54}\text{Fe}) = 15.7$. Values of the nucleon and alpha-particle densities which would give similar matches at other temperatures were listed in Table 2. In this section we turn to the question of whether the evolution of ^{28}Si burning carries the system through points where these particular sets of quasi-equilibrium abundances are achieved and the values, if any, of temperature and density for which this happens.

The quasi-equilibrium distribution at fixed temperature is determined by two independent parameters. Possible choices for this pair include (1) $n(^{56}\text{Ni})/n(^{54}\text{Fe})$ and f and (2) n_α and n_p/n_n . The comparison for the first set of parameters follows directly from the discussion of Figure 12. For the natural abundances discussed in § II (Cameron 1967) the fraction of mass between $A = 28$ and $A = 64$ (inclusive) which is contained in ^{28}Si is about 25 per cent if one uses the meteoritic abundance for iron or about 36 per cent if one uses one-fifth of the meteoritic abundance. Continuing to adopt the latter choice for the present analysis, we look for solutions at about $f = 0.35$ (or slightly higher if we remember from § II that type A solutions underestimate the abundances of many of the neutron-rich nuclei below the iron group). Even allowing for the possibility that the meteoritic abundance should be used for iron, a good match will not be obtained for $f \leq 0.2$. From the natural ratio for $n(^{56}\text{Fe})/n(^{54}\text{Fe})$ the quasi-equilibrium calculation should give $[\log n(^{56}\text{Ni}) - \log n(^{54}\text{Fe})] = 1.2$.

Examination of Figure 12 shows that the desired parameters are fairly closely approached but not quite reached at $T_9 = 4.0$. The action of beta decay keeps $n(^{56}\text{Ni})/n(^{54}\text{Fe})$ from rising above about 10 at any density. On the other hand, at $T_9 = 4.8$ the desired point is reached, at densities slightly below $\rho = 10^9 \text{ g cm}^{-3}$.

An analogous comparison for the second set of parameters is made in Figure 13, where evolutionary tracks of n_p/n_n are plotted at several temperatures and densities. The "target point," i.e., the best-fit values at each temperature from Table 2, are also displayed in the figure. This point depends upon the temperature but is independent of the density. Characteristically one sees, as n_α increases, that n_p/n_n rises until such time as beta decay causes it to peak and subsequently begin to fall. This falloff in n_p/n_n appears to exclude solutions at temperatures as low as $T_9 = 3.8$. At $T_9 = 4.0$ there is somewhat better success but still not a very good match. The effect of the beta decay is

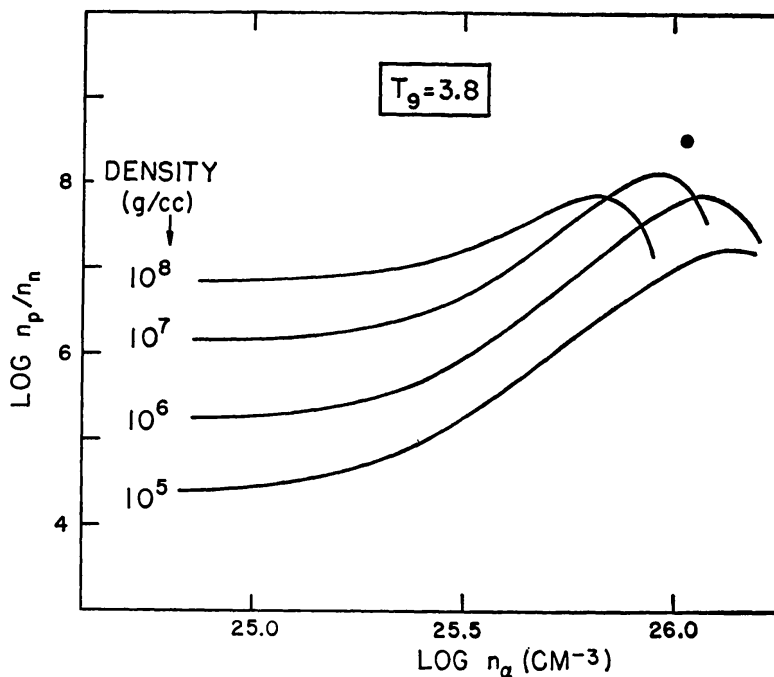


FIG. 13a.—Evolution during ^{28}Si burning at $T_9 = 3.8$ of the ratio n_p/n_n as a function of n_α for several densities. Circled cross represents the best match at $T_9 = 3.8$ to the natural solar-system abundances; its coordinates are taken from Table 2.

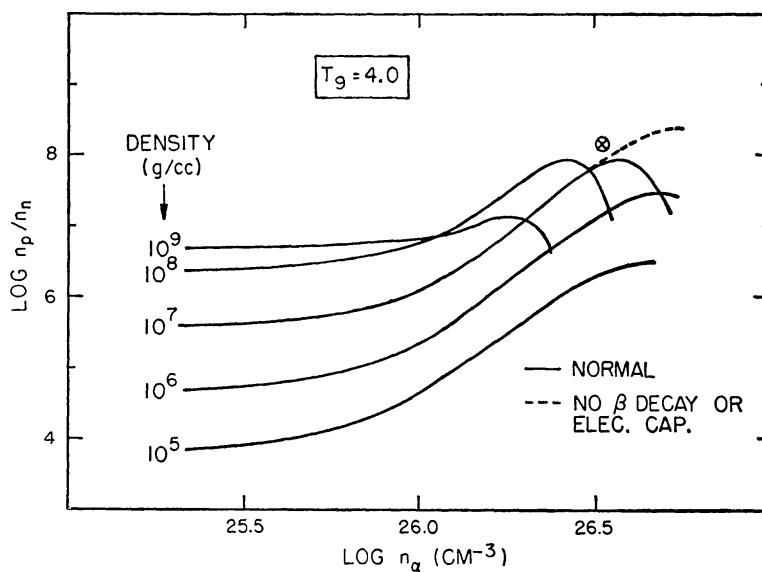


FIG. 13b.—Evolution during ^{28}Si burning at $T_9 = 4.0$ of the ratio n_p/n_n as a function of n_α for several densities. Circled cross represents the best match at $T_9 = 4.0$ to the natural solar-system abundances; its coordinates are taken from Table 2. Dotted line indicates evolution at $\rho = 10^7 \text{ g cm}^{-3}$ were there no beta decay or electron capture.

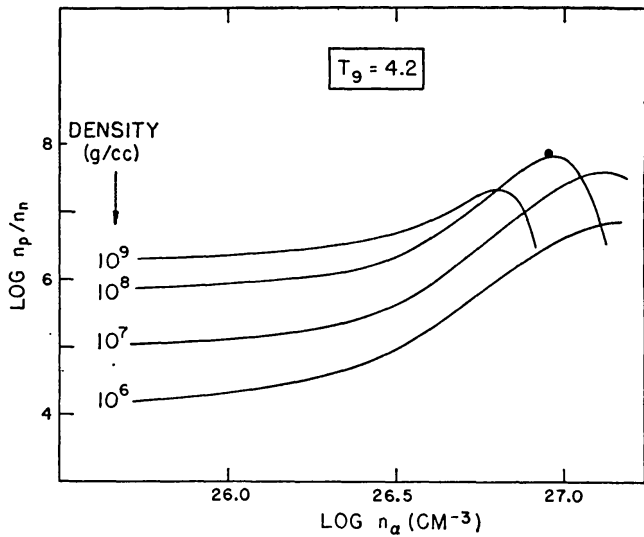


FIG. 13c

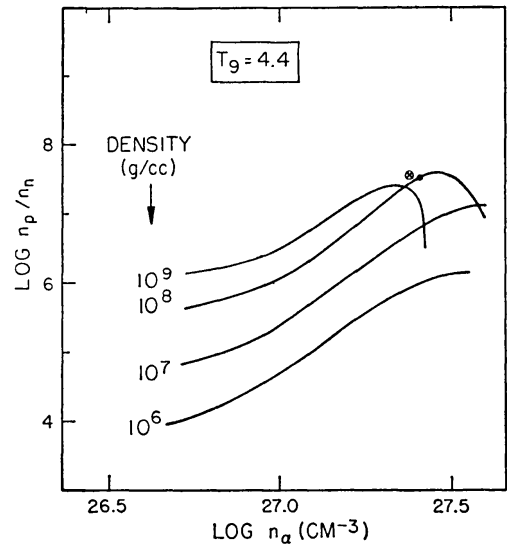


FIG. 13d

FIG. 13c.—Evolution during ^{28}Si burning at $T_9 = 4.2$ of the ratio n_p/n_n as a function of n_a for several densities. Circled cross represents the best match at $T_9 = 4.2$ to the natural solar-system abundances; its coordinates are taken from Table 2.

FIG. 13d.—Evolution during ^{28}Si burning at $T_9 = 4.4$ of the ratio n_p/n_n as a function of n_a for several densities. Circled cross represents the best match at $T_9 = 4.4$ to the natural solar-system abundances; its coordinates are taken from Table 2. Solid dot corresponds to the point at $\rho = 10^8 \text{ g cm}^{-3}$ where $f = 0.35$; the abundance distribution of Fig. 14a corresponds to this point.

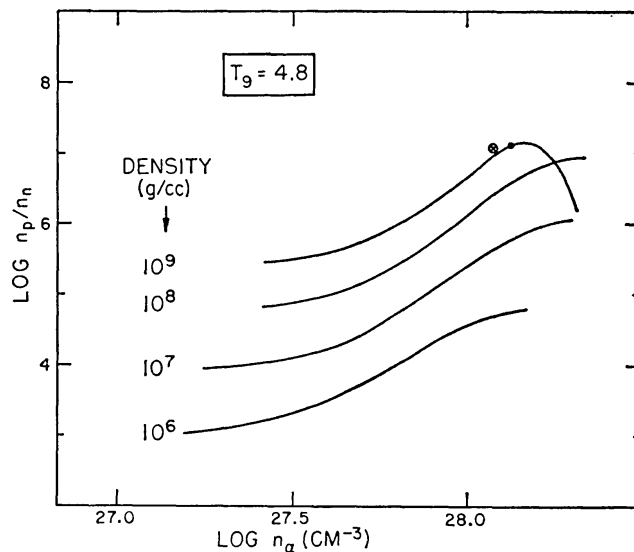


FIG. 13e.—Evolution during ^{28}Si burning at $T_9 = 4.8$ of the ratio n_p/n_n as a function of n_a for several densities. Circled cross represents the best match at $T_9 = 4.8$ to the natural solar-system abundances; its coordinates are taken from Table 2. Solid dot corresponds to the point at $\rho = 10^9 \text{ g cm}^{-3}$ where $f = 0.35$; the abundance distribution of Fig. 14b corresponds to this point.

explicitly displayed at $\rho = 10^7 \text{ g cm}^{-3}$, where the results of a calculation with no decay are also shown. Were it not for the decay, a trajectory for a density of about $3 \times 10^7 \text{ g cm}^{-3}$ would pass through the desired point.

Results displayed in Figures 13c–13e indicate that good fits can be achieved at temperatures between $T_9 = 4.2$ and $T_9 = 4.8$. In each case, one of the plotted curves passes close to the point, and with intermediate choices of density still better fits can be obtained. Extrapolation of the present results indicates that a similarly good fit can be obtained at $T_9 = 5.0$, for a density somewhat above $\rho = 10^9 \text{ g cm}^{-3}$.

Above $T_9 = 5.0$ one will find it increasingly difficult to match the abundances of the alpha-particle nuclei as a whole. While an arbitrary desired value of n_α might be attained in the evolution of ^{28}Si , examination of Figure 5 shows that no value of n_α will provide

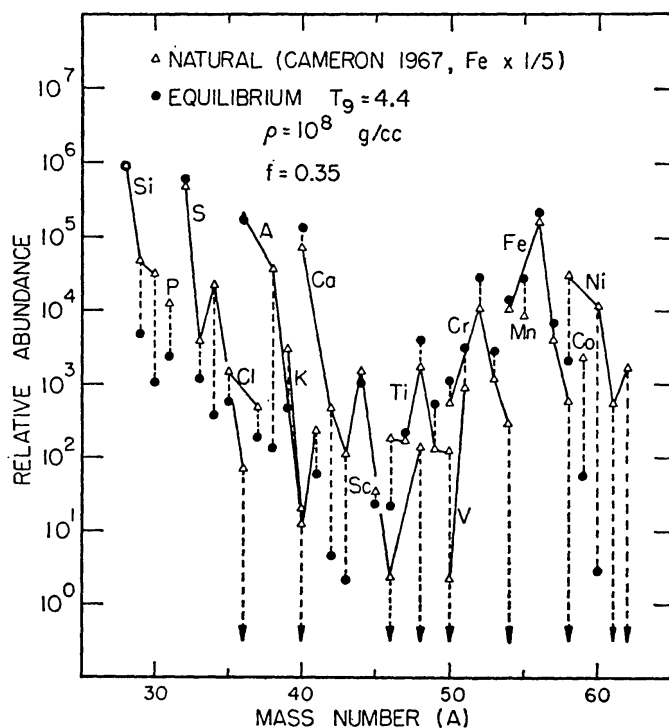


FIG. 14a.—Comparison of natural solar-system abundances with quasi-equilibrium abundances reached in ^{28}Si burning at $T_9 = 4.4$, $\rho = 10^8 \text{ g cm}^{-3}$, and $f = 0.35$.

simultaneous fits for the entire group. In fact, even the fit at $T_9 = 5.0$ is of marginal quality. Were one to use the meteoritic abundance for iron, rather than one-fifth of this abundance, the ^{56}Ni point would be raised, making the agreement still worse at high temperatures.

A more detailed comparison of calculated and observed abundances may be made by exploring the success of the present solutions in matching the abundances of the nuclei between $A = 28$ and $A = 62$. A comparison of this sort has already been made at $T_9 = 4.2$ in Figure 3. The values used, $\log n_\alpha = 26.96$ and $\log (n_p/n_n) = 7.86$, were selected a priori for a good fit. However, as can be seen in Figure 13c, the evolutionary track at $\rho = 10^8 \text{ g cm}^{-3}$ passes quite close to this point, going through $\log (n_p/n_n) = 7.82$ at $\log n_\alpha = 26.96$. This implies a 5 per cent disagreement in the value of n_p and a 10 per cent disagreement in the ratio $n(^{56}\text{Ni})/n(^{54}\text{Fe})$. Such discrepancies are too small to note in Figure 3, and this figure is an excellent representation of the abundances from ^{28}Si burning at $T_9 = 4.2$ and $\rho = 10^8 \text{ g cm}^{-3}$ for $f = 0.4$.

Similar abundance comparisons at $T_9 = 4.4$ and $T_9 = 4.8$ are shown in Figures 14a

and 14*b* for points (indicated by heavy dots) on the evolutionary tracks in Figure 13. These points, both for $f = 0.35$, are close to the target points from Table 2 but do not exactly match them. Because of the slightly high value of n_α at $T_9 = 4.4$, the calculated value of $n(^{56}\text{Ni})$ is slightly too high in Figure 14*a*. Otherwise the fit at $T_9 = 4.4$ is about as good as can be obtained for any type *A* solution at this temperature. At $T_9 = 4.8$, the value used for n_α is again higher than the best-fit value. As might be anticipated from examination of Figure 5, this results in a good match at $A = 56$ but a sizable discrepancy at $A = 48$ and 52. The growing inability to match simultaneously the abundances of all the alpha-particle nuclei argues against pursuing the ^{28}Si -burning calculation above $T_9 = 5.0$.

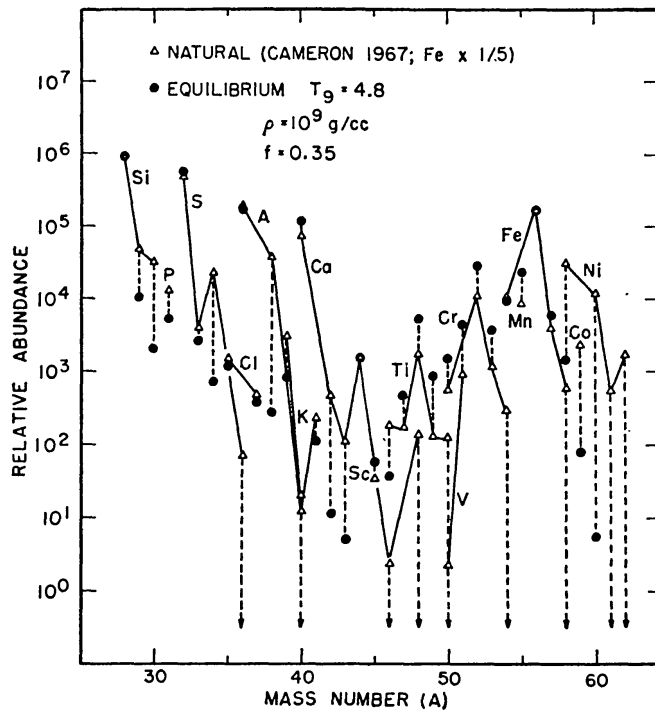


FIG. 14*b*.—Comparison of natural solar-system abundances with quasi-equilibrium abundances reached in ^{28}Si burning at $T_9 = 4.8$, $\rho = 10^9 \text{ g cm}^{-3}$, and $f = 0.35$.

We conclude that for temperatures between $T_9 = 4.0$ and $T_9 = 5.0$, ^{28}Si burning can indeed lead naturally to alpha-particle and nucleon densities which give the natural abundances of the alpha-particle nuclei and the natural ratio $n(^{56}\text{Fe})/n(^{54}\text{Fe})$. For the lower temperatures this occurs at densities between $\rho = 10^7 \text{ g cm}^{-3}$ and $\rho = 10^8 \text{ g cm}^{-3}$ and at the higher temperatures near $\rho = 10^9 \text{ g cm}^{-3}$. A precise delineation of a region of acceptable fits or a search for the very best fit among the acceptable fits is not attempted. It is most unlikely that the observed solar-system abundances are the consequences of processes limited to one single temperature and density. Therefore, quantitative comparisons of observations with results calculated at a single constant temperature and density are of interest for illustrative purposes only. *The important conclusion of the present analysis is that there exists a region, extending from about $T_9 = 3.8$ and $\rho = 10^7 \text{ g cm}^{-3}$ to $T_9 = 5.0$ and $\rho = 10^9 \text{ g cm}^{-3}$, within which a superposition of ^{28}Si -burning histories, over a range of temperatures and densities, can account for important features of the natural solar-system abundances. In particular, they account for the abundances of the $A = 4n$ nuclei and the abundances of the dominant iron-group nuclei from $A = 49$ to $A = 57$. The quasi-equilibrium abundances of the remaining nuclei between $A = 28$ and $A = 62$ are less than the natural abundances, and secondary processes must therefore be invoked to explain these abundances.*

A comment on this analysis can be made for burning in which other alpha-particle nuclei, most probably ^{24}Mg and ^{32}S , may be present initially in appreciable quantities. These nuclei undergo photodisintegration more rapidly than does ^{28}Si , and this leads to a quasi-equilibrium with ^{28}Si in a considerably shorter time than in pure silicon burning. The burning of a gas in which initially $^{32}\text{S}/^{28}\text{Si} = 2$, for example, achieves a silicon quasi-equilibrium with a silicon mass fraction equal to 0.5 faster than the value $f = 0.5$ is achieved in the burning of pure ^{28}Si . The quasi-equilibrium abundance distributions are identical if beta decays have been unimportant. For evolutionary tracks like those in Figure 13, however, the shortened time can have the effect of delaying the turnover in n_p/n_n . A thorough analysis of the silicon quasi-equilibrium when beta decays have been effective therefore depends upon the initial composition. The final products of carbon and oxygen burning, which serve as the initial composition for silicon burning, are not yet well established. It may, in fact, happen that carbon or oxygen burning merges continuously into a silicon quasi-equilibrium. This point needs further research for its clarification.

VI. THERMONUCLEAR ENERGY GENERATION

The determination of the rate of thermonuclear energy generation is essential to the understanding of the relationship between the nuclear processes and the possible stellar environment. As an aid toward the eventual development of a self-consistent picture for this relationship, we here consider the energy generation under idealized conditions of constant temperature and pressure. We first discuss the total amount of nuclear energy that has been liberated at given stages in the burning process, and then we discuss the time rate of the nuclear energy generation.

The conversion of ^{28}Si to the iron group is, for the most part, accompanied by a decrease in rest mass and a release of nuclear energy, because the binding energy per nucleon increases as one proceeds along the nuclear stable valley from $A = 28$ to $A = 56$. An exception to this primarily exoergic trend is provided by the disintegration of ^{28}Si into lighter elements, particularly protons and alpha particles. In the conditions of the present study, the protons are particularly important in energy considerations because of the large energy expended in the production of free nucleons (8.4 MeV per nucleon) and because the number densities of free protons are large (usually in excess of the alpha-particle number density). As will be discussed further below, the role of the free protons is very appreciable near the high end of the range of temperatures considered ($T_9 = 5.0$), but over most of the temperature interval of interest the exoergic production of iron-group elements is dominant.

The nuclear energy released in reaching any stage of the ^{28}Si conversion can be calculated from the number densities and masses of the constituents. In the present program it was calculated at each step of the iteration from the expression for the mass decrease, ΔM :

$$\Delta M = \sum A n(^A Z) \left[\frac{E(^{28}\text{Si})}{28} - \frac{E(^A Z)}{A} \right], \quad (33)$$

where E is the mass excess per atom, and the summation is taken over all nuclear species, including free nucleons. Results of these calculations are shown for several representative cases in Figures 15 and 16. The energy released per (converted) nucleon, $\Delta M/N_B(1-f)$, is plotted in Figure 15 as a function of the fraction f of ^{28}Si remaining and in Figure 16 as a function of the density ρ . Several trends are apparent:

1. After an initial endoergic stage when the abundance of ^{24}Mg and lighter constituents is first built up, the energy released per nucleon increases as the ^{28}Si depletion progresses (at constant temperature and density). For a broad intermediate interval following this initial period, the most abundant nucleus other than ^{28}Si is ^{32}S , for which the energy released is 45 keV per nucleon. The dominance of ^{32}S in determining the energy

released is particularly striking at $T_9 = 4.0$, $\rho = 10^7 \text{ g cm}^{-3}$, and $f = 0.65$, when together ^{28}Si and ^{32}S contain 92 per cent of the nucleons, and the energy released has been about 52 keV per converted nucleon. Still later in the conversion the iron-group nuclei become the most important. The energy released is 195 keV per nucleon for ^{56}Ni production and 290 keV per nucleon for ^{54}Fe production. It is to be noted that the process $2 \text{ }^{28}\text{Si} \rightarrow ^{54}\text{Fe} + 2p$ is endoergic (-23 keV per nucleon) but that the production of ^{54}Fe itself is exoergic if the free-proton density is kept low by the nuclear rearrangements consequent upon electron capture. This distinction is relevant for the present purposes because both situations are encountered. We can consider two examples, both at $\rho = 10^7 \text{ g cm}^{-3}$ and

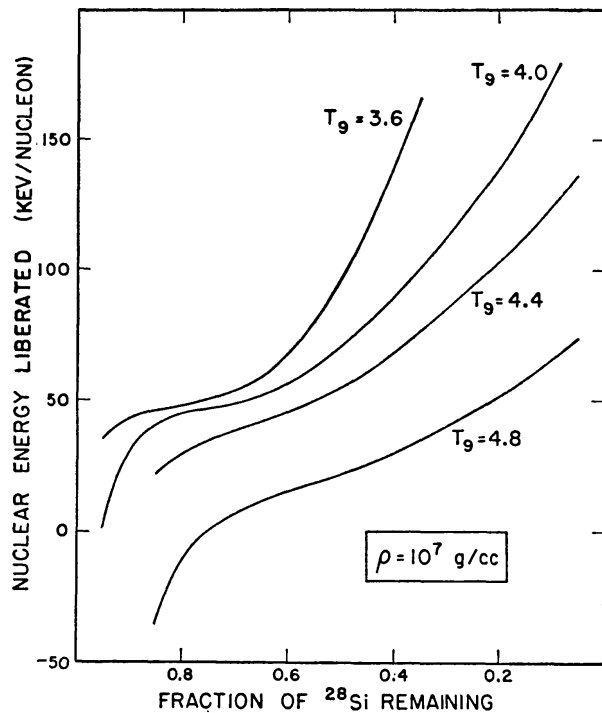


FIG. 15

FIG. 15.—Cumulative nuclear energy released in ^{28}Si burning. Ordinate is cumulative energy release per converted nucleon, $\Delta M/N_B(1-f)$, at $\rho = 10^7 \text{ g cm}^{-3}$ for several temperatures.

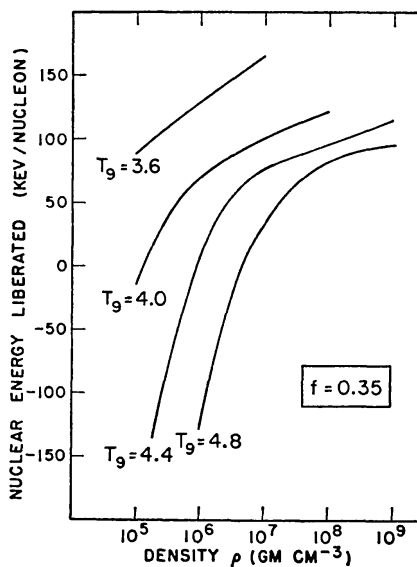


FIG. 16

FIG. 16.—Dependence on density of nuclear energy released in ^{28}Si burning. Ordinate is cumulative energy released per converted nucleon, $\Delta M/N_B(1-f)$, at $f = 0.35$ for several temperatures.

$f = 0.35$, in cases in which $n(^{54}\text{Fe}) > n(^{56}\text{Ni})$. At $T_9 = 3.6$ the conversion has been slow enough to allow appreciable beta decay and electron capture, \bar{Z}/\bar{N} being reduced to 0.981. Here $n(^{54}\text{Fe})/n(^{56}\text{Ni}) = 5$ and $n_p/n(^{54}\text{Fe}) = \frac{1}{2.50}$. Thus the endoergic proton production is unimportant. On the other hand, at $T_9 = 4.8$, $n(^{54}\text{Fe})/n(^{56}\text{Ni}) = 2$, and thus ^{54}Fe again is the main iron-group nucleus, but $n_p/n(^{54}\text{Fe}) = 4$ and the net effect of ^{54}Fe production is endoergic.

2. At a given ^{28}Si depletion and density, the energy released decreases with increasing temperatures. This trend is a result of the greater dissociation into free protons and alpha particles. Again considering the case $\rho = 10^7 \text{ g cm}^{-3}$ and $f = 0.35$, this dissociation accounts for the difference in energy liberation at $T_9 = 4.0$, where $n(^{56}\text{Ni}) > n(^{54}\text{Fe})$, and at $T_9 = 4.8$, where the ^{56}Ni has been, in effect, partially dissociated into $^{54}\text{Fe} + 2p$.

3. For fixed temperature and ^{28}Si fraction, the energy released per nucleon increases with increasing density. This effect arises because the magnitudes of n_p and n_α are stabilized by the abundance ratios $n(^AZ)/n(^{28}\text{Si})$. These ratios vary relatively slowly with density at fixed f , whereas the magnitudes of $n(^AZ)$ are approximately proportional

to the density. Thus the protons and alpha particles constitute a decreasing fraction of the total mass as the density increases, and their endoergic production becomes less significant.

In summary, we see from Figures 15 and 16 (and more extensively from Table 4) that, for a wide range of conditions relevant to ^{28}Si burning, the energy released has been between 50 and 200 keV per converted nucleon. However, the energy liberation can be substantially less than 50 keV at sufficiently high temperatures, at sufficiently low densities, or early enough in the ^{28}Si burning. In fact, under conditions which are not very extreme, the burning can consume rather than produce energy.

While the foregoing considerations are of interest for the understanding of the nuclear energetics, the more important quantity for astrophysical problems is the time rate of nuclear energy generation. For circumstances in which the energy released per nucleon can be taken to be roughly constant (e.g., 50–200 keV per converted nucleon), this time rate of nuclear energy generation is proportional to the time rate of ^{28}Si depletion.

A model for the calculation of the energy generation has been developed by Finzi and Wolf (1966), under the simplifying assumption that ^{56}Ni is the major product of ^{28}Si conversion and, in the spirit of this approximation, that the energy contribution of other constituents may be ignored. We reproduce their argument, with minor modifications.

Assume that each photodisintegration of ^{28}Si , which is assumed to occur at the rate $\lambda_{\gamma\alpha}(^{24}\text{Mg})n(^{24}\text{Mg})$, results in the reaction $^{28}\text{Si} + ^{28}\text{Si} \rightarrow ^{56}\text{Ni} + 10.92 \text{ MeV}$. It is then elementary to show that the lifetime of ^{28}Si is

$$\begin{aligned} \frac{1}{\tau(^{28}\text{Si})} &= 10^{35.72} \left(\frac{T_9}{4}\right)^{3/2} \left[\frac{n(^{28}\text{Si})}{n(^{56}\text{Ni})}\right]^{1/7} \langle\sigma_{\alpha,\gamma}(^{20}\text{Ne})v_{\alpha}\rangle e^{-142.07/T_9} \\ &\simeq 10^{15.88} \left(\frac{T_9}{4}\right)^{3/2} \left[\frac{n(^{28}\text{Si})}{n(^{56}\text{Ni})}\right]^{1/7} e^{-157.50/T_9} \text{ sec}^{-1} \end{aligned} \quad (34)$$

and the time rate of energy release, ϵ , is then

$$\epsilon \simeq 1.74 \times 10^{-5} \frac{n(^{28}\text{Si})}{2\rho\tau(^{28}\text{Si})} \text{ ergs g}^{-1} \text{ sec}^{-1}. \quad (35)$$

With the additional approximation that $X(^{28}\text{Si}) + X(^{56}\text{Ni}) = 1$, which is consistent with the assumption that the basic reaction is $2 ^{28}\text{Si} \rightarrow ^{56}\text{Ni}$, one would insert in the expression for τ the approximation

$$\frac{n(^{28}\text{Si})}{n(^{56}\text{Ni})} \simeq \frac{2f}{1-f} \quad (36)$$

and obtain therefrom expressions for τ and for ϵ that depend only upon f and T_9 . Thus

$$\epsilon = 10^{33.154} \left(\frac{T_9}{4}\right)^{3/2} f \left(\frac{2f}{1-f}\right)^{1/7} e^{-157.50/T_9} \text{ ergs g}^{-1} \text{ sec}^{-1}. \quad (37)$$

This calculation focuses more clearly on the crucial issues than did previous ones and has the merit of physical simplicity. However, several of its assumptions are not always well satisfied:

1. In taking ^{56}Ni to be the only product of ^{28}Si conversion, the calculation overestimates the alpha-particle density and therefore underestimates the concentration of ^{24}Mg in equilibrium with ^{28}Si . Thus ϵ is underestimated. This effect is particularly pronounced at low values of f , where $n(^{56}\text{Ni})$ is very low; at low temperatures ($T_9 \leq 3.6$), where the action of beta decay and electron capture cause ^{54}Fe to be the dominant iron-group product; and at high temperatures ($T_9 \geq 4.8$), where the dissociation $^{56}\text{Ni} \rightarrow ^{54}\text{Fe} + 2p$ is favored. However, even large fractional errors in $n(^{56}\text{Ni})$ lead to compara-

tively small fractional errors in ϵ , because the dependence is only through a term in $[n(^{56}\text{Ni})]^{1/7}$.

2. The production of nuclei other than ^{56}Ni leads to an energy release which is usually less than for ^{56}Ni alone. As was seen in Figure 14, a typical average for the energy liberated (at $T_9 = 4.0$) is about 100 keV per nucleon, corresponding to an overestimate in ϵ of about a factor of 2. Near $T_9 = 5.0$ the error in ϵ can be much larger.

3. In assuming a downward flow from ^{28}Si equal to $\lambda_{\gamma\alpha}(^{24}\text{Mg})n(^{24}\text{Mg})$, the calculation neglects the upward flow from alpha-particle capture in ^{20}Ne and thereby overestimates ϵ (see Fig. 8). The error is greatest at high temperatures and near the end of the conversion.

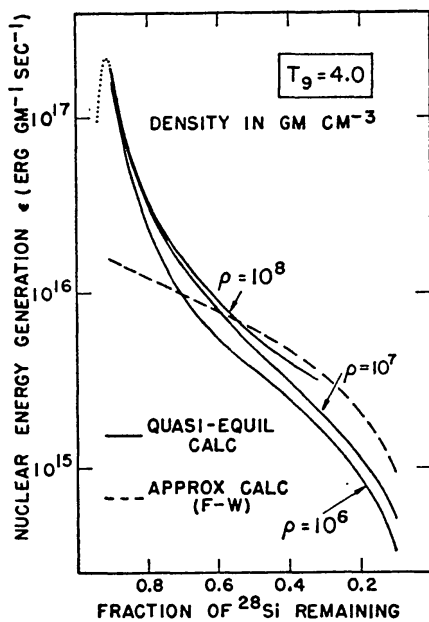


FIG. 17

FIG. 17.—Time rate of nuclear energy generation in ^{28}Si burning as a function of the fraction f of ^{28}Si remaining. Solid curves are from the present calculation at $T_9 = 4.0$ for several densities. Dotted curve is from an approximate (density-independent) calculation by Finzi and Wolf (1966).

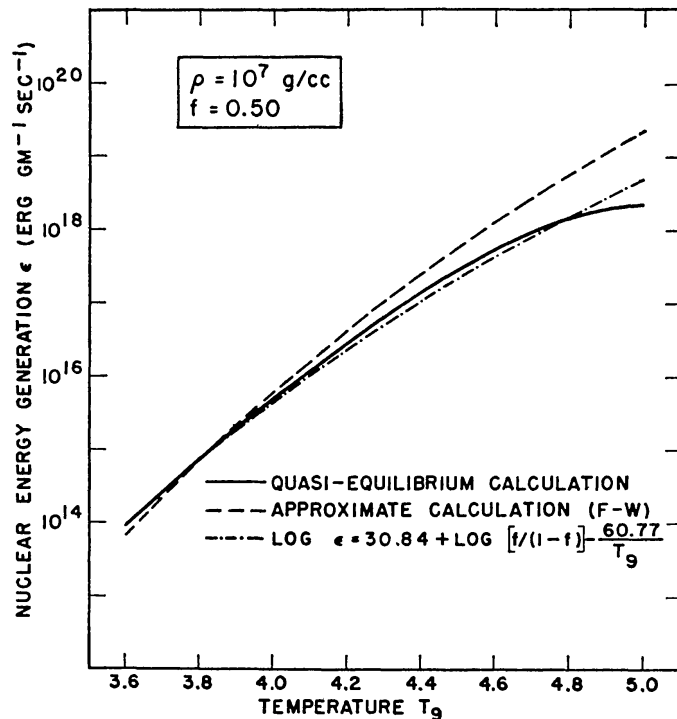


FIG. 18

FIG. 18.—Time rate of nuclear energy generation in ^{28}Si burning as a function of temperature, at $f = 0.5$. Solid curve is from the present calculation at $\rho = 10^7 \text{ g cm}^{-3}$. Dotted curves are from (a) an approximate (density-independent) calculation by Finzi and Wolf (1966); and (b) an empirical match to the solid curve near its end points.

A more precise determination of ϵ , which avoids these approximations, is possible through the quasi-equilibrium calculation described in § V. At each step of the iteration, ϵ can be calculated from the increment in ΔM and from the time interval. Results of such calculations are displayed in Figures 17 and 18. These results show that ϵ increases rapidly with increasing temperature, that ϵ decreases as the conversion proceeds to smaller f , and that ϵ is relatively insensitive to density. These dependences can be understood in terms of the time rate for ^{28}Si conversion, discussed in § Va, or from the qualitatively equivalent model of Finzi and Wolf.

The results of the Finzi-Wolf model are also shown in Figures 17 and 18. It is seen that the main trends of the present, more complete calculation are well reproduced and that the quantitative agreement is reasonably good over large regions. However, there are discrepancies of about a factor of 10 at extreme points in these figures, and even greater discrepancies exist at still less representative points.

A somewhat better match to the quasi-equilibrium calculation is given by the empirical expression:

$$\log \epsilon \simeq 30.84 + \log [f/(1 - f)] - 60.77/T_9. \quad (38)$$

This expression is similar to the expression from the Finzi-Wolf analysis but differs slightly in functional form and in parameters. It is intended to match the results of the quasi-equilibrium calculation at $\rho = 10^7 \text{ g cm}^{-3}$, which are displayed in Figures 17 and 18. In particular, it gives an exact match at $\rho = 10^7 \text{ g cm}^{-3}$, $f = 0.5$, for $T_9 = 3.6$ and $T_9 = 4.8$. It gives a good match at intermediate temperatures, as seen in Figure 17. The match is not quite so successful at other values of f , as can be shown by a comparison (not plotted) with the results in Figure 17. It is to be emphasized that this empirical expression can be relied on only near $T_9 = 4.0$, $\rho = 10^7 \text{ g cm}^{-3}$, and $f = 0.5$. It is particularly deficient in that it contains no dependence on density, which, as seen in Figure 16, is a serious failing at low densities and high temperatures. For more accurate representations of the results of the quasi-equilibrium calculation, the reader is referred to Table 4.

The rate of nuclear energy generation, ϵ , can be compared to other energy sources and sinks which may exist in the stellar environment. The case $T_9 = 4.2$ and $\rho = 10^8 \text{ g cm}^{-3}$ will be considered as a somewhat typical situation, in the sense that here the quasi-equilibrium abundances and the natural solar-system abundances are in relatively good agreement. Under these conditions the energy release is roughly between 10^{17} and 10^{16} ergs $\text{g}^{-1} \text{ sec}^{-1}$ for f between 0.6 and 0.2. The cumulative energy which has been liberated at $f = 0.35$, reached at $t = 1.8 \text{ sec}$, is 7×10^{16} ergs g^{-1} or about 70 keV per nucleon (considering all nucleons, not just the converted nucleons). In the brief time interval required to reach $f = 0.35$, beta decay and electron capture can account for less than 2 per cent of this energy in neutrino losses. Neutrino luminosity from pair annihilation accounts for only about 1 per cent of the total energy (Fowler and Hoyle 1964, eq. [21]). Increases in thermal kinetic energy due to an increase in temperature or in the number of nuclear particles can also account for only a small fraction of the total energy output. Finally, it can be noted that the energy release of 7×10^{16} ergs g^{-1} corresponds to a velocity of about 3600 km sec^{-1} , if all converted to kinetic energy, which does not differ greatly from possible speeds of the mantle plus envelope in typical type II supernovae (as discussed by Fowler and Hoyle 1964, p. 58).

VII. THE APPROACH TO QUASI-EQUILIBRIUM

The quasi-equilibrium with ^{28}Si cannot be established at once. As the first alpha particles are liberated by the photodisintegration of ^{28}Si , they are consumed in a simple flow from ^{28}Si toward the iron group. The heavier elements must build up in abundance before their own photodisintegration becomes prominent enough to balance (approximately) the capture flow coming from smaller atomic weight. It is at this point, when the rate of formation of ($^A Z$) from lighter nuclei and the rate of destruction of ($^A Z$) to lighter nuclei substantially exceed $dn(^A Z)/dt$, that the quasi-equilibrium assumption becomes a good approximation. Thus a minimum test for quasi-equilibrium is that the production and destruction rates for each nuclear species be much greater than the rate of change of the abundance of that nucleus as computed from two successive quasi-equilibrium distributions. This condition is, however, not sufficient to guarantee that the quasi-equilibrium could have been established. It only guarantees that the equilibrium, once achieved, can be maintained.

The most serious obstacle in ^{28}Si burning for the attainment of equilibrium is connected with the abundance minimum near $A = 44$. Reference to Figures 3 and 14 illustrates that the quasi-equilibrium abundances in this region are several orders of magnitude smaller than the abundances on either side. The danger to quasi-equilibrium is that the current through this abundance minimum may not be large enough to provide for the

buildup of the more abundant iron peak. The relevant nuclear reaction rates, calculated from nuclear systematics, have been tabulated by TCG. Inspection of these rates suggests that there is indeed a bottleneck at ^{44}Ti . The ^{44}Ti quasi-equilibrium abundance is typically a factor of 100 less than that of ^{40}Ca . The upward flow from ^{44}Ti is carried primarily by the $^{44}\text{Ti}(\alpha, p)^{47}\text{V}$ and $^{44}\text{Ti}(n, \gamma)^{45}\text{Ti}$ reactions. The (α, p) reaction wins over the competing (α, γ) reaction because the (α, p) Q -value is -0.5 MeV, and proton emission from the compound nucleus ^{48}Cr is more probable than gamma emission for typical incident alpha-particle energies of about 5 MeV. Other reactions, such as $^{42}\text{Ca}(\alpha, p)^{45}\text{Sc}$, sometimes contribute appreciably, but they are not the dominant paths. The rate at

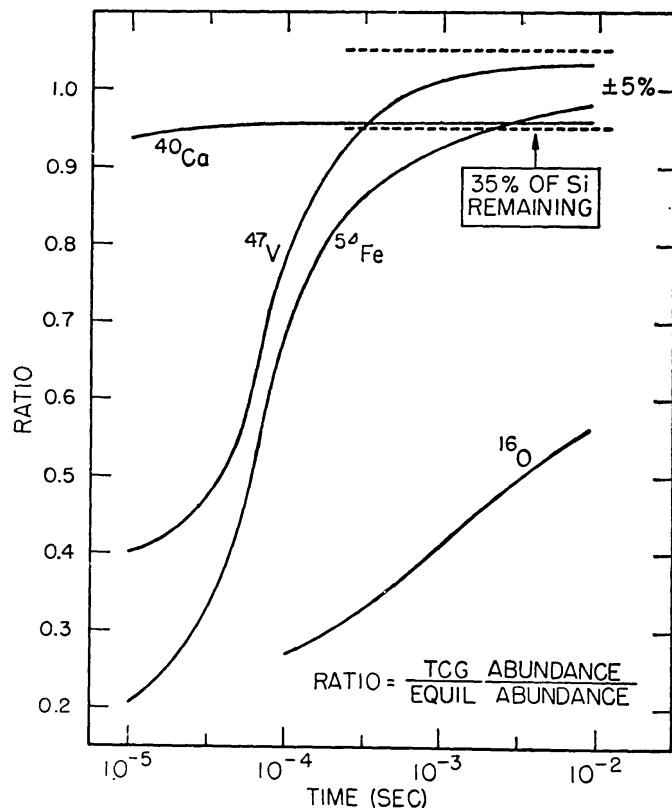


FIG. 19.—Approach to quasi-equilibrium in ^{28}Si burning. Abundances calculated by Truran, Cameron, and Gilbert (1966) are compared with quasi-equilibrium abundances obtained by using the TCG values of n_α , n_p , and n_n in eq. (3). Horizontal dotted lines represent a region (± 5 per cent) in which disagreements may be attributed to computational errors rather than to a violation of quasi-equilibrium.

which nuclei pass from $A \leq 44$ to $A > 44$ is thus largely dependent on $n(^{44}\text{Ti})$, n_α , and n_n . If these concentrations are not sufficiently great to provide for the rate of growth of the entire iron peak, the abundances of the iron group will lag behind their quasi-equilibrium values.

This lag does occur, as can be seen by examining the extent to which the results of the TCG numerical integration at $T_9 = 5.0$ and $\rho = 1.3 \times 10^7 \text{ g cm}^{-3}$ correspond to quasi-equilibrium. In Figure 19 we have plotted the variation with time of the ratios of the concentrations of ^{16}O , ^{40}Ca , ^{47}V , and ^{54}Fe , as given by TCG, to the quasi-equilibrium values from equation (3). The TCG densities for $n(^{28}\text{Si})$, n_α , n_p , and n_n , at the successive times, were used in the later calculation. It can be seen that ^{40}Ca attains its quasi-equilibrium value almost at once, whereas ^{47}V and ^{54}Fe lag appreciably. However, for these nuclei as well, the quasi-equilibrium abundances and the TCG abundances have reached good agreement (within 5 per cent) by the time that the ^{28}Si fraction has been reduced to $f = 0.35$. (The fact that the TCG abundance for ^{54}Fe does not quite

reach the quasi-equilibrium value even by the end of the period considered is not taken as evidence that quasi-equilibrium is not attained. For other iron-group nuclei, not included in Fig. 19, the TCG abundance exceeds the quasi-equilibrium abundance by several per cent. Discrepancies of a few per cent are not considered here to be computationally significant.) It should be added that n_a , n_p , and n_n attain their internal equilibrium much earlier in the burning. On the other hand, $n(^{16}\text{O})$ does not reach its equilibrium value even by the end of the period considered and must be determined in a quite different fashion, as discussed in § III.

The time scale in Figure 19 is taken from TCG, and that comparison is concerned only with questions of abundance and not with time. However, it has already been seen in Figure 10 and the associated discussion that the time scales are in good agreement for the TCG calculation and the present calculation. It is concluded from these and other comparisons that quasi-equilibrium is a good representation of the actual conditions of ^{28}Si burning at $T_9 = 5.0$ and $\rho = 1.3 \times 10^7 \text{ g cm}^{-3}$ after the ^{28}Si concentration has been reduced below $f = 0.5$. Although the agreement is not good during the relatively rapid first stages of the burning, we are in fact primarily interested in the later stages, because it is here, near $f = 0.35$ or 0.40 , that a match to the natural abundances is sought.

The case $T_9 = 5.0$ and $\rho = 1.3 \times 10^7 \text{ g cm}^{-3}$ has been examined in particular detail because it provides the one example in which the quasi-equilibrium results can be compared in detail with those of TCG. It does not, however, represent the most probable conditions for ^{28}Si burning. The situation at other temperatures and densities, as well as for this case, can, in principle, be examined through an analysis of the internal consistency of the quasi-equilibrium calculation, without recourse to comparisons such as the one made with the TCG results. The criterion for quasi-equilibrium to be established in the face of a bottleneck at ^{44}Ti is that the total number of reactions at this bottleneck be large compared to the quasi-equilibrium number of nuclei above ^{44}Ti . Thus, for quasi-equilibrium to be valid at time t , it is required that

$$\int_0^t r(\tau) d\tau \gg \sum_{A > 44} n(^A Z, t), \quad (39)$$

where $r(\tau)$ is the sum of the contributing reaction rates at time τ and $n(^A Z, t)$ is the number density of $(^A Z)$ at time t . The term in r from the $^{44}\text{Ti}(a, p)^{47}\text{V}$ reaction, for example, is the product $n_a n(^{44}\text{Ti}) \langle \sigma_{a,p} (^{44}\text{Ti}) v_a \rangle$. An approximate evaluation of the integrated reaction rate (the left-hand side of relation [39]) was carried out, summing the contributions of the $^{44}\text{Ti}(a, p)^{47}\text{V}$, $^{44}\text{Ti}(n, \gamma)^{45}\text{Ti}$, and $^{42}\text{Ca}(a, p)^{45}\text{Sc}$ reactions. The cross-section terms, $\langle \sigma v \rangle$, were taken from TCG, and the number densities at successive times τ from the quasi-equilibrium ^{28}Si -burning calculation. The total number of nuclei above ^{44}Ti (the right-hand side of relation [39]) is also obtained from this calculation.

The comparison of the two sides of relation (39) is displayed in Figure 20 for two cases: (a) $T_9 = 5.0$ and $\rho = 1.0 \times 10^7 \text{ g cm}^{-3}$ and (b) $T_9 = 4.2$ and $\rho = 1.0 \times 10^8 \text{ g cm}^{-3}$. Case a is chosen for its similarity to the conditions of Figure 19; case b is chosen because the temperature and density are probably more typical of the actual conditions of ^{28}Si burning. It is seen that in both cases the criterion of relation (39) is well fulfilled when the ^{28}Si depletion has progressed to $f = 0.4$ but that it is not fulfilled early in the ^{28}Si burning. The criterion is fulfilled slightly earlier for case b than for case a. This suggests that the comparison at $T_9 = 5.0$ and $\rho = 1.3 \times 10^7 \text{ g cm}^{-3}$ represents a somewhat unfavorable case, and in more typical circumstances the quasi-equilibrium calculation is a slightly better representation of ^{28}Si burning than was implied by the earlier examination of this case.

The conclusion reached from this one test was confirmed by a rough survey at other temperatures and densities in which the products of the reaction rates and elapsed time at $f = 0.65$ were compared with the total numbers of nuclei above $A = 44$. In agreement

with the previous more restricted result, it was found that the quasi-equilibrium requirements were better fulfilled for most temperatures and densities in the interval $T_9 = 3.4$ – 5.0 and $\rho = 10^5$ – 10^9 g cm $^{-3}$ than for the reference conditions at $T_9 = 5.0$ and $\rho = 10^7$ g cm $^{-3}$.

An exception to this generalization occurs in the region of low densities and high temperatures. Here the quasi-equilibrium is approached more slowly. Among a host of competing effects, the slow attainment of equilibrium under these conditions (and, to a lesser extent, at $T_9 = 5.0$ and $\rho = 10^7$ g cm $^{-3}$) can be attributed chiefly to the fact that the concentrations of alpha-particle nuclei, such as ^{56}Ni and ^{44}Ti , are relatively low and the concentrations of neutron-rich nuclei, such as ^{54}Fe , are relatively high (see Fig. 12). Then, considering the situation at fixed f , specifically $f = 0.65$, it follows that (1) the

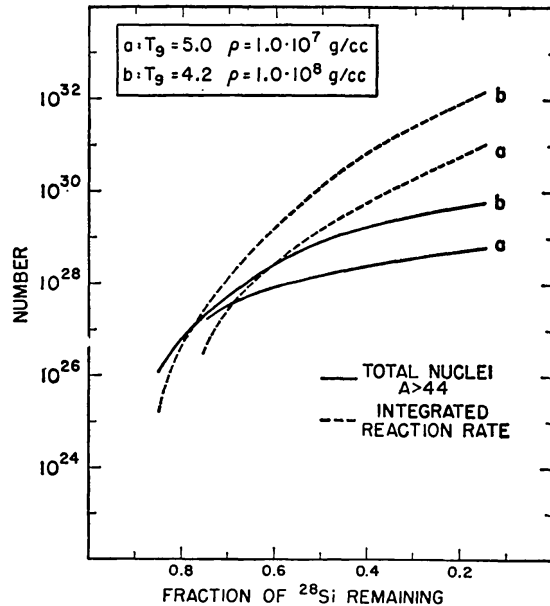


FIG. 20.—Examination of impediment to the attainment of quasi-equilibrium caused by the slow rate of reactions at ^{44}Ti . Solid curves give as a function of f the total number of nuclei above $A = 44$. Dotted curves give as a function of f the total (cumulative) number of $^{44}\text{Ti}(\alpha, p)^{47}\text{V}$, $^{44}\text{Ti}(n, \gamma)^{45}\text{Ti}$, and $^{42}\text{Ca}(\alpha, p)^{45}\text{Sc}$ reactions, as calculated using quasi-equilibrium densities found from the present calculation.

low magnitude of $n(^{44}\text{Ti})$ makes the reaction rate low and (2) the small fractional reduction in the very large number density of ^{32}S frees enough nucleons to increase substantially the total number of nuclei above $A = 44$, particularly ^{54}Fe . Both of these effects work against the attainment of equilibrium. However, it is to be noted that the low-density, high-temperature conditions, in giving an abundance peak at $A = 54$, cannot provide a match to the natural abundances. Therefore, they presumably do not correspond to the actual conditions of ^{28}Si burning, and one is less concerned with quantitative precision than in the case of more typical conditions.

In summary, it appears that quasi-equilibrium is well fulfilled (within 5 or 10 per cent) in the most relevant circumstances after about half the ^{28}Si is burned. Quantitative details of the validity of this approximation depend on the fraction which has been burned, the temperature, and the density. In general, the approximation is best at low values of f and for temperatures and densities which match the natural abundance peak at $A = 56$.

If necessary, the quasi-equilibrium calculation could probably be modified to give better results early in the burning. It seems that nuclei up to ^{44}Ti are early in quasi-equilibrium with ^{28}Si and that the iron group is in quasi-equilibrium with ^{56}Ni , n_α , and n_p but that there is an early impediment to the transfer of nuclei from the lower pool

to the upper pool. A refined approximation, therefore, would be the modification of the computational procedure so that it explicitly follows the transfer of one group of quasi-equilibrium nuclei into the other group of quasi-equilibrium nuclei. This modification could be made but has not been attempted in the present work.

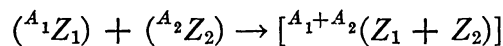
VIII. COULOMB-ENERGY CORRECTIONS

The equilibrium relations contain exponentials of the energy difference between combined and dissociated states of the composite nuclei. In first approximation these energy differences are simply the differences of the atomic-mass excess of the particles, inasmuch as the number of electrons remains the same in each dissociation. The Coulomb interaction energy between nuclei and electrons, which is usually ignored for conditions relevant in laboratory experiments, may in the present problem amount to a non-trivial fraction of kT and hence should be considered.

The atomic-mass excess of an isolated neutral atom is smaller than the mass excess of the nucleus plus electrons by an amount equal to the atomic binding energy. In the conversion to nuclear-mass excesses, therefore, the atomic values should be augmented by their atomic binding. Empirical adjustment of the Thomas-Fermi atomic model (Foldy 1951; we have changed Foldy's numerical coefficient from 15.73 to 15.6) yields, as a good approximation to the atomic binding,

$$W(^AZ; \text{atom}) \simeq -15.6Z^{7/3} \text{ eV} . \quad (40)$$

In the thermal environment characteristic of silicon burning, on the other hand, the nuclei are completely ionized. A Coulomb interaction between the ions and the electrons nonetheless persists because of the polarization of the plasma surrounding each ion. Because the electron density near each nucleus is considerably larger than for a neutral atom at terrestrial densities, the plasma polarization energy, which we will call $W(^AZ; \text{plasma})$, is generally greater than the normal atomic binding energy $W(^AZ; \text{atom})$. The nuclear process



liberates the increase in nuclear binding energy plus the increase in the plasma binding energy. These two Coulomb corrections may be included by using for the mass of each ion

$$M(^AZ; \text{plasma}) = M(^AZ; \text{atom}) - Zm_e - W(^AZ; \text{atom}) + W(^AZ; \text{plasma}) . \quad (41)$$

The calculation of the plasma interaction energy is a difficult matter. For qualitative orientation we wish to examine the value given by the Debye-Hückel model, although the requirements for the validity of that model (cf. Salpeter 1954) are not satisfied in all silicon-burning circumstances. In that approximation

$$W(^AZ; \text{plasma}) = -\frac{1}{2} \frac{Z^2 e^2}{R_D} , \quad (42)$$

where the Debye radius is designated by R_D :

$$R_D = \left(\frac{M_u kT}{4\pi e^2 \rho \zeta^2} \right)^{1/2} \quad (43)$$

and where

$$\zeta = \left[\sum_Z (Z^2 + Z) \frac{X_Z}{A_Z} \right]^{1/2} \quad (44)$$

is something like an average ionic charge. Numerically, taking $\zeta \approx 3$ for partially burned ^{28}Si ,

$$W(^A Z; \text{plasma}) = -2.40Z^2 \left(\frac{\rho_7}{T_9} \right)^{1/2} \text{ keV}, \quad (45)$$

where $\rho_7 = \rho/10^7$. It is quite evident that, in the Debye-Hückel approximation, the plasma interaction energy is much larger than the atomic binding energy. As seen from the negative sign and the quadratic Z dependence, the composite particles are more tightly bound than in the absence of the plasma interactions.

The main consequences of the plasma interaction in changing equilibrium abundances in the region from ^{28}Si to ^{56}Ni can be understood by considering the alpha-particle nuclei alone. Thus we consider reaction chains which connect ^{28}Si and δ_α alpha particles to the nucleus ($^A Z$). The true energy release, Q^c , which includes the correction for the plasma interaction, differs from the value Q taken from the atomic masses by $\Delta Q = Q^c - Q$, where

$$\Delta Q = -[W(^A Z; \text{plasma}) - W(^{28}\text{Si}; \text{plasma}) - \delta_\alpha W(^4\text{He}; \text{plasma})]. \quad (46)$$

Using equation (45), this gives

$$\Delta Q/kT = b\delta_\alpha(1 + \delta_\alpha/13), \quad (47)$$

where

$$b = 1.6\rho_7^{1/2}T_9^{-3/2}. \quad (48)$$

The corrected number density, $n^c(^A Z)$, is then

$$n^c(^A Z) = C(^A Z)n(^{28}\text{Si})(n_\alpha^c)^{\delta_\alpha}e^{\Delta Q/kT}, \quad (49)$$

where n_α^c is the alpha-particle number density in the corrected calculation. For a given fraction f of ^{28}Si remaining, $n^c(^A Z)$ would differ by the very large factor $\exp(\Delta Q/kT)$, were $n_\alpha^c = n_\alpha$. However, it is not possible for all concentrations to rise and ρ and f still to remain constant. To hold the total density fixed, n_α^c will be related to n_α by the expression

$$n_\alpha^c = n_\alpha \exp[-b(1 + \langle\delta_\alpha\rangle/13)], \quad (50)$$

where $\langle\delta_\alpha\rangle$ is an average value of δ_α such that the requirement

$$\Sigma AC(^A Z)n(^{28}\text{Si})n_\alpha^{\delta_\alpha} = \Sigma AC(^A Z)n(^{28}\text{Si})(n_\alpha^c)^{\delta_\alpha}e^{\Delta Q/kT} \quad (51)$$

is satisfied. Under typical conditions of ^{28}Si burning, $\langle\delta_\alpha\rangle$ is in the neighborhood of $\langle\delta_\alpha\rangle = 6$. Substituting the value of n_α^c from equation (50) in equation (49), one finds

$$n^c(^A Z) = n(^A Z) \exp[b\delta_\alpha(\delta_\alpha - \langle\delta_\alpha\rangle)/13]. \quad (52)$$

Thus, for example, under conditions where $\langle\delta_\alpha\rangle = 6$,

$$n^c(^{56}\text{Ni}) \simeq n(^{56}\text{Ni})e^{b/2}. \quad (53)$$

This correction factor, while not negligible at all densities and temperatures of interest, is far smaller than the correction factor $\exp(\Delta Q/kT)$ which would apply were the alpha-particle density fixed.

More quantitative statements are not appropriate without further analysis, because in the region of temperatures and pressures where the correction becomes appreciable, say $T_9 = 4$ and $\rho_7 = 10$, the Debye-Hückel criteria of validity become seriously violated.

A corollary to the changes in abundances implied by the Coulomb corrections is a change in time scale. The corrected value of the alpha-particle density is less than the

uncorrected value by the factor $\exp[b(1 + \frac{1}{13}\langle\delta_\alpha\rangle)]$, and therefore, in equilibrium, $n^c(^{24}\text{Mg})$ will tend to be increased by the same factor. This factor is partially compensated by the increase in the average binding energy of the alpha particle in ^{28}Si , which reduces $n^c(^{24}\text{Mg})$ by the additional factor $\exp[-b(1 - \frac{1}{13})]$. In first approximation, the effective photodisintegration rate of ^{28}Si is proportional to $n^c(^{24}\text{Mg})$, so that the corrected time scale is smaller than the uncorrected time scale by the factor $\exp[-b(\langle\delta_\alpha\rangle + 1)/13]$. For example, were $b = 0.2$ and $\langle\delta_\alpha\rangle = 6$, this would correspond to a reduction in the time by about 10 per cent. However, a time shift of this magnitude is insignificant in the context of ^{28}Si burning, because the value of $\lambda_{\gamma\alpha}(^{24}\text{Mg})$ is not known to that accuracy and because the same shift may also be achieved by changing the burning temperature by the very small amount $\Delta T_9 \simeq 0.01$.

The calculations of the present paper have been made without the Coulomb corrections discussed in this section, and at the present time we see no compelling reason to include them. As seen above, although the abundance ratios at fixed n_α , ρ , and T are altered considerably by these corrections, the distributions at fixed f , ρ , and T are not much altered. Furthermore, the time scale without Coulomb corrections at temperature T is nearly indistinguishable from one at $T + \Delta T$ where the increment ΔT is small. The astrophysical circumstances are not known with sufficient precision to distinguish the two situations.

IX. DISCUSSION

The study described in this paper has examined silicon burning under conditions of constant temperature and density. The site of this burning has not been specified. However, even if we could assign one specific site to the burning process, such as a shell exterior to the core of a supernova, it is unreasonable to suppose that the temperature and density are constant, either in space or time, during any one burning history or that the temperature-density histories of different supernovae are identical. A more realistic analysis must include evolutionary histories of the stars, in which the temperature and density are changed in accordance with an appropriate model of the stellar dynamics. The observed solar-system abundances are then to be attributed to the superposition of a number of such silicon-burning sequences.

In making comparisons with natural abundances, an abundance has been chosen for iron which is one-fifth of the meteoritic value tabulated by Cameron (1967). The introduction of this reduction factor was motivated by the fact that the abundance for iron found from solar photospheric studies is substantially less than the abundance found in meteorites. It must be recognized, however, that there is no firm basis for preferring the photospheric abundance to the meteoritic abundance, especially since the solar coronal abundance substantially exceeds the photospheric value. A general review of the conflicting evidence relating to the abundance of iron has recently been presented by Urey (1967), with references to the relevant literature. In view of the continuing uncertainty, the correct abundance for iron must be viewed to be an open issue, and the factor of $\frac{1}{5}$ may turn out to be incorrect.

It is therefore of interest to examine the consequences of using the meteoritic abundance for iron, which raises the natural abundances of all iron isotopes by a factor of 5 over the values used in the earlier parts of the present paper. With this change the best agreement between the quasi-equilibrium solutions and natural abundances will be achieved at relatively low temperatures. This is evident, for example, from Figure 5, where a high value for the point at $A = 56$ implies a relatively steep curve (shifted upward in absolute position), corresponding to $T_9 \approx 4.0$ or less. The match to the total array of points will not be particularly good, with rather large discrepancies at $A = 40$ and $A = 52$.

A more complete comparison is presented in Figure 21 between the natural abundances (without the factor $\frac{1}{5}$) and the quasi-equilibrium abundances. Results are shown

for $T_9 = 4.0$, $\rho = 10^7 \text{ g cm}^{-3}$, and $f = 0.25$. The match in Figure 21 is poorer than those achieved with the lower iron abundance (Figs. 3 and 14). Perhaps the most flagrant discrepancy is at ^{55}Mn , where the quasi-equilibrium abundance in Figure 21 exceeds the natural abundance by a factor of 7. The discrepancy throughout the chromium isotopes may also prove troublesome to an interpretation of this kind.

It is difficult at the present time to assess the implications of the disagreements which appear in Figure 21 between the calculated and observed abundances. Despite the differences in details, there is agreement in the broad major features, namely, the abundance peak at $A = 56$ and the relatively high abundances for much of the iron group

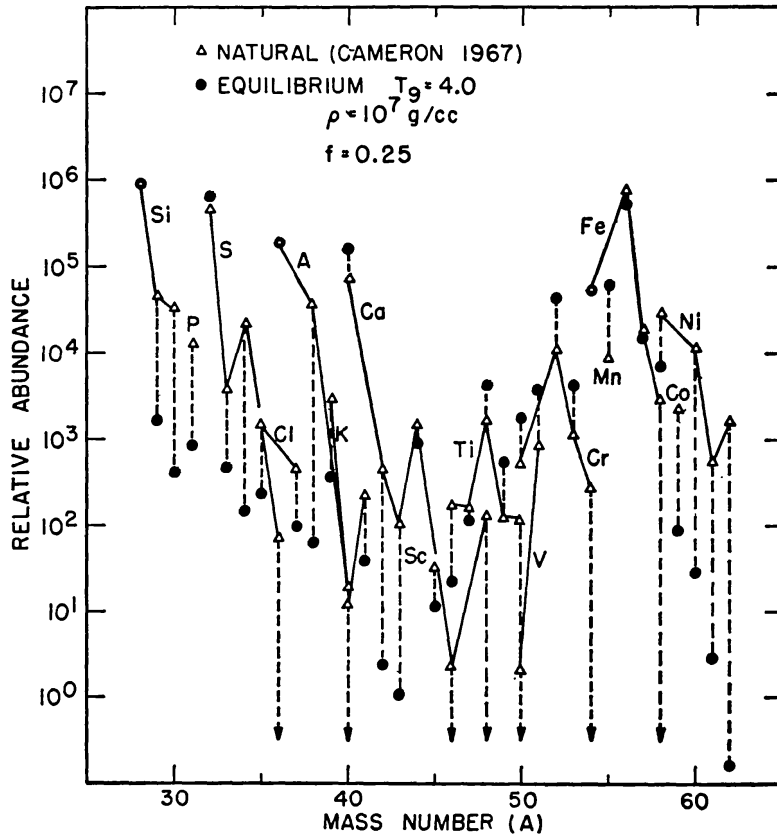


FIG. 21.—Comparison of natural solar-system abundances with quasi-equilibrium abundances at $T_9 = 4.0$, $\rho = 10^7 \text{ gm cm}^{-3}$, and $f = 0.25$. The meteoritic iron abundance is used in this comparison.

and for the $A = 4n$ nuclei. Thus the main conclusion expressed at the end of § V applies in its essential qualitative features for either choice of iron abundance. It is possible, although not assured, that extensions of this model would eliminate the quantitative discrepancies. Individual points whose quantitative impact should be investigated include (a) the consequences of realistic superpositions of distributions resulting from different values of T , ρ , and f ; (b) the dependence of the quasi-equilibrium abundances on the initial composition (assumed here to be pure ^{28}Si) and on the initial charge-to-mass ratio (assumed here to be exactly $\frac{1}{2}$); (c) the readjustments in abundances which occur when freezing first disrupts the equilibrium coupling between different groups of nuclei; and (d) the changes in abundance produced by the subsequent secondary processes that are invoked particularly to explain the abundance of the neutron-rich nuclei outside the iron group but that must affect all nuclei to some extent. Until such studies are carried out, it would be premature to conclude that the present model is in decisive *quantitative* agreement or disagreement with any plausible choice of iron abundance.

No attempt has been made in the present analysis to trace histories in which the temperature and density vary with time. However, it is possible to use the results for constant temperature and density, as presented in Table 4, to construct rough approximations to such histories. Details of implementing this procedure are described in the Appendix. As discussed in the Appendix, it is particularly important to take cognizance of the fact that the free-particle densities change rapidly with changes in temperature and therefore, for example, that the actual nuclear energy generation during intervals of rising temperature is less than the nuclear energy generation when the temperature is constant.

The proposition of this paper that the large natural abundance of ^{56}Fe is due to the decay of ^{56}Ni following the expulsion of silicon-burning zones from supernovae suggests some major revisions of long-standing astrophysical arguments. The Fowler and Hoyle (1964) contention that the dominance of ^{56}Fe points to the universality of the weak interaction was based on the assumption that ^{56}Fe was synthesized during a complete nuclear equilibrium near the presupernova core. If that scheme for the production of ^{56}Fe is replaced by the scheme of this paper, their conclusion regarding the universality of the weak interaction could, of course, not be drawn. Present arguments and information do not establish conclusively the extent to which either of these schemes is correct. The radioactive decays of ^{56}Ni and of other unstable but abundant alpha-particle nuclei (^{52}Fe , ^{48}Cr , ^{44}Ti) have, in addition, important implications for the thermal budget of the nebula and for gamma-ray astronomy. The energy released by these decays before the expanding nebula becomes thin may maintain a high thermal temperature in the expanding gas with resultant effect on the supernova light curves (Colgate and McKee 1968), in much the same spirit as the older californium hypothesis ($B^2\text{FH}$). The 6-day decay of ^{56}Ni and the 77-day decay of ^{56}Co would seem to dominate these considerations. The gamma rays of nuclear de-excitation following these electron captures should be quite profuse from young supernova remnants (Clayton, Colgate, and Fishman 1968).

It does not appear likely that nucleosynthesis in silicon burning is related to silicon burning in the core of a presupernova star. While such burning probably does occur, it is difficult for the material to escape from the core, and, further, the temperatures necessary to account for the observed abundances ($T_9 \geq 4.0$) are probably too high to allow controlled core burning to occur. Presumably the core burning stabilizes briefly at a lower temperature, where the nuclear energy generation can be in balance with the energy losses.

A more probable site for the silicon burning that is responsible for the observed products of nucleosynthesis is in a shell ejected from the supernova. This possibility has been discussed frequently, most recently by Truran, Arnett, and Cameron (1967) and by Finzi and Wolf (1967). One imagines that silicon burning progresses to some value of f and passes through a temperature maximum before the material is ejected into space. Although the quasi-equilibrium approximation is a good one during the high-temperature burning, it cannot remain good as the matter is ejected. When the cooling begins, the abundances will adjust at first to quasi-equilibrium at a lower temperature, but, if the temperature falls rapidly, the nuclear abundances may not be able to readjust quickly enough to match the new quasi-equilibrium distribution. In particular, this may well be the case for $f \sim 0.35$, for which the time scale of nuclear burning becomes fairly long. The necessary freezing calculation will depend explicitly on the time scale of the expansion and on the nuclear reaction rates. Thus the quasi-equilibrium calculation does not obviate the need for knowledge of nuclear cross-sections in this mass region.

One may seek in the freezing calculations an explanation of the abundances which are higher in nature than is predicted by quasi-equilibrium, namely, the abundances of most of the nuclei with $28 < A < 50$, other than the alpha-particle nuclei. The synthesis of these nuclei is apparently due to secondary processes, starting with nucleon capture in the abundant alpha-particle nuclei. Because proton reactions in these nuclei will be less

hindered by the Coulomb barrier than will alpha-particle reactions, proton-capture reactions will persist relatively far into the freezing period, provided that the free protons are not exhausted. If, nevertheless, these nuclei cannot be produced during freezing by proton capture (followed by beta decay), they may have to be attributed to neutron-capture processes starting with the alpha-particle nuclei as seeds. The answers to these and other interesting questions remain for future investigation. Thus concludes this "Handbuch des Siliziumbrennens."

We are very indebted to Drs. A. Finzi and R. A. Wolf for allowing us to draw upon their unpublished notes concerning energy generation in silicon burning and to Barbara Zimmerman and Kikuko Matsumoto for their invaluable help in developing the computer program. We are also indebted to Dr. J. W. Truran for providing us with computer outputs of some of his results, to Mr. G. Michaud for communicating to us results of his analysis of reaction rates, to Jan Rasmussen for preparation of the manuscript, to Elizabeth Jacobsohn for assistance in the preparation of tables, and to Bonnie Felton for editorial assistance.

David Bodansky wishes to thank the John Simon Guggenheim Memorial Foundation for fellowship support and the California Institute of Technology for hospitality during 1966–1967. Donald D. Clayton wishes to thank the Alfred P. Sloan Foundation for fellowship support and to thank both the California Institute of Technology and the Institute of Theoretical Astronomy for visiting appointments during the 1966–1967 academic year. William A. Fowler wishes to thank the Institute of Theoretical Astronomy and Churchill College, Cambridge, England, for hospitality during the summer of 1967.

APPENDIX

USE OF PRESENT RESULTS FOR TRACING EVOLUTIONARY HISTORIES

Approximations to realistic evolutionary histories in silicon burning can be obtained by replacing the actual history by a series of discrete steps, each at constant temperature and density. With suitable interpolation, the results presented in Table 4 can be used to describe the behavior during the successive steps.

The system is imagined to burn for some period in state α , at T_α and ρ_α , and then change, essentially instantaneously, to state β at T_β and ρ_β . To study the burning in state β , it is necessary to relate the initial fraction of ^{28}Si remaining, $(f_\beta)_{\text{initial}}$, to the final value of state α , $(f_\alpha)_{\text{final}}$. The quasi-equilibrium assumption implies that, when the transition is made from α to β , the heavy nuclei, $A \geq 28$, can immediately readjust to quasi-equilibrium at the new temperature and density, but that the total number of these nuclei, S , is constant. The constancy of S is then the basic condition imposed on the transition from α to β . In general,

$$\Delta S \simeq \left(\frac{\partial S}{\partial f}\right) \Delta f + \left(\frac{\partial S}{\partial T}\right) \Delta T + \left(\frac{\partial S}{\partial \rho}\right) \Delta \rho . \quad (\text{A1})$$

The nuclear composition is much more sensitive to changes in temperature than to comparable fractional changes in density. Thus the requirement $\Delta S = 0$ reduces to

$$\left(\frac{\partial S}{\partial f}\right) \Delta f \simeq -\left(\frac{\partial S}{\partial T}\right) \Delta T . \quad (\text{A2})$$

For a change in temperature from T_α to T_β , the corresponding change in f is then

$$(f_\beta)_{\text{initial}} - (f_\alpha)_{\text{final}} = \psi(T_\beta - T_\alpha) , \quad (\text{A3})$$

where

$$\psi = -\left(\frac{\partial S}{\partial T}\right) / \left(\frac{\partial S}{\partial f}\right). \quad (\text{A4})$$

Values of $\psi(T, \rho, f)$ are listed in Table A1.

A special problem arises in considering the energy generation. If, for example, one considers a period during which the temperature rises, the temperature increase will be accompanied by a very rapid rise in the free-proton and free-alpha-particle densities. Thus the true rate of energy release may be much less than the constant-temperature values of ϵ given in Table 4. In problems involving changing temperatures one should use from Table 4 the energy liberated per nucleon, g , rather than the tabulated time rate of energy release, ϵ . The true time rate of energy generation can then be calculated from the change in g and the elapsed time, for given changes in f , T , and ρ . As an extreme case, we may note that the total energy liberated is about the same at $T_9 = 4.0$, $\rho = 10^8 \text{ g cm}^{-3}$, and $f = 0.50$ as at $T_9 = 5.0$, $\rho = 10^8 \text{ g cm}^{-3}$ and $f = 0.40$. Thus, if the temperature were to rise from $T_9 = 4.0$ to $T_9 = 5.0$ during the time f was falling from 0.50 to 0.40, then there would be no nuclear energy release during this period.

TABLE A1

VALUES OF $\psi(T, \rho, f)$ OBTAINED FROM AN EVALUATION OF THE APPROXIMATE EXPRESSION $\psi = -(\Delta S / \Delta T_9) / (\Delta S / \Delta f)$

TEMP. (T_9)	log ρ^*	FRACTION OF ^{28}Si REMAINING (f)							
		0.85	0.75	0.65	0.55	0.45	0.35	0.25	0.15
3.6.....	{5	+0.05	+0.10	+0.11	+0.07
	{6	.02	+ .03	.00	- .06
	{7	.01	- .01	- .07
3.8.....	{5	.08	+ .13	+ .17	+ .18	+0.15	+0.12
	{6	.02	+ .05	+ .07	+ .05	+ .01	+ .01
	{7	.02	+ .01	+ .01	- .02	- .07	- .11
	{8	.02	.00	- .05
4.0.....	{6	.05	+ .07	+ .10	+ .10	+ .07	+ .05	+0.03	+0.02
	{7	.03	+ .03	+ .03	+ .02	.00	- .02	- .03
	{8	.03	+ .01	.00	- .04	- .06
	{9	+0.03	- .01	- .09
4.2.....	{6	+ .10	+ .13	+ .13	+ .12	+ .10	+ .07	+ .05
	{7	+ .04	+ .05	+ .04	+ .03	+ .01	.00	.00
	{8	+ .03	+ .02	.00	- .02	- .04
	{9	+ .01	- .01	- .08
4.4.....	{6	+ .12	+ .15	+ .17	+ .16	+ .14	+ .12	+ .09
	{7	+ .06	+ .07	+ .06	+ .05	+ .03	+ .02	+ .01
	{8	+ .03	+ .03	+ .01	.00	- .01	- .02	- .02
	{9	+ .02	+ .01	- .02	- .06
4.6.....	{6	+ .14	+ .17	+ .19	+ .20	+ .19	+ .17	+ .15
	{7	+ .08	+ .09	+ .09	+ .07	+ .05	+ .04	+ .03
	{8	+ .04	+ .03	+ .03	+ .01	.00	.00	- .01
	{9	+ .04	+ .02	.00	- .02	- .04
4.8.....	{6	+ .16	+ .17	+ .20	+ .22	+ .23	+ .22	+ .20
	{7	+ .10	+ .11	+ .11	+ .10	+ .08	+ .06	+ .05
	{8	+ .06	+ .04	+ .04	+ .02	+ .01	.00	.00
	{9	+0.06	+0.02	+0.01	-0.01	-0.02	-0.03	-0.03

* The density ρ is in grams per cubic centimeter.

REFERENCES

- Brancazio, P. J., and Cameron, A. G. W. 1967, *Canadian J. Phys.*, **45**, 3297.
- Burbidge, E. M., Burbidge, G. R., Fowler, W. A., and Hoyle, F. 1957, *Rev. Mod. Phys.*, **29**, 547 (B²FH).
- Cameron, A. G. W. 1967, Proceedings of the International Association of Geochemistry and Cosmochemistry, Paris, May 8–11, 1967 (to be published).
- Chandrasekhar, S., and Henrich, L. R. 1942, *A p. J.*, **95**, 288.
- Clayton, D. D., Colgate, S. A., and Fishman, G. J. 1968, *A p. J.* (to be published).
- Clifford, F. E., and Tayler, R. J. 1965, *Mem. R.A.S.*, **69**, 21.
- Colgate, S. A., and McKee, C. 1968, paper presented at A.A.S. meeting, Charlottesville, Virginia, April 1968 (to be published).
- Finzi, A., and Wolf, R. A. 1966 (private communication).
- . 1967, *A p. J.*, **150**, 115.
- Foldy, L. L. 1951, *Phys. Rev.*, **83**, 397.
- Fowler, W. A. 1966a, in *High Energy Astrophysics*, ed. L. Gratton (New York: Academic Press).
- . 1966b, in *Abundance Determinations in Stellar Spectra*, ed. H. Hubenet (New York: Academic Press).
- . 1968, Proceedings of the International Association of Geochemistry and Cosmochemistry, Paris, May 8–11, 1967 (to be published).
- Fowler, W. A., Burbidge, E. M., Burbidge, G. R., and Hoyle, F. 1965, *A p. J.*, **142**, 423.
- Fowler, W. A., Caughlan, G. R., and Zimmerman, B. A. 1967, *Ann. Rev. Astr. and Ap.*, **5**, 525 (FCZ).
- Fowler, W. A., and Hoyle, F. 1964, *A p. J. Suppl.*, No. 91, **9**, 201.
- Hansen, C. J. 1966, unpublished Ph.D. thesis, Yale University, New Haven, Connecticut.
- Hayashi, C., Nishida, M., Ohyama, N., and Tsuda, H. 1959, *Progr. Theoret. Phys.*, **22**, 101.
- Hoyle, F. 1946, *M.N.R.A.S.*, **106**, 343.
- Klein, O., Beskow, G., and Treffenberg, L. 1946, *Ark. f. mat., astr., och fys.*, Vol. **33B**, No. 1.
- Mattauch, J. H. E., Thiele, W., and Wapstra, A. H. 1965, *Nucl. Phys.*, **67**, 1.
- Peat, D. W., and Pemberton, A. C. 1967 (to be published).
- Pokrowski, G. I. 1931, *Phys. Zs.*, **32**, 374.
- Salpeter, E. E. 1954, *Australian J. Phys.*, **7**, 373.
- Tolman, R. C. 1922, *J. Am. Chem. Soc.*, **44**, 1902.
- Truran, J. W., Arnett, W. D., and Cameron, A. G. W. 1967, *Canadian J. Phys.*, **45**, 2315.
- Truran, J. W., Cameron, A. G. W., and Gilbert, A. 1966, *Canadian J. Phys.*, **44**, 563 (TCG).
- Urey, H. C. 1967, *Quart. J.R.A.S.*, **8**, 23.
- Urey, H. C., and Bradley, C. A., Jr. 1931, *Phys. Rev.*, **38**, 718.